

ABSTRACT

DATTA, PREETA. Polymerization under Confinement. (Under the direction of Dr. Jan Genzer).

This Ph.D. Thesis focuses on understanding polymerization reactions under different degrees of confinement, from growing polymers in micro-channels using thermal frontal polymerization to surface-grafted templates via “grafting through” approach. This work demonstrates that by suitable choice of theta solvent, it is possible to induce gelation and thereby, reduce the termination rate in free radical polymerization reactions giving rise to high molecular weight polymers. Specifically, free radical synthesis of acrylamide via thermal frontal polymerization, was studied. In conjunction with gelation, the frontal mode of heat transport localized the reaction and eliminated convection in confined systems. Using such systems, it is possible to synthesize fairly monodisperse (PDI ~ 1.2) polymers well below the theoretical limit (1.5) of polydispersity index in free radical polymerization. The major impact and novelty of this Ph.D. Thesis is the development of a new paradigm shift in polymer synthesis from current sophisticated chemistries to simple, convenient and energy-efficient free radical chemistry. This Ph.D. Thesis also examines polymer synthesis via template polymerization using a “grafting through” approach. “Grafting through” polymerization is based on a bulk radical polymerization reaction utilizing a self-assembled monolayer that contain polymerizable units. Free polymer chains formed in solution can incorporate the surface-bound monomers, and thereby, get covalently bonded to the surface. As more growing chains attach to the surface-bound monomers, an immobilized polymer layer is formed on the surface. The proximity of the surface-bound polymerizable units promotes the “grafting through” process but prevents more free growing chains to “graft to” the polymerizable units. A combination of Monte Carlo simulation and surface-sensitive characterization tools was used to demonstrate that the packing density of the template (that brings these counter-active effects into play) and the dimensionality of the template are key factors in controlling the structure and sequence distribution in surface-tethered growing polymer chains. The contribution of this work is significant in furthering the present understanding of novel polymer synthesis via template polymerization.

Polymerization under Confinement

by
Preeta Datta

A dissertation submitted to the Graduate Faculty of
North Carolina State University
in partial fulfillment of the
requirements for the degree of
Doctor of Philosophy

Chemical Engineering

Raleigh, North Carolina

2015

APPROVED BY:

Kirill Efimenko

Orlando Rojas

Michael Dickey

Orlin Velez

Jan Genzer
Committee Chair

DEDICATION

To my mother, Amita

BIOGRAPHY

Preeta was born and brought up in the Indian metropolitan city of Calcutta. After graduating from Jadavpur University, she went to do her Masters from the prestigious Indian Institute of Science, Bangalore. While at IISc, she worked on molecular simulation in Prof Ganapathy Ayappa's group. She got motivated to do doctoral research, decided to explore a new country and joined NCSU in 2009. She got interested in polymers while attending a class that Dr Genzer was teaching in Fall 2009. She started working in the Genzer lab soon after. While at NCState, she served briefly at the Student Conduct Board and also, served as the departmental Graduate Recruiting Captain in 2013 and the departmental Ambassador for Office of International Services (until May, 2015).

ACKNOWLEDGMENTS

I am at a loss of words to thank my advisor, Dr. Jan Genzer, for his excellent supervision and guidance during the course of my doctoral research. He's always been there with his cheerful demeanor and immense patience, motivating me to work even in the most disappointing situations. I think I cannot ask for a better advisor than him and working for him to be one of the best decisions I took in my life. In fact, a part of me doesn't want to leave.

I also acknowledge Dr. Efimenko; his practical and very critical approach towards research and problem solving helped me keep on track. Thank you Drs. Dickey, Velez, Khan, Henderson and Rojas for letting me use your lab facilities and suggestions.

This thesis would not have been possible without a few individuals, namely Rohan, Phil and Dr. Genzer. They have painstakingly taken time away from their busy schedules to proof-read this thesis at a very short notice. Thanks to Matt and Gilbert for their valuable suggestions. I am grateful to the past Genzer group members – Erich, Casey and Julie, for being the go-to people in my early years in the group. The current Genzer group members and visitors, including Steven, Sean, Duncan, Ying and Stephie, are not only excellent coworkers but great company too. Special mention for Edwin for patiently listening to research-related woes. Thanks to Rich Lamy of Burlington Precision Instruments, Elaine Zhou of AIF and our own, Ms. Sandra Bailey, for their resourcefulness. Overall, my stay at NCState has been wonderful, thanks to the amazing people in the department.

Thank you Vivek for your care and support during the first few years of my academic journey. I am lucky to have made a few friends who made my stay in Raleigh so enjoyable.

I am grateful to a couple of my school teachers and college professors who encouraged me at an impressionable age. I have to mention my aunt and my father, who weren't directly involved in my Ph.D. She made my young mind curious about science and he encouraged my younger self to dare.

Last but not the least, I must thank the individuals who discouraged me at every stage of my career and life. Criticism and discouragement constitute the magic potion that drives me.

TABLE OF CONTENTS

LIST OF TABLES.....	viii
LIST OF FIGURES.....	ix
1. Polymerization under Confinement.....	1
1.1 Introduction.....	2
1.2 Thermal Frontal Polymerization.....	4
1.3 Template polymerization using “grafting through” approach.....	6
1.4 References.....	6
2. Effect of confinement on thermal frontal polymerization.....	9
2.1 Introduction.....	10
2.2 Experimental Details.....	11
2.3 Results & Discussions.....	13
2.4 Conclusions.....	17
2.5 Acknowledgements.....	17
2.6 Appendix.....	18
2.7 References.....	22
3. Controlling Polydispersity in Free Radical Polymerization systems.....	24
3.1 Introduction.....	27
3.2 Molecular Weight Distribution of the polymer.....	31
3.3 Understanding the front zones.....	32
3.4 The role of convection.....	33
3.5 Role of ‘gelation’ – choice of solvent.....	36
3.6 Directional heat supply.....	39
3.7 Bimodal nature of the molecular weight distribution.....	43
3.8 Discussion.....	47
3.9 References.....	48
4. Computer Simulation of Template Polymerization using a Controlled Reaction Scheme.....	51
4.1 Introduction.....	51
4.2 Simulation Model.....	54
4.3 Results and Discussion.....	57
4.4 Conclusions.....	70
4.5 Acknowledgements.....	71
4.6 Appendix.....	73
4.7 References.....	74

5. “Grafting Through” Polymerization using surface-bound monomers.....	78
5.1 Computer Simulation.....	80
5.1.1 <i>Set-up and Method</i>	80
5.1.2 <i>Results and Discussion</i>	83
5.2 Experimental Set-up.....	92
5.2.1 <i>General Methods and Materials</i>	92
5.2.2 <i>Sample Preparation</i>	92
5.2.2.1 <i>Methacrylate Silane deposition and modification</i>	92
5.2.2.2 <i>Polymerization of surface-bound monomers</i>	93
5.2.3 <i>Results and Discussion</i>	93
5.3 Conclusions.....	96
5.4 Appendix.....	98
5.5 References.....	101
6. Outlook.....	104
6.1 Confined Frontal Polymerization as a means to synthesize low PDI polymers.....	105
6.2 Confined Frontal Polymerization as a separation method to study reaction kinetics..	106
6.3 “Grafting through” polymerization for molecular imprinting and patterning.....	106

LIST OF TABLES

Table 2.1. The average molecular weight of the polymer samples corresponding to different degrees of confinement.....	14
--	----

LIST OF FIGURES

Figure 1.1. The different confinement scenarios in radical polymerization.....	4
Figure 2.1. Schematic diagram of the positive feedback mechanism in a frontal polymerization system.....	11
Figure 2.2. IR image of top glass surface, snapshot of front, pixel intensity of optical image and temperature inside reactor (top to bottom).....	12
Figure 2.3. Optimal images of the front (top view) corresponding to different degrees of confinement, at different time intervals after initiation.....	13
Figure 2.4. Front position at different time intervals after initiation (inset: front velocity as a function of vertical confinement).....	15
Figure 2.5. Normalized molecular weight distribution (log base 10) corresponding to different degrees of confinement.....	15
Figure A2.1. a) DSC trace of potassium persulfate at 5°C heating rate. b) Linear portion of Arrhenius plot derived from DSC trace in Figure 2.1a	20
Figure A2.2. (top) Molecular weight distribution of polymer at different distances from the heat source at the end of consecutive runs. (bottom) Variation of overall average molecular weight of the polymer with time after initiation for channel height of 0.4 mm.....	21
Figure 3.1. Degree of polymerization distribution (analogous to molecular weight distribution) for polymer samples taken after 60 mins of ignition at varying distances away from heat source (shown in different colors in the legend) corresponding to different reactor heights (or gaps).....	28
Figure 3.2. Variation of polydispersity index (PDI) of polymer samples with distance from heat source and reactor height (shown as y-axis) 60 mins after ignition.....	31
Figure 3.3. Kinetic data on M_n (left) and PDI (right) for samples located at different distances away from heat source corresponding to a highly confined reactor (0.4 mm height).....	31
Figure 3.4. The different reaction zones in frontal polymerization (on a dark background) with the respective monomer conversions (top); IR spectra of DMSO, acrylamide (AAm) and the samples from the different zones.....	33

- Figure 3.5.** Time evolution of the fronts corresponding to different degrees of vertical confinement. The inset shows the cross-section of the front manifesting convection, note the distinct layering..... 34
- Figure 3.6.** Comparison of the temperature (left ordinate, red lines) and the initiator half-life (right ordinate, green lines) profiles corresponding to 0.4 mm (heavily suppressed convection) and 2 mm (with convection) vertical confinement for various reaction times ranging from 10 to 60 mins..... 35
- Figure 3.7.** Comparison of front profiles of a 0.4 mm thick horizontal setup and one that is inclined horizontally at 10 degrees (top views)..... 36
- Figure 3.8.** Motion of suspended particles (shown in black) inside the reaction chamber of height 2 mm (left) and 0.4 mm (right), demonstrating the presence of convection. The red and green arrows mark the initial and the final positions of the particles respectively (from top to bottom)..... 37
- Figure 3.9.** Storage (E') and loss (E'') moduli as a function of angular frequency, measured at constant strain of 0.01, for 0.4 mm thick polyacrylamide film in air (solid) and soaked in DMSO (dashed)..... 38
- Figure 3.10.** Effect of dilution on M_n and PDI for different reactor heights. For very dilute systems, the front did not propagate..... 39
- Figure 3.11.** Comparison of M_n and PDI of polymers grown via frontal polymerization and uniform heating at different degrees of dilution. Note that for dilute systems (1:5 and 1:10), the front did not propagate (*cf.* **Figure 3.9**)..... 41
- Figure 3.12.** Comparison of M_n and PDI of polymers grown via uniform heating with glass and metal windows (bottom) and schematic diagram of the reactor with different windows (top)..... 42
- Figure 3.13.** A typical example of peak resolution of degree of polymerization distribution of a polymer sample..... 44
- Figure 3.14.** Detailed analysis of molecular weight distribution using peak fitting for polymer samples at different distances from heat source corresponding to different reactor heights (along each column). The top row compares the experimental and fitted PDI values. Peak 1 (red) and 2 (blue) correspond to the two weighted Schulz-Zimm peaks fitted to the bimodal distribution. The middle row shows the PDIs and number average degree of polymerization (analogous to M_n) for the fitted peaks. The bottom row shows the weights of the two peaks used to fit the experimental data..... 46

- Figure 3.15.** DSC curve showing exothermic peak for mixture of acrylamide and potassium persulfate in DMSO..... 46
- Figure 4.1.** a) Rod-like substrates (black) with grafted bound monomers (magenta), (b) Ring-like substrates (black) with grafted monomers (magenta), (c) copolymers formed by combination of free monomers (green) and bound monomers (magenta) – high grafting density of monomers, (d) copolymers with bound “unimers” – low grafting density of monomers on substrate..... 57
- Figure 4.2.** Comparison of the number and sequence length distributions of B bound monomers in A-B copolymers for different number of initiators ($[I] = 12$ and 125) and free monomers ($[A] = 3125$ and 6250) for rod-like substrates..... 59
- Figure 4.3.** Comparison of the number distribution of B in A-B copolymers, averaged over 10 simulation runs, for different grafting densities on rod-like substrates (σ_B)..... 60
- Figure 4.4.** Effect of the number of initiators ($[I]$) and the number of bound B monomers ($[B]$) on the number distribution and sequence length distribution of B in copolymers A-B..... 62
- Figure 4.5.** Distributions of “mers” in A-B copolymers for $[I] = 125$, $[B] = 64$, $[A] = 6250$ and $\sigma = 1$. Unimers to octamers are observed to be formed under these conditions (the red lines demarcate the different substrates)..... 63
- Figure 4.6.** Effect of flexibility of the bound B monomers on the number distribution and sequence length distribution of B in A-B copolymers, for $[I] = 12$ and 125 64
- Figure 4.7.** The average number of A polymers and A-B copolymers as well as the average A-B composition as a function of the grafting density of the B monomers (σ_B) in fixed (left column) and flexible (right column) conformations..... 66
- Figure 4.8.** Comparison of the number distribution of B monomers in A-B copolymers for rod and ring-like substrates..... 68
- Figure 4.9.** Effect of the orientation of the bound B monomer on their number distribution in A-B copolymers, for $[I] = 12$, $[A] = 3125$ and $\sigma_B = 0.47$ (blue), 0.43 (red)..... 70
- Figure A4.1.** Comparison of sequence length distribution of A monomers in polymer chains at different grafting densities of bound monomers B for two different initial numbers of free A monomers in solution..... 74

- Figure 5.1.** The cubic lattice for simulation – the dimensions of the box are changed to vary the bund B monomer packing density (σ_B), keeping the volume constant. The blue motifs denote the monomers bound to the substrate..... 81
- Figure 5.2.** Comparison of the number distribution of B in A-B copolymers, averaged over 50 simulation runs, for different grafting densities on planar substrates (σ_B) at two different initiator concentrations ($[I] = 12, 125$)..... 84
- Figure 5.3.** Effect of the monomer packing density (σ_B) on the sequence length distribution of B in copolymers A-B..... 86
- Figure 5.4.** Snapshots from a typical simulation run showing the self-limiting nature of the grafting of polymer chains to the substrate..... 87
- Figure 5.5.** Distributions of “loops” and “trains” in A-B copolymers for $\sigma = 0.18$ and 1 (top and bottom respectively) at different monomer conversions (X)..... 88
- Figure 5.6.** Effect of the monomer packing density (σ_B) and number of initiators ($[I]$) on the sequence length distribution of B in copolymers A-B..... 89
- Figure 5.7.** The average number of A polymers and A-B copolymers as well as the average A-B composition as a function of the grafting density of the B monomers (σ_B) for $[I] = 12$ and $[I] = 125$ 91
- Figure 5.8.** Top, left (a) Cartoon depicting the experimental procedure, (b) ellipsometry dry thickness measurements, (c) Br content estimated from XPS measurements, (d)-(f): TOF-SIMS fragments as a function of fractional coverage by MPS..... 96
- Figure A5.1.** Cosine of the water contact angles measured along the length of the gradient of OTS and OTS/MPS..... 99
- Figure A5.2.** A typical high resolution XPS data showing C (top) and Br (bottom) peaks... 100

1. Polymerization under Confinement

1.1 Introduction

Behavior of polymers under confinement is a classical problem in polymer physics and it has been the subject of numerous experimental, theoretical and simulations based studies [1, 2]. The length-scale and dimensionality of confinement can influence the rate of propagation and termination of a polymerization process. At one end of the spectrum of length scales, there are the industrial bulk polymerization reactors while at the other end, there are the nano-reactors (~10nm). The non-linear scaling behavior of the polymerization reaction can influence the nature of the products. As the size of a reactor decreases, the dissipation of exothermic heat to the reactor wall increases since the surface to volume ratio of the reactor increases. Therefore, the polymerization domain can change from monomer deficient to the energy deficient as the reactor size decreases under the same operating conditions, thereby changing the initiation and propagation kinetics. Confinement in nanoreactors, *i.e.* the compartmentalization of reactants to monomer droplets or polymer particles (~ 20–200 nm), significantly improves the progression of a controlled/living radical polymerization based on the persistent radical effect such as nitroxide-mediated radical polymerization and atom transfer radical polymerization. Nano-confinement causes segregation effect, which increases radical life-time and thereby improves the control over the molecular weight distribution. Such nano-scale reactors offer novel means of improving the performance of controlled/living radical polymerizations and have been studied extensively by various researchers [3-6]. Some examples of such reactors are nanoporous glass, hollow latex spheres, mesoporous silica, reverse micelle, porous dipeptide, inter-penetrating networks (IPNs) of PDMS, and core of electrospun fibers. The porosity of such materials enables monomer absorption, and subsequent polymerization in the cavities. The effect of confinement on various polymerization reactions is remarkable. Apart from the degree of confinement, the extent of the influence depends on the nature of the confining walls. For example, the rate of polymerization of acrylic acid drops down considerably in the presence of confinement effects imposed by PDMS IPNs. In case of free radical polymerization of acrylates in hydrophilic and hydrophobic nanoporous media (average pore diameter ~13 nm), the propagation rates in

acrylate polymerization become appreciable resulting in equilibrium polymerization at high temperature. For polymer synthesized in nanoconfined environment, the negative change in entropy upon propagation results in a decrease in equilibrium conversion and a shift of the ceiling temperature to lower temperatures.

The dimensionality of confinement is another aspect that plays a crucial role. The confinement encompasses the broad range from free polymer chains in a good solvent to surface-grafted polymer brushes. The dimensionality and degree of confinement can affect chain mobility and thereby affect propagation and termination rates. Often, the two aspects of confinement, dimensionality and degree, can act in conjunction to affect polymer molecular weight and in some cases also morphology (*vide infra*). Surface-initiated polymerization is a good example of such extreme confinement [7-15], wherein a loss of translational entropy of the growing chains affects their structure and conformation. The grafted polymers adopt a so-called “mushroom” conformation if the distance between neighboring chains is greater than the radius of gyration of the chain (R_g). When the average distance between two neighboring chains is less than R_g , the macromolecular grafts enter the so-called “brush” conformation, in which steric effects due to neighboring chains cause the polymers to stretch perpendicularly to the surface. In this analogy, dimensionality and degree of confinement is imposed by the high grafting density, forcing the chains to grow preferentially in one direction. The conformations of polymer brushes on surfaces are governed by a complex interaction between molecular weight, grafting density, solvent quality, and the curvature of the substrate. The interplay among the microscopic properties of polymer brushes, such as, the molecular weight, the grafting density, the chemical composition of the grafts as well as the sequence distribution of the chemical units along the grafted chain, influences the macroscopic behavior of surface-grafted polymers (*i.e.*, wettability, lubricity, modulus, response to stimulus).

This Ph.D. Thesis examines two different model systems, thermal frontal polymerization and “grafting through” polymerization, to gain a fundamental insight into the underlying mechanism of polymerization in different confinement conditions. The length-scales, dimensionalities, and the modes of confinement are widely dissimilar in these two

situations. Yet these two situations are intermediate with respect to confinement, as compared to the two extreme cases, i.e., bulk polymerization and polymerization following the “grafting from” protocol. In free radical polymerization, bimolecular termination cannot be avoided, unless under “controlled” conditions. Compared to other controlled/“living” polymerization methods, radical-based polymerization reactions have several advantages, especially in terms of compatibility with both aqueous and organic media as well as a high tolerance toward a wide range of functional groups. This work demonstrates that it is possible to achieve better control on radical polymerization products by tuning the reaction environment. The following sections serve an introduction to the two different modes of polymerization explored in this Thesis.

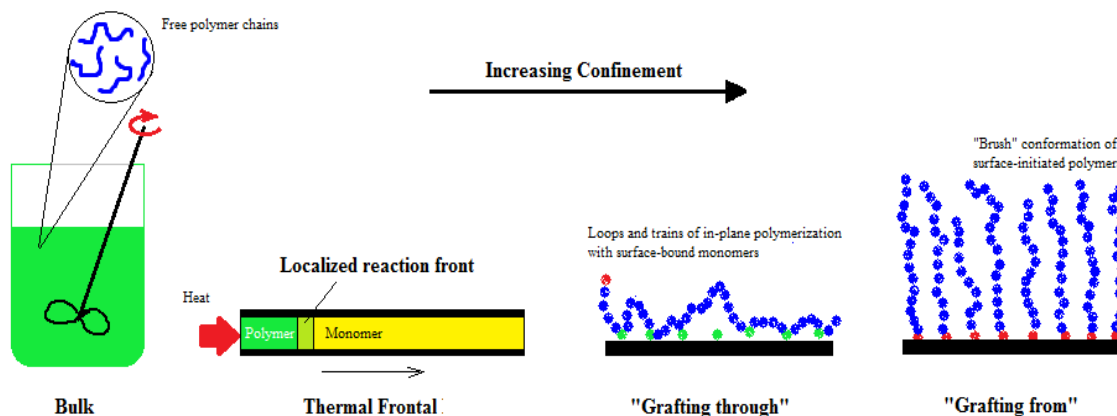


Figure 1.1. The different confinement scenarios in radical polymerization.

1.2 Thermal Frontal Polymerization

Thermal frontal polymerization is a mode of polymerization, in which a localized exothermic reaction zone propagates in an unstirred reaction vessel as a result of the interplay of thermal diffusion and Arrhenius reaction kinetics, initiated by an external heat source [16-

20]. Such a mode of polymerization can be sustained only if the polymer is not miscible with the monomer or is insoluble in it and the solvent (if used). Fronts propagate via a positive feedback mechanism and do not necessarily propagate with a constant velocity or maintain a constant shape. Buoyancy-driven and/or intrinsic thermal instabilities can affect these fronts. If the reactor is horizontal, the front is inherently unstable because of convection. Studies on descending fronts of acrylamide/bis-acrylamide polymerization in DMSO as a function of tube orientation reveal that the front velocity projected along the axis of the tube increased with $1/\cos(\phi)$, where ϕ is the angle of inclination. Convection is often eliminated by addition of thickening agents or by applying high pressure or by adjusting the reactor orientation. Free radical polymerization of acrylamide (AAm) in dimethyl sulfoxide (DMSO) initiated by potassium persulfate is a convenient system for studying frontal polymerization. Previous studies have established that the resulting polyacrylamide (PAAm) forms gels in DMSO and the vertical fronts formed are not destroyed by Raleigh-Taylor instability. Imidization of acrylamide can lead to a crosslinked product; however, this occurs in trace amounts (< 6%) and does not take place in the presence of inert fillers such as barium carbonate or polyacrylamide. This particular system has several advantages for studying frontal polymerization, including, no volatile side products (*i.e.*, no gas bubbles), polyacrylamide gels in DMSO (*i.e.*, fronts are not destroyed by “fingering”), low volatility of DMSO (*i.e.*, no vapors, hence no bubbling), visibility of a distinct front due to density differences. This Ph.D. Thesis explores the effect of physical confinement on horizontal fronts in thermal frontal polymerization systems by examining the molecular properties of polymerization products. The molecular weight distribution of a polymer is a record of the kinetic history of the polymerization process, and can provide useful insight into the reaction conditions. **Chapter 2** comprises of work published in the journal of Polymer Chemistry in 2012 and **Chapter 3** contains an in-depth investigation of the role of the growth environment on polymerization product molecular weight distribution.

1.3 Template polymerization using “grafting through” approach

“Grafting through” polymerization is based on a bulk radical polymerization reaction utilizing a self-assembled monolayer that contain polymerizable units [21-25]. Free polymer chains formed in solution can incorporate the surface-bound monomers, and thereby, get covalently bonded to the surface. As more growing chains attach to the surface-bound monomers, an immobilized polymer layer is formed on the surface. The proximity of the surface-bound polymerizable units promotes the “grafting through” process but prevents more free growing chains to “graft to” the polymerizable units. This is the first study that uses a combination of Monte Carlo simulation and surface-sensitive characterization tools to demonstrate that the packing density of the template (that brings these counter-active effects into play) and the dimensionality of the template are key factors that control the structure and sequence distribution in surface-tethered growing polymer chains. **Chapter 4** reports on understanding the effect of monomer packing density and the effect of substrate shape on the nature of the polymer chains in case of one dimensional substrates such as nano-rods and nano-wires. **Chapter 5** extends the previous study to two dimensional substrates and provides experimental validation of the simulation results.

1.4 References

1. P. G. De Gennes, “Scaling Theory of Polymer Adsorption”, *J. Phys.*, 1976, **37**, 1445–1452.
2. S. Alexander, “Polymer Adsorption On Small Spheres: A Scaling Approach”, *J. Phys.*, 1977, **38**, 977–981.
3. H. Y. Zhao, Z. N. Yu, F. Begum, R. C. Hedden, S. L. Simon, "The Effect of Nanoconfinement on Methyl Methacrylate Polymerization: T-g, Molecular Weight, and Tacticity", *Polymer*, 2014, **55**(19), 4959-4965.

4. F. Begum, H. Y. Zhao, and S. L. Simon, "Modeling Methyl Methacrylate Free Radical Polymerization: Reaction in Hydrophobic Nanopores", *Polymer*, 2012, **53**(15), 3261 – 3268.
5. F. Begum, H. Y. Zhao, and S. L. Simon, "Modeling Methyl Methacrylate Free Radical Polymerization: Reaction in Hydrophilic Nanopores," *Polymer*, 2012, **53**(15), 3238 – 3244.
6. F. Begum and S. L. Simon, "Modeling Methyl Methacrylate Free Radical Polymerization in Nanoporous Confinement," *Polymer*, 2001, **52**, 1539 – 1545.
7. S. T. Milner, "Polymer Brushes", *Science*, 1991, **251**, 905–914.
8. B. Zhao and W. J. Brittain, "Polymer Brushes : Surface-Immobilized Macromolecules", *Prog. Polym. Sci.*, 2000, **25**, 677–710.
9. I. Luzinov, S. Minko and V. V. Tsukruk, "Adaptive and Responsive Surfaces through Controlled Reorganization of Interfacial Polymer Layers", *Prog. Polym. Sci.*, 2004, **29**, 635–698.
10. P. Uhlmann, H. Merlitz, J. Sommer and M. Stamm, "Polymer Brushes for Surface Tuning", *Macromol. Rapid Commun.*, 2009, **30**, 732–740.
11. M. A. Cohen Stuart, W. T. S. Huck, J. Genzer, M. Müller, C. Ober, M. Stamm, G. B. Sukhorukov, I. Szleifer, V. V. Tsukruk, M. Urban, et al., "Emerging Applications of Stimuli-Responsive Polymer Materials", *Nat. Mater.*, 2010, **9**, 101–113.
12. E.D. Bain, S. Turgman-Cohen, J. Genzer, "Computer simulation approaches for polymerization in grafted systems", *Macromol. Theory & Simul.*, 2013, **22**, 8.
13. E.D. Bain, K. Dawes, A.E. Özçam, X. Hu, C.B. Gorman, J. Šrogl, J. Genzer, "Surface-initiated polymerization by means of novel, stable, non-ester-based radical initiator", *Macromolecules*, 2012, **45**, 3802.
14. S. Turgman-Cohen, J. Genzer, "Simultaneous bulk- and surface-initiated controlled radical polymerization from planar substrates", *J. Am. Chem. Soc.*, 2011, **133**, 17567.

15. S. Turgman-Cohen, J. Genzer, "Computer simulation of concurrent bulk- and surface-initiated living polymerization", *Macromolecules*, 2012, **45**, 2128.
16. J. Pojman, D. Fortenberry, V. Ilyashenko, "Frontal Polymerization as an Analog of SHS", *Int. J. Self-Propag. High-Temp. Synth.*, 1997, **6**, 355-376.
17. R.P. Washington, O. Steinbock, "Frontal Polymerization Synthesis of Temperature-Sensitive Hydrogels", *J. Am. Chem. Soc.*, 2001, **123**, 7933-7934.
18. J.A. Pojman, "Frontal Polymerization", in *Encyclopedia of Polymer Science: A comprehensive reference*, (K. Matyjaszewski & M. Möller, Eds.), Amsterdam, 2001, **4**, 957-979.
19. B.A. Grzybowski, "Chemistry in motion: Reaction-diffusion systems for micro- and nanotechnology", John Wiley & Sons, Hoboken, 2009.
20. J.A. Pojman, Q. Tran-Cong-Miyata (Eds), "Nonlinear dynamics with polymers: Fundamentals, methods and applications", Wiley-VCH, Weinheim, 2010.
21. M. Henze, D. Madge, O. Prucker and J. Rühle, "'Grafting Through': Mechanistic Aspects of Radical Polymerization Reactions with Surface-Attached Monomers", *Macromolecules*, 2014, **47** (22), 2929-2937.
22. S. Polowinski, "Template Polymerization", *ChemTec Publishing*, 1997.
23. G. Challa and Y.Y. Tan, "Template Polymerization", *Pure & Applied. Chem.*, 1981, **53**, 647-651.
24. D. M. Rosenbaum and D. R. Liu, "Efficient and Sequence-Specific DNA-Templated Polymerization of Peptide Nucleic Acid Aldehydes", *J. Am. Chem. Soc.*, 2003, **125** (46), 13924-13925.
25. J. Gons, E. J. Vorenkamp, G. Challa, "Radical polymerization of methyl methacrylate in the presence of stereoregular poly(methyl methacrylate). V. Kinetics of initial template polymerization", *Journal of Polymer Science: Polymer Chemistry*, 1975, **13** (7), 1699-1709.

2. Effect of confinement on thermal frontal polymerization*

* Based on P. Datta, K. Efimenko and J. Genzer, *Polymer Chemistry*, 2012, **3**, 3243-3246.

2.1 Introduction

Thermal frontal polymerization involves spontaneous conversion of monomer units to polymers via a localized exothermic radical reaction initiated by an external heat source, which self-propagates in an unstirred reaction vessel [1,2]. Front propagation occurs through positive feedback mechanisms as a result of the interplay between heat diffusion and Arrhenius type reaction kinetics [3,4]. The reactive front and its stability are affected by various factors, *i.e.*, initiation temperature, initiator concentration, monomer concentration in solution, and reactor geometry [5,6,7]. Most previous frontal polymerization studies have employed a vertical reactor in order to obtain a stable propagating front [8,9]. In contrast, in horizontal channels, convection gives rise to front instabilities and “fingering” [10,11,12,13]. Here we report the first investigation of the effect of confinement on frontal polymerization in horizontal channels.

Figure 2.1 depicts a schematic diagram of the thermal frontal polymerization process in a horizontal reaction chamber. Since the front propagation properties are strongly correlated to the heat generated in/removed from inside the polymerization reactor, it is important to estimate the heat losses in the system/mechanism during heat transfer processes and find an appropriate correlation with the overall system geometry. Previous studies of “bulk” systems have suggested that predominant heat loss to the ambient conditions occurs due to heat convection through the reaction media/glass interface [5,14]. This heat loss is proportional to the total surface area of the reaction chamber. For long channels with a high aspect ratio cross-section, heat loss takes place primarily through the top and bottom surfaces, and can thus be assumed to be independent of the channel height. It is important to point out that the exothermic heat generated in the confined system depends on the reaction volume, and is therefore, proportional to the channel height. Thus, by tuning the vertical confinement of the reaction channel, we can control the heat diffusion into the unreacted monomers and thereby tune the reaction kinetics.

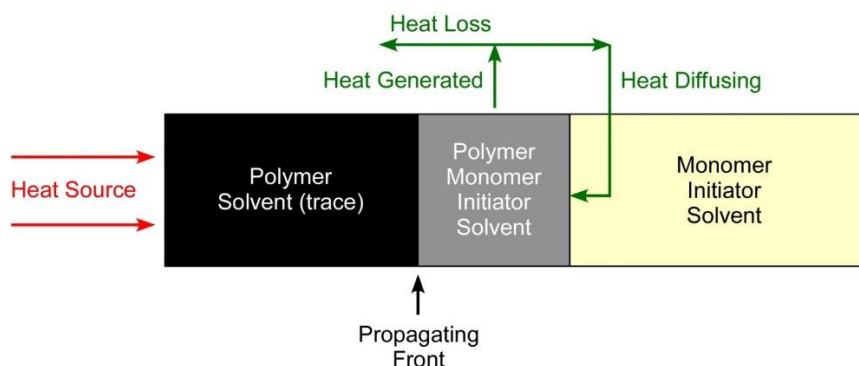


Figure 2.1. Schematic diagram of the positive feedback mechanism in a frontal polymerization system.

2.2 Experimental Details

The reaction chamber consists of a Teflon jacket sandwiched between two thick (≈ 6 mm) borosilicate glass plates (to minimize heat loss); the thickness of the Teflon jacket is varied from 0.4 to 5 mm to achieve different degrees of vertical confinement. Acrylamide ($> 99\%$, Sigma-Aldrich) monomer is dissolved in dimethyl sulfoxide (DMSO, Fisher) with potassium persulfate (Sigma-Aldrich) acting as the reaction initiator. We have chosen this system due to well established polymerization mechanism without detrimental side reactions, including, no volatile side products (*i.e.*, no gas bubbles), formation of polyacrylamide gels in DMSO (*i.e.*, fronts are not destroyed by “fingering”), low volatility of DMSO (*i.e.*, no vapors, hence no bubbling), visibility of a distinct front due to density differences [15]. Trace amounts of hydroquinone (Acros) are used as an inhibitor to eliminate spontaneous polymerization thus to achieve a better control of the polymerization process. For all the experiments, 1:750 ratio of initiator to monomer (by moles) is used. Infrared (IR) thermal images as well as regular photographic snapshots of the system are captured at regular time intervals to record the temperature profiles and polymerization front position, using FLIR A325sc (FLIR) and Canon Rebel iX (Canon) cameras, respectively. A typical example of the temperature profiles are

shown in **Figure 2.2**. An hour after initiation, the assembly is dismantled and the reaction is quenched by immersing the specimens into liquid nitrogen. Samples of the polymerization product are taken at equispaced intervals (1 cm) and characterized using size exclusion chromatography (SEC) in aqueous medium (eluent: 0.1 M sodium nitrate solution). More details pertaining to our experimental set up and analytical methods are provided in Supplementary information.

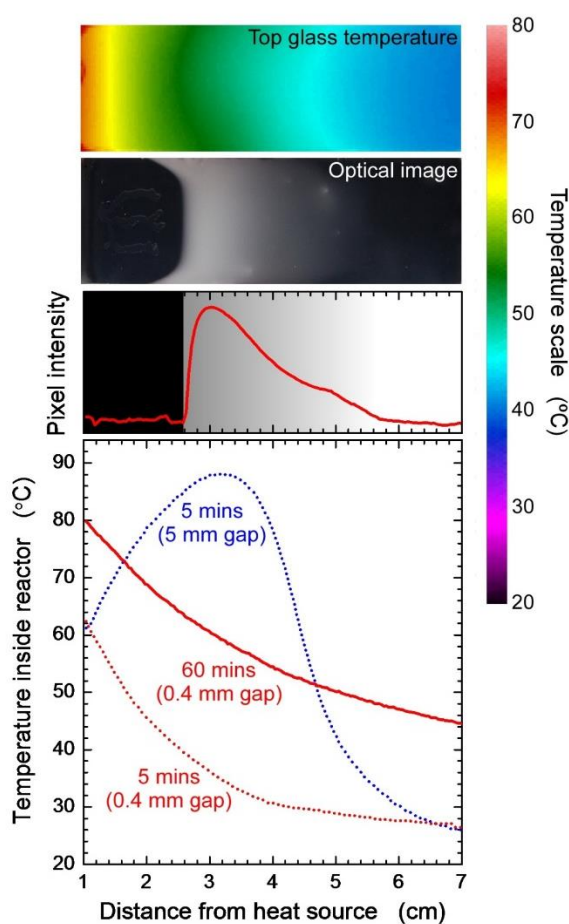


Figure 2.2. IR image of top glass surface, snapshot of front, pixel intensity of optical image and temperature inside reactor (top to bottom).

2.3 Results & Discussion

The propagating wave-front is marked by a characteristic white zone, often accompanied by random protrusions originating ahead of the front. As heat loss takes place primarily from the top and the bottom glass surfaces, the temperature inside the channel should reach a maximum at the center and decrease symmetrically with increasing distance away from the centerline. However, as the channel height decreases, the difference between the glass surface temperature and the centerline temperature decreases, asymptotically approaching zero. This is manifested in **Figure 2.3**, which shows the top-view of the propagating fronts corresponding to different confinement at specific time intervals- the parabolic profile flattens out with increasing degree of confinement. The non-uniformity of the temperature profile leads to convection heat transfer inside the system and leads to separation of top and bottom layers of the white zone in the less confined systems ($>2\text{mm}$).

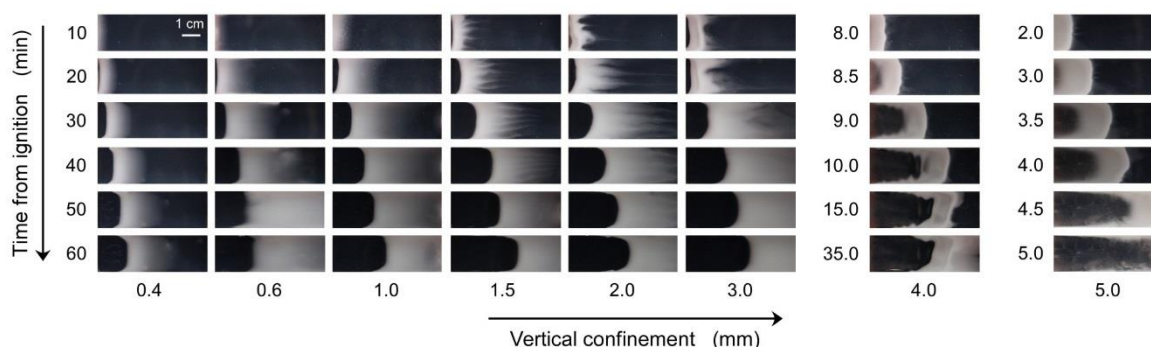


Figure 2.3. Optimal images of the front (top view) corresponding to different degrees of confinement, at different time intervals after initiation. There are three regions of interest present in the system (from left to right): dark, hazy, and dark. They are depicted schematically in **Figure 2.1**. The dark region on the left (close to the heating source) comprises polymer (*i.e.*, PAAm). It is separated by the diffusing front from the region containing PAAm, AAm and the DMSO solvent. The haziness results from immiscibility of PAAm in AAm/DMSO mixtures. The dark region on the right, ahead of the hazy field, comprises a mixture of AAm and DMSO. The chemical composition of the three regions was established from IR spectroscopy.

The analysis of the front propagation indicates clearly that at initial stages of the reaction the propagation velocity is constant for all confinement conditions. However, the deviation from this behavior is recorded for later stages of the reaction as velocity decreases with increasing confinement, as shown in **Figure 2.4**. We note that the results present herein are pertinent to the current dimensions of the system we investigated (*i.e.*, 6 cm length scale). That is, we cannot make definite conclusions about what will the behavior be in larger systems. In order to explain this behavior, one needs to carefully investigate the heat propagation/loss patterns in these systems. In “bulk-like” systems convection favors frontal propagation. As the degree of confinement increases the heat convection is suppressed significantly and polymerization reaction is affected predominantly by the heat diffusion along the channel direction, the resulting molecular weight of the polymer decreases with increasing distance from the external heating source (*cf.* **Figure 2.5**). The overall molecular weight (averaged over all samples corresponding to same degree of confinement) of the specimens shows an increase in case of confined systems (≈ 190 kDa for bulk systems to a maximum of ≈ 350 kDa for confined systems) as shown in **Table 2.1**.

Table 2.1 The average molecular weight of the polymer samples corresponding to different degrees of confinement.

Channel height (mm)	PAAm average molecular weight (kDa)
0.4	322
0.6	276
1.0	231
2.0	272
5.0	189

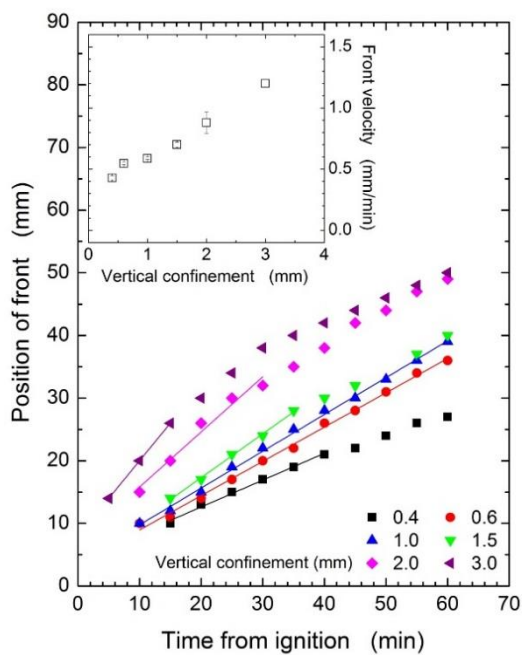


Figure 2.4. Front position at different time intervals after initiation (inset: front velocity as a function of vertical confinement).

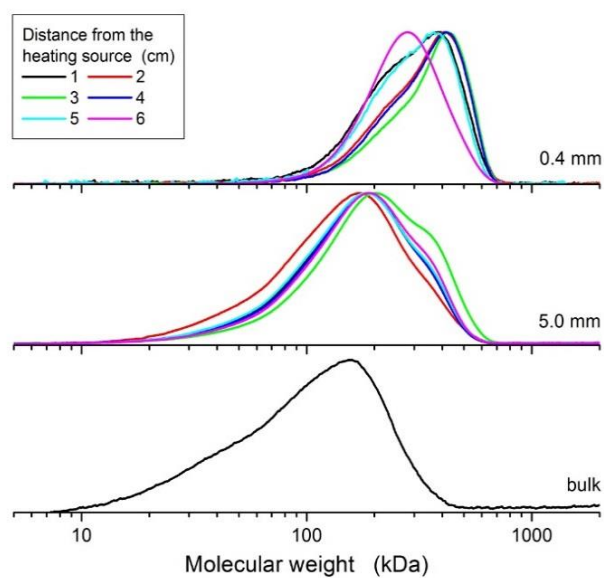


Figure 2.5. Normalized molecular weight distribution (log base 10) corresponding to different degrees of confinement.

To corroborate our experimental finding that the average molecular weight of the polymerization products increases with increasing vertical confinement of the system, we calculate the average molecular weights using Gillespie's algorithm [16] (see Supplementary information). We calculate the rate of initiation from the thermal decomposition kinetics of potassium persulfate obtained from DSC studies [17] (see Supplementary information). The rates of propagation and termination of acrylamide polymerization in DMSO are obtained from literature [18,19]. To account for the caging effect of the sulphate radical in an aprotic solvent (DMSO) [20] and the inhibiting effect of hydroquinone, we use an initiation efficiency factor of 0.01 (arbitrarily chosen as a low value due to the presence of the initiator inhibitor; we do not imply that this is the real value for initiator efficiency present in our system). We calculate the average molecular weights of the polymer formed at different distances from the heated end for the two extreme cases: channel heights 0.4 and 5 mm. The average molecular weight for the highly confined system (0.4 mm) is significantly higher (265 kDa) than the one with 5 mm vertical height (129 kDa); whose values are in accordance with our experimental findings (*cf.* **Table 2.1**). The molecular weights predicted by the Gillespie's algorithm are lower than the experimental values, which can be attributed to the fact that Gillespie's algorithm does not take into account the gelation effect and that our estimate for the initiation efficiency factor may be slightly off. Nevertheless, the trends obtained from the Gillespie's algorithm are consistent with the experimental observations.

We reconcile our observations as follows. The front propagation occurs through a positive feedback mechanism, *i.e.*, thermal energy decomposes initiators giving rise to free radicals in the initiation step, these free radicals add on monomers and heat is generated in the chain propagation step, the net heat generated raises the local temperature which in turn leads to decomposition of larger number of initiator molecules and thus increases the rate of reaction front propagation. In this study, all parameters except the vertical height of the reaction channel are kept constant. However, the volume of reaction mixture being small, the rates of heat generation and temperature gradients are also small in highly confined systems (*cf.* **Figure 2.2**, that shows the temperatures on the top glass surface for the two extreme cases: 0.4 and 5

mm). Thus, in highly confined systems a smaller number of radicals are generated, resulting in a smaller number of chains with a higher molecular weight.

2.4 Conclusions

In conclusion, we report on the first study of the effect of vertical confinement on thermal frontal polymerization. By tuning the height of the reactor, convection can be eliminated and the temperature gradients can be controlled. We observe that reducing the reactor height slows down the front propagation and the overall polymerization process, thereby producing polymers with higher molecular weights.

2.5 Acknowledgements

We thank the National Science Foundation for supporting this work through the grant No. CBET-0853667. We also thank Professor John Pojman (Louisiana State University) for fruitful discussions and useful suggestions.

APPENDIX

2.6 Appendix

Calculating the rate of initiation using Differential Scanning Calorimetry (DSC)

The thermal decomposition of potassium persulfate leads to formation of free radicals that initiate the polymerization process. The kinetics of the thermal decomposition of the initiator was characterized using differential scanning calorimetry (DSC). The DSC trace of potassium persulfate is shown in **Figure A2.1a**. The Arrhenius constants for the initiator decomposition were obtained as following. The heat of reaction ΔH_{tot} is evaluated by integrating the dH/dt curve (zeroed to the baseline value) with respect to temperature and dividing by the heating rate ($^{\circ}\text{C}/\text{min}$) [17]. Then the reaction conversion $x(T)$ at each temperature is calculated by integrating the heat evolved up to the temperature of interest (ΔH_i) and dividing by the total heat of reaction (ΔH_{tot}). The rate constant k_d of initiator decomposition, assuming a first order reaction, is given by:

$$k_d(T) = \frac{\Delta H}{\Delta T} \frac{1}{\Delta H_{tot}(1-x(T))} \quad (\text{A2.1})$$

In order to calculate k_d values for each temperature, we generate an Arrhenius plot in the form of $\ln k_d$ vs. $1/T(\text{K})$. The linear portion of the plot, typically the values between 1% and 50% of initiator conversion, is fitted to a line, and the slope and intercept of the best-fitting line are used to determine the activation energy and the pre-exponential factor, respectively. **Figure 2.6.A1.b** shows the Arrhenius plot derived from the DSC trace for potassium persulfate. The activation energy was determined to be ≈ 134 kJ/mol, and the pre-exponential factor $\approx 10^{18} \text{ s}^{-1}$.

Theoretical Molecular Weight calculations using Gillespie's Stochastic Simulation Algorithm (GSSA)

The temperature at a specific location inside the frontal polymerization system is a function of time after initiation and distance from the heat source. Since the polymer chain

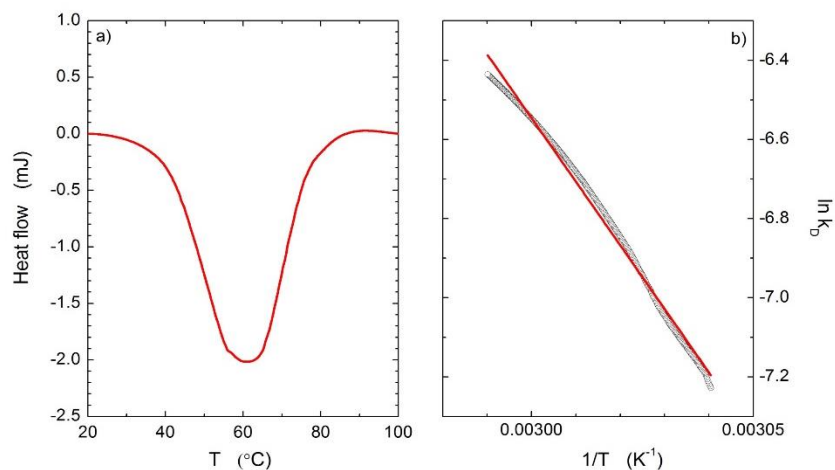


Figure A2.1. a) DSC trace of potassium persulfate at 5°C heating rate. b) Linear portion of Arrhenius plot derived from DSC trace in **Figure 2.1a**.

lengths depend on by the rates of initiation and propagation, which are inherently temperature-dependent, the molecular weight of the polymerization products is a function of the location (distance from heat source) and the time elapsed after initiation. We discretize the system by dividing it into equally spaced bins and assume the temperature of each bin to be uniform within a specific time interval. The glass-air top-surface temperature of each bin at a specific time is obtained from a line of best-fit to the experimental temperature profiles corresponding to a specific channel height (from the IR images). We assume conductive heat transfer from the interior of the bin to the top glass surface, across polyacrylamide and glass layers, in order to calculate temperature inside each bin. We use a stochastic Monte Carlo scheme based on Gillespie's algorithm to simulate bulk FRP in each of the discrete bins for a specific time-interval. The Gillespie's algorithm has been previously implemented in a bulk FRP set-up by Bain *et al.* [16]. It evaluates reaction probabilities using empirical kinetic parameters and models the time dependence of reactions, resulting in significantly accurate predictions of reaction kinetics. The GSSA method considers each reacting species independently, allowing calculation of the distributions of molecular weight and sequence distribution for polymerized

chains. The program calculates bulk rate constants at the reaction temperature according to the kinetic equations for acrylamide polymerization in DMSO reported in literature [18-20]. We keep count of the number of polymers generated, the average molecular weight, the number of monomers, the number of initiators and the monomer concentration in each bin after each discrete time interval. Since the radicals are short-lived, we rightly assume that the polymer chains generated in each time interval are dead at the end of the simulation run. The unconverted monomer and initiator concentrations at the end of each run serves as the input parameters for the simulation for the next time interval. At the end of the entire simulation run, we calculate the weighted average molecular weight in each bin by summing over all the discrete time intervals. The overall molecular weight of the polymer product is then calculated by summing over all the bins with appropriate weightage.

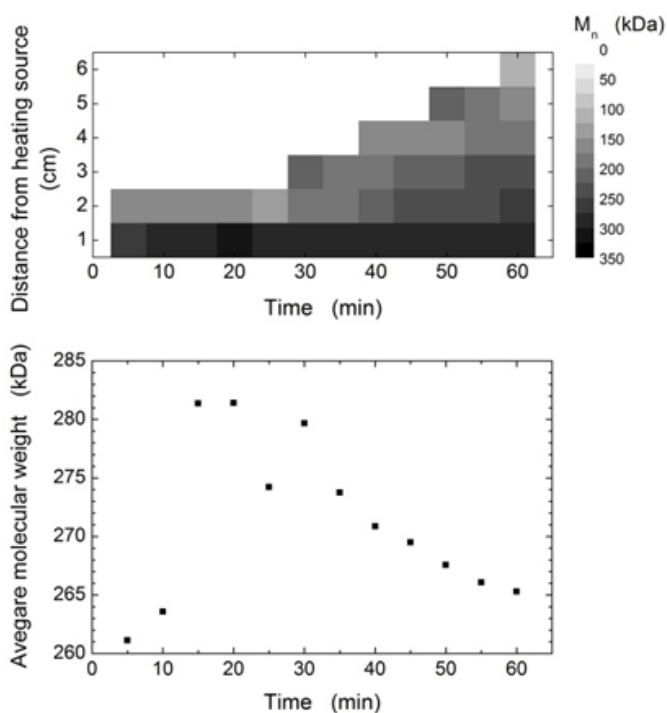


Figure A2.2. (top) Molecular weight distribution of polymer at different distances from the heat source at the end of consecutive runs. (bottom) Variation of overall average molecular weight of the polymer with time after initiation for channel height of 0.4 mm.

The molecular weight distributions corresponding to different distances from heating source and the overall average molecular weight of the polymerization products calculated at the end of the consecutive runs corresponding to a channel height of 0.4 mm are shown in **Figure A2.2**.

2.7 References

1. J. Pojman, D. Fortenberry and V. Ilyashenko, "Frontal Polymerization as an Analog of SHS," *Int. J. Self-Propag. High-Temp. Synth.* 1997, **6**, 355-376.
2. R. P. Washington and O. Steinbock, "Frontal Polymerization Synthesis of Temperature-Sensitive Hydrogels," *J. Am. Chem. Soc.* 2001, **123**, 7933-7934.
3. J. A. Pojman, "Traveling Fronts of Methacrylic Acid Polymerization," *J. Am. Chem. Soc.*, 1991, **113**, 6284-6286.
4. P. M. Goldfeder, V. A. Volpert, V. M. Ilyashenko, A. M. Khan, J. A. Pojman, and S. E. Solovyov, "Mathematical Modeling of Free-Radical Polymerization Fronts," *J. Phys. Chem. B* 1997, **101**, 3474-3482.
5. J. A. Pojman, J. Willis, D. Fortenberry, V. Ilyashenko and A. Khan, "Factors Affecting Propagating Fronts of Addition Polymerization: Velocity, Front Curvature, Temperature Profile, Conversion and Molecular Weight Distribution," *J. Polym. Sci. Part A: Polym Chem.* 1995, **33**, 643-652.
6. Pojman, J. A.; Masere, J.; Petretto, E.; Rustici, M.; Huh, D.-S.; Kim, M. S.; Volpert, V. "The Effect of Reactor Geometry on Frontal Polymerization Spin Modes," *Chaos* 2002, **12**, 56-65.
7. M. Bazile Jr., H. A. Nichols, J. A. Pojman, and V. Volpert, "The Effect of Orientation on Thermoset Frontal Polymerization", *J. Polym. Sci. Part A: Polym Chem.* 2002, **40**, 3504-3508.
8. V. A. Volpert, V. A. Volpert and J. A. Pojman, "Effect of Thermal Expansion on Stability of Reaction Front Propagation", *Chem. Eng. Sci.* 1994, **14**, 2385-2388.
9. V. A. Volpert, V. A. Volpert, J. A. Pojman and S. E. Solovyov, "Hydrodynamic Stability of a Polymerization Front", *Eur. J. Appl. Math.* 1996, **7**, 303-320.

10. J. A. Pojman, R. Craven, A. Khan and W. West, "Convective Instabilities Induced by Traveling Fronts of Addition Polymerization", *J. Phys. Chem.*, 1992, **96**, 7466-7472.
11. J. A. Pojman, V. M. Ilyashenko and A. M. Khan, "Spin Mode Instabilities in Propagating Fronts of Polymerization," *Physica D* 1995, **84**, 260-268.
12. B. McCaughey, J. A. Pojman, C. Simmons and V. A. Volpert, "The Effect of Convection on a Propagating Front with a Liquid Product: Comparison of Theory and Experiments," *Chaos* 1998, **8**, 520-529.
13. G. Bowden, M. Garbey, V. M. Ilyashenko, J. A. Pojman, S. Solovyov, A. Taik and V. Volpert, "The Effect of Convection on a Propagating Front with a Solid Product: Comparison of Theory and Experiments", *J. Phys. Chem. B* 1997, **101**, 678-686.
14. J. A. Pojman, V. M. Ilyashenko and A. M. Khan, "Free-Radical Frontal Polymerization: Self-Propagating Thermal Reaction Waves," *J. Chem. Soc. Faraday Trans.* 1996, **92**, 2824-2836.
15. J. A. Pojman, G. Curtis and V. M. Ilyashenko, "Frontal Polymerization in Solution," *J. Am. Chem. Soc.* 1996, **115**, 3783-3784.
16. E. D. Bain, K. Dawes, A. E. Özçam, X. Hu, C. C. Gorman, J. Šrogl, and J. Genzer, "Surface-Initiated Polymerization by Means of Novel, Stable, Non-Ester-Based Radical Initiator", *Macromolecules* 2012, **45**, 3802-3815.
17. J. C. M. Torfs, L. Deij, A. J. Dorrepaal and J. C. Heijins, "Determination of Arrhenius kinetic constants by differential scanning calorimetry", *Analytical Chemistry* 1984, **56**, 2863-2867.
18. V. F. Gromov, N. I. Galperina, T. I. Osmanov, P. M. Khomikovskii and A. D. Abkin, "Effect of Solvent on Chain Propagation and Termination Reaction Rates in Radical Polymerization", *European Polymer Journal* 1980, **16**, 529-535.
19. V. F. Kurenkov and L. I. Abramova, "Homogeneous Polymerization of Acrylamide in Solutions", *Polym.-Plast. Technol. Eng.* 1992, **31**, 659-704.
20. D. Hunkeler, "Mechanism and Kinetics of the Persulfate-Initiated Polymerization of Acrylamide", *Macromolecules* 1991, **24**, 2160-2171.

3. Controlling polydispersity in free radical polymerization systems

3.1 Introduction

One of the major challenges in polymer synthesis is the control of molecular weight distribution (MWD) of the produced polymers. The polydispersity index (PDI) is a statistical measure of the dispersion of a MWD, given by the ratio of the second to the first moment of the MWD. In the case of polymers, the first and second moments are given by the weight average (M_w) and number average (M_n) molecular weights, respectively. Conventional free radical polymerizations (FRPs) generate polymers with a broad distributions of molecular weights (MW). Theoretically, the lower limit on PDI for a FRP process is 1.5, imposed by the mode of chain termination. In principle, fairly monodisperse polymers can be obtained by free radical polymerization if the process proceeds via a “living” mechanism wherein all the growing chains are initiated at approximately the same time and termination of the propagating chains is heavily suppressed [1]. In the past, researchers have shown that polymerization in microreactors (e.g., porous substrates) produces polymers with narrower MW distributions (or low PDI values) relative to bulk reaction [2]. Onset of gelation during synthesis also narrows down the MWD of polymers due to decreased mobility of the growing chains thus minimizing the likelihood of termination. This is the first study that demonstrates that fairly monodisperse polymers can be produced via FRP without addition of any stable free radicals (e.g., nitroxides, as in nitroxide-mediated polymerization) or ligands (e.g., Cu-salts and metal organic ligands, as in atom transfer radical polymerization).

Properties of polymers synthesized in confined spaces depend primarily on: 1) the nature of the confining space (*i.e.*, geometry, dimension, deformability of walls, *etc.*) [2-4], 2) the type of polymerization reaction employed, and 3) the interactions among the growing chains in the confined space as well as chemical affinity towards the confining cavity (*i.e.*, polymer/wall interactions). Polymerizations carried out under confinement, in conjunction with altered kinetics and diffusion limitation produce polymers whose MW, PDI, topology, and/or composition differ significantly from polymers synthesized using identical methods and reaction conditions under no confinement (*e.g.*, bulk or solution). A recent Monte Carlo study [5] reported that the diffusivity (D) of self-avoiding polymers in various confinements (slit,

tube and cube with a characteristic spacing h) scales as $MW^{1/3}$ and h^2 . For FRPs, significant increases in MW and decreases in PDI are generally observed. For example, Aida and coworkers reported that relative to bulk polymerization M_n increased from ≈ 40 to ≈ 400 kDa for polymerization of methyl methacrylate (MMA) in the 2.7 nm diameter pores of zeolite MCM-41 and PDI decreased from 2.8 to 1.7, respectively. The zeolite did not serve any apparent catalytic role; it was only used to generate nano-confinement, in which the polymerization took place. Similar results were obtained for PMMA synthesized in confined pore glass having 4.4 ~ 5 nm pores sizes [2], and for various other vinyl-based polymers formed in nano-channels of porous coordination polymers (PCPs), mesoporous silica whose walls were decorated with immobilized radical initiators, or in microreactors. In addition to changes in MW and PDI, variations in tacticity have been observed for FRP of styrene, MMA, and vinyl acetate (VA) and a decrease in branching of PVA has also been noted. Because the spatial dimensions of the pores are comparable to the sizes of the polymer segments, distribution of heterogeneities in segmental motion exists, wherein less mobile segments reside close to the wall of the pore. Polymer/wall interactions affect not only the local segmental dynamics but also the overall chain locomotion inside the confining cavity, as reported by Zhao & Simon [2]. As the overall diffusion of polymer chains slows down, monomer diffusion drives the polymerization kinetics and auto-acceleration due to gel effect sets in at a relatively early stage of FRP in nanoscale confinement, which ultimately governs the polymerization kinetics. As a result of slow polymer motion inside confined space, the rate of chain termination decreases dramatically, which results in polymers with high MW and $PDI \approx 1.5$. In bulk polymerizations, as the viscosity increases, the gel effect comes into play causing auto acceleration by decreasing the rate of termination. In case of monomers, such as methyl methacrylate or acrylamide, the gel effect influences the overall polymerization kinetics. The decrease in chain termination is linked to diffusion-control phenomena. The termination reaction between two growing chains becomes more hindered as mobility in the system is gradually restricted due to conversion of monomer to polymer [6-13].

This chapter illustrates how thermal frontal polymerization reaction in vertically-confined reactors (height \sim hundreds of μm to a few mm) can create fairly monodisperse polymers free-radically. The combination of all three effects, *i.e.*, confinement, gelation, and front propagation in FRP leads to high MW polymers with relatively low molecular weight PDI (PDI \sim 1.2). This chapter elaborates on the effect of spatial confinement on convective instabilities and subsequently, the propagation dynamics and nature of polymerization products in horizontal fronts. In bulk or unconfined systems, the sharper temperature gradients and convection cause the reaction front to deform and move faster, resulting in rapid polymerization and non-uniform distribution of polymer chains. Under confinement, temperature gradients are suppressed and in the absence of convection, the polymerization front is well-defined. As a result, the initiation and propagation steps are slower and longer polymer chains with lower polydispersity are formed.

3.2 Molecular weight distribution of the polymer

In the previous chapter of this Ph.D. Dissertation, it was noted that reducing the reactor height slows down the front propagation and the overall polymerization process, thereby producing polymers with higher molecular weights. **Figure 3.1** shows the degree of polymerization distribution (analogous to molecular weight distribution) of the polymers corresponding to increasing distances away from the heat source, produced at different degrees of confinement. The bimodal nature of these distributions is the topic of discussion in a later section of this chapter. The MWD was further analyzed to calculate the PDI of the polymer products at 1 cm intervals away from the heated end corresponding to different reactor heights (*cf.* **Figure 3.2**). The overall PDI values of the specimens show a decrease in case of confined systems (>2 for bulk systems to a minimum of ≈ 1.2 for highly confined systems) as shown in **Figure 3.2**. Interestingly, the PDI values calculated for reactor heights less than 2 mm, are much lower than the theoretical limit of 1.5 imposed by the nature of chain termination in FRP systems.

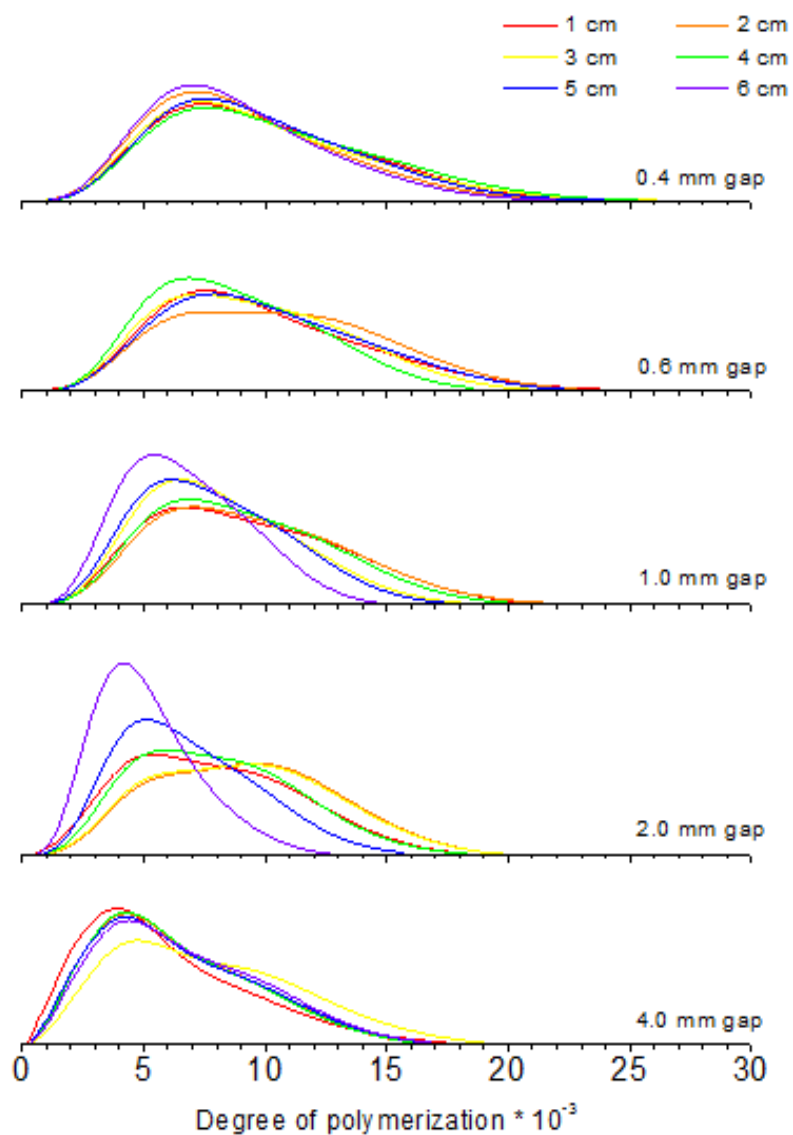


Figure 3.1. Degree of polymerization distribution (analogous to molecular weight distribution) for polymer samples taken after 60 mins of ignition at varying distances away from heat source (shown in different colors in the legend) corresponding to different reactor heights (or gaps).

As in the previous chapter on frontal polymerization (*i.e.*, Chapter 2 in this Ph.D. Thesis), the PDIs of the polymerization products were calculated using Gillespie's algorithm in order to corroborate experimental findings. The calculated PDI values for highly confined systems (1.75 for 0.4 mm vertical height) are significantly lower than those corresponding to bulk-like or unconfined systems (1.98 for 5 mm). However, the PDIs calculated using Gillespie's algorithm are greater than the corresponding experimental values for both the bulk-like (5 mm vertical height) and the highly confined system (0.4 mm vertical height). This can be attributed to the fact that Gillespie's algorithm does not account for the gel effect which can reduce chain termination significantly in acrylamide/DMSO systems and thus produce chains with high MW and relatively low PDI.

Figure 3.2 shows the dependence of PDI of the samples taken from different positions away from heat source, polymerized under different degrees of confinement. Polymerization products of higher M_n (as noted in Chapter 2) and lower PDI are produced under greater degree of vertical confinement. At larger distances from the heat source, the polymer produced is comparatively less polydisperse. This can be attributed to a slow front propagation velocity and the suppression of convection in vertically confined systems. In order to better understand frontal polymerization in confined geometries, the molecular weight distributions of the products from particular locations in 0.4 mm high reactor were monitored over 60 min in intervals of 10 min (*cf.* **Figure 3.3**). It is to be noted that such measurements involved individual reactions quenched at different time periods after ignition. The kinetic data reveal that at any given location (along each column, *cf.* **Figure 3.3**), the polymer MW increases with increasing time while the PDI decreases. This indicates accelerated chain initiation and suppressed chain termination, or in other words, the presence of gelation.

The key factor that set apart such a confined frontal polymerization system from a bulk polymerization is the absence of convection [15-22] and the localization of the reaction zone [14, 23, 24]. These factors in conjunction with the gel effect are believed to produce fairly uniform polymer chains. The following sections examine each of these factors and puts to test the validity of the hypothesis.

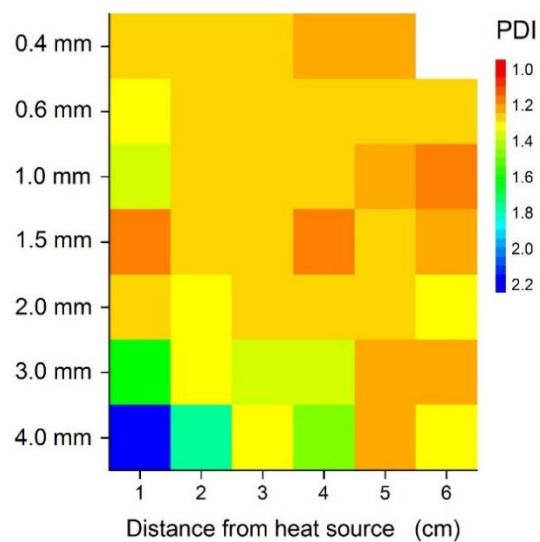


Figure 3.2. Variation of polydispersity index (PDI) of polymer samples with distance from heat source and reactor height (shown as y-axis) 60 mins after ignition.

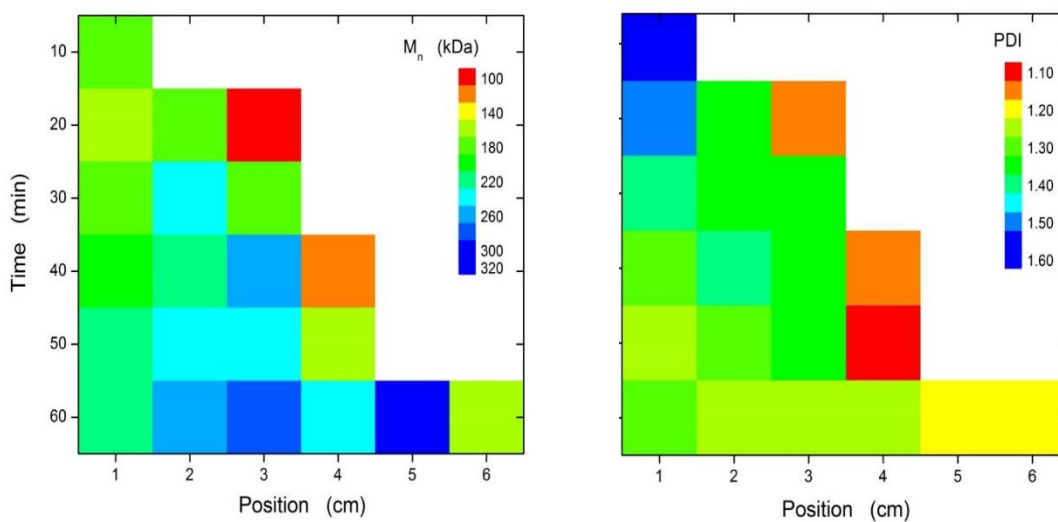


Figure 3.3 Kinetic data on M_n (left) and PDI (right) for samples located at different distances away from heat source corresponding to a highly confined reactor (0.4 mm height).

3.3 Understanding the front zones

In order to understand the front dynamics during polymerization [14], the different zones in the thermal frontal polymerization system need to be identified. Regions of varying optical density in the reaction chamber were observed (*cf.* **Figure 3.4**). Those include transparent and cloudy zones at increasing distances from the initiating heat source. Polyacrylamide (PAAm) is not very soluble in dimethyl sulfoxide (DMSO) and phase separates in presence of acrylamide, giving rise to cloudiness. To gain further insight into the chemical composition of the various reaction zones in the reactor, samples of the polymerization product were collected from equidistant intervals (1 cm) and the polymer was precipitated into methanol. The extracted samples were analyzed using gas chromatography equipped with mass spectrometer (GC-MS) to estimate the monomer-to-polymer conversion. **Figure 3.4** shows the three different zones in the reaction chamber with the respective monomer conversions (obtained from GC-MS analysis) and the corresponding Fourier transform infrared (FT-IR) spectra of DMSO (solvent), acrylamide (monomer), opaque and transparent polymerization product samples. The transparent region closest to the heat source has a monomer conversion of >99% whereas the cloudy regions have lower monomer conversion further away from the heat source. The presence of the vinyl peaks in the opaque sample confirms that polymerization takes place ahead of the distinct interface between transparent and cloudy zones. The sharp interface marks the end of the polymerization zone.

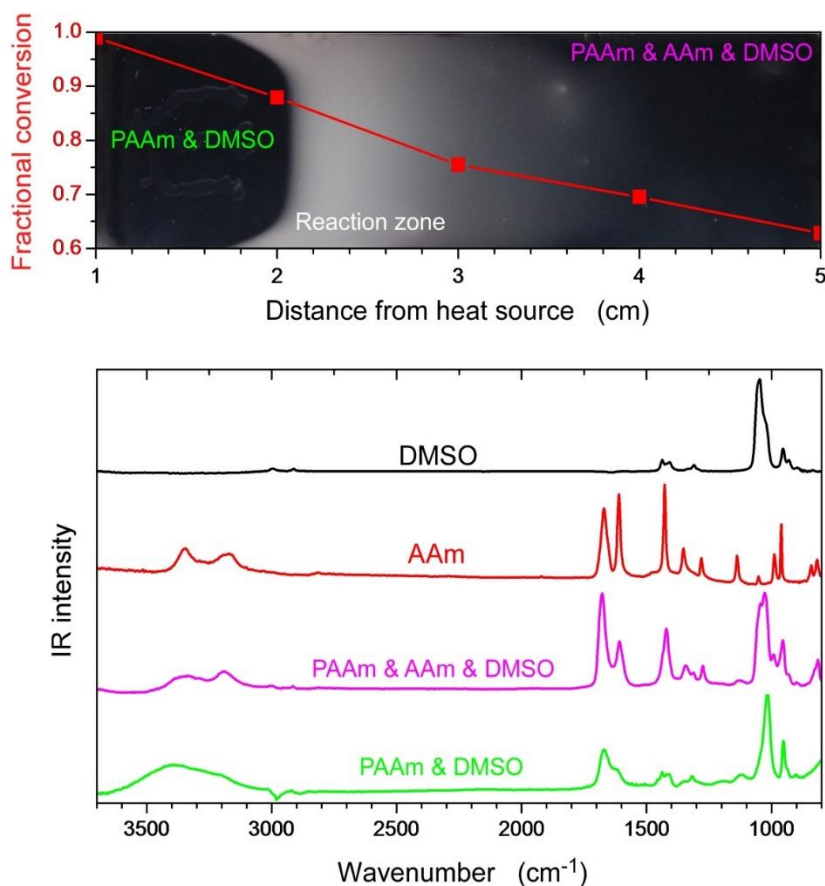


Figure 3.4. The different reaction zones in frontal polymerization (on a dark background) with the respective monomer conversions (top); IR spectra of DMSO, acrylamide (AAm) and the samples from the different zones.

3.4 The role of convection

Figure 3.5 shows the evolution of the reaction fronts corresponding to different degrees of confinement with time. For the greater vertical confinement (*i.e.*, 0.4 mm), the front is roughly flat without appearances of convective effects. In contrast, the front shape becomes parabolic and protrusions start to appear as the vertical dimension of the reaction chamber is increased beyond 1 mm. The moving reaction front tends to separate into layers due to convection beyond 1 mm reactor height. A close-up of a cross-section of the reaction front

where the lower layer lags behind the upper one is shown in the inset to **Figure 3.5**. This is a manifestation of convection currents set up due to temperature gradients in the system. **Figure 3.6** compares the temperature profiles and the corresponding initiator half-life times of two extreme cases of vertical confinement (*i.e.*, 0.4 and 2 mm). In case of 2 mm vertical confinement, the temperature gradients along the direction of front propagation are sharper and increases rapidly relative to 0.4 mm confinement. The higher temperature gradients in the former case give rise to convection currents in the system; hotter material (closer to the heat source) expands and rises up and forward to replace colder material ahead of the front. A schematic representation of the convection-induced separation of the moving front into layers is shown (*cf.* **Figure 3.6**). The bottom of the front lags behind while the top layer moves forward. The non-uniformity of the temperature profile leads to convection-induced separation of top and bottom layers. In contrast, convection is heavily suppressed in a highly confined system (*i.e.*, 0.4 mm). It is noted that the temperature corresponding to the sharp interface (*i.e.*, between the transparent and the cloudy zones) is roughly constant at $\approx 65^{\circ}\text{C}$ in case of the highly confined system (0.4 mm). The higher half-lifetimes of the initiators in highly confined systems indicate longer and slower chain propagation under approximately isothermal conditions. On the other hand, for the system with a vertical height of 2 mm, the interface temperature is initially higher ($\approx 80^{\circ}\text{C}$) and decreases slowly to $\approx 65^{\circ}\text{C}$ as time progresses. Therefore, in less confined systems, chain propagation is much faster and not uniform over the reactor volume. Convection is predominant in the initial stages of front propagation when the front temperature is also higher.

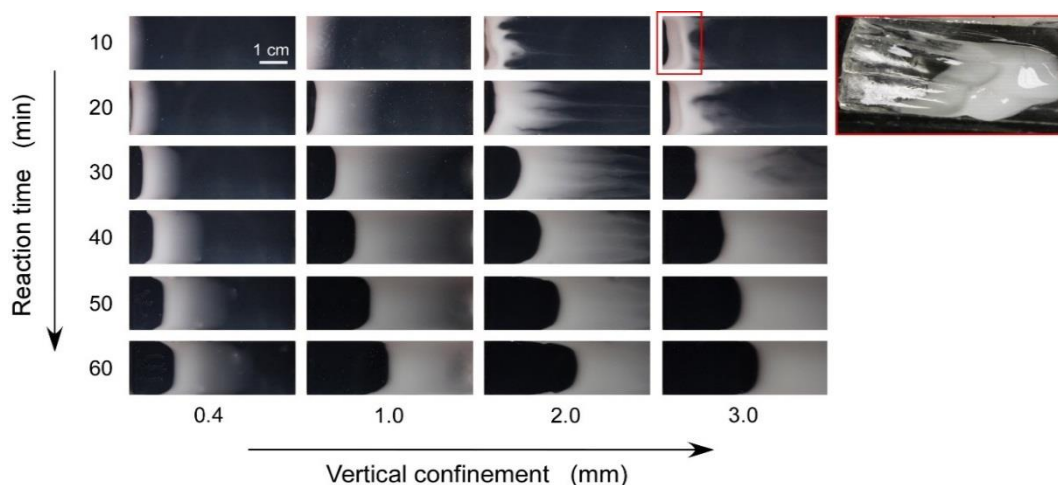


Figure 3.5. Time evolution of the fronts corresponding to different degrees of vertical confinement. The inset shows the cross-section of the front manifesting convection, note the distinct layering.

As the temperature gradients are higher in thicker systems, the generated free radicals, having a shorter average half-life time, are activated and polymerization progresses rapidly thus generating more heat of reaction which further increases the temperature gradients. Convection assists in faster front propagation; it increases heat transfer so the front propagation velocity is increased. In highly confined systems or at distances away from the heat source, the lower temperature gradients lead to more controlled initiation and chain growth steps, *i.e.*, fewer number of initiators with longer half-lives are activated and the chains grow slowly. The uniformity of the temperature at the sharp interface at all times indicates that chain propagation occurs at roughly the same temperature in case of highly confined systems. As a result, the polymer product possesses lower PDI as compared to less confined systems where polymerization is faster.

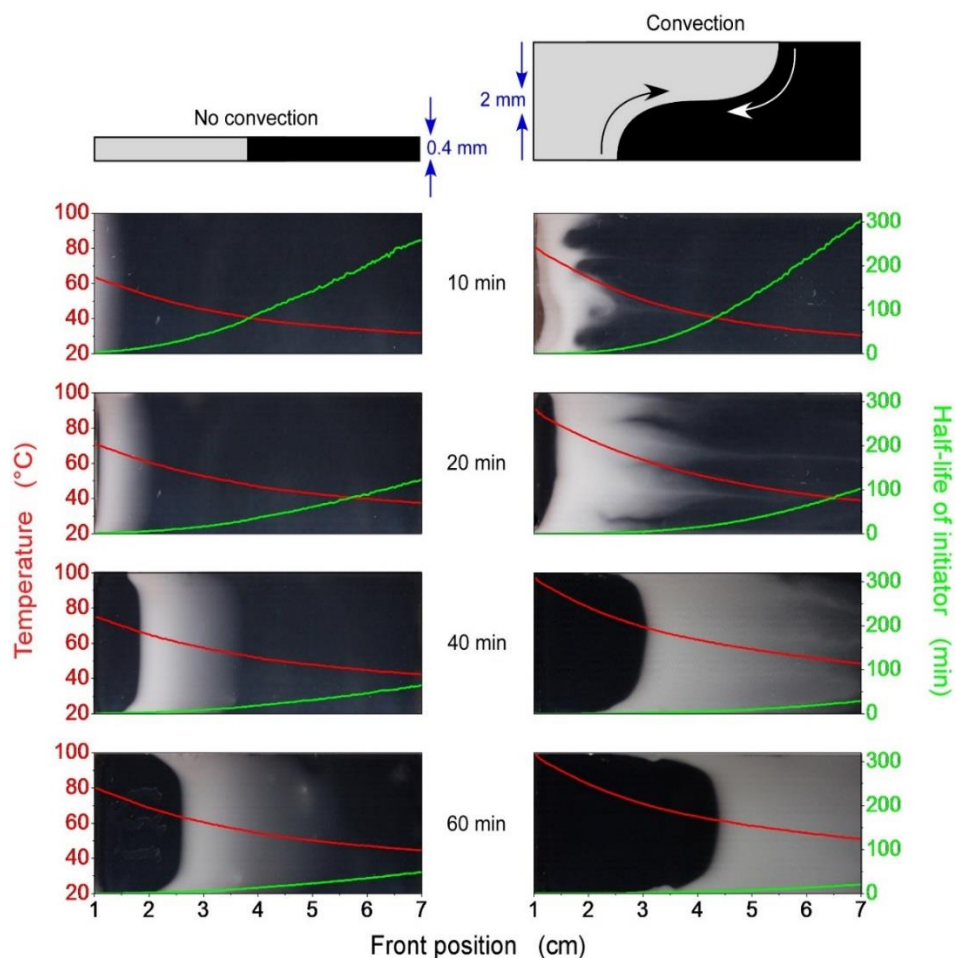


Figure 3.6. Comparison of the temperature (left ordinate, red lines) and the initiator half-life (right ordinate, green lines) profiles corresponding to 0.4 mm (heavily suppressed convection) and 2 mm (with convection) vertical confinement for various reaction times ranging from 10 to 60 mins.

To validate the hypothesis that confinement suppresses convection in frontal polymerization systems, the time evolutions of the front profiles in 0.4 mm thick reaction chambers placed horizontal and inclined at 10° to the horizontal were compared. **Figure 3.7** shows the front profiles under these geometrical constrains corresponding to different time periods after ignition. If convection was predominant, the front of the inclined system would have propagated ahead of the horizontal front at the same time after ignition. There is no

significant difference in front profile nature or time evolution caused by changing system inclination. Further, the presence of convection currents in reactors was tested with suspended particles (*cf.* **Figure 3.8**). The particles do not demonstrate any visible displacement in a highly confined reactor (*i.e.*, 0.4 mm, on the right) while they move around in less confined geometries (*i.e.*, 2 mm, on the left). In the light of these evidences, it is concluded that convection is heavily suppressed under vertical confinement on the order of 0.1 mm.

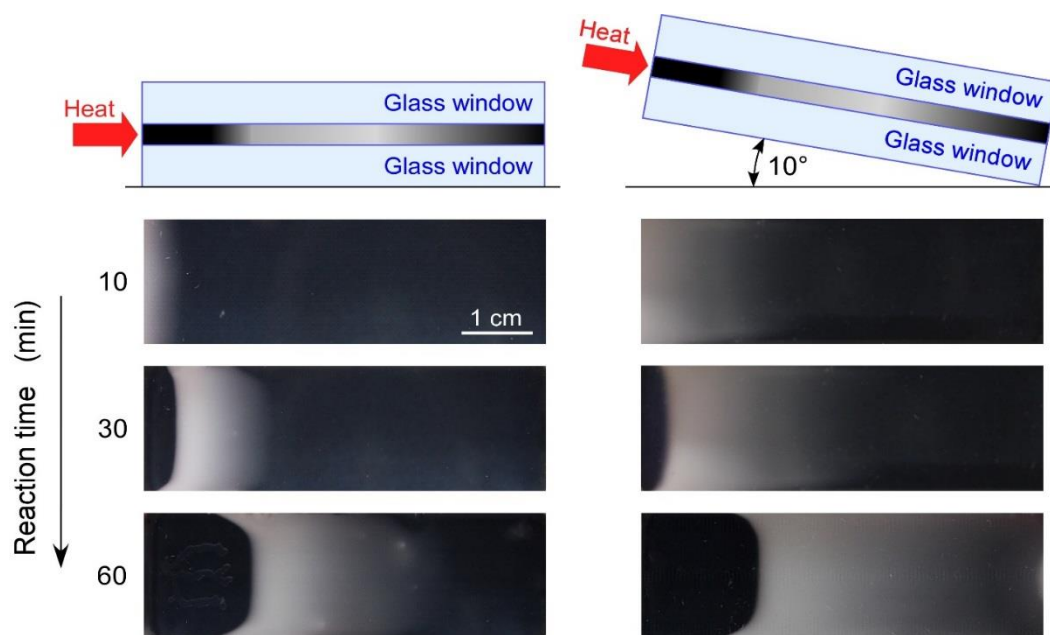


Figure 3.7. Comparison of front profiles of a 0.4 mm thick horizontal setup and one that is inclined horizontally at 10 degrees (top views).

3.5 The role of ‘gelation’ – choice of solvent

As described in a previous section, gelation can lead to a reduced rate of termination and therefore, longer yet more uniform polymer chains. DMSO is not a good solvent for PAAm. With increasing conversion, the polymer can gel in the solvent by physical

crosslinking (or entanglements). Chemical crosslinking is not possible due to the inherent lack of bifunctionality in the chemical structure of acrylamide monomer. Imidization of acrylamide can lead to a crosslinked product; however, this occurs in trace amounts ($< 6\%$) and does not take place in presence of inert fillers such as barium carbonate or polyacrylamide [Ref. Pojman chapter]. Samples of the formed polymer are subject to modulus measurement at a constant strain of 1%, in air and soaked in DMSO. These polymer samples were collected from a 0.4 mm high reactor at the end of 60 mins and had residual DMSO trapped in them. The storage and loss moduli changes proportionately with frequency, indicating that the polymer is indeed forming a physical gel in presence of trapped DMSO (*cf.* **Figure 3.9**). The relatively low values value of the moduli over low values of angular frequency suggests that the gel is a weak one. The overall lower values of moduli measured for samples measured in DMSO implies that the excess solvent can swell the gel and weaken it.

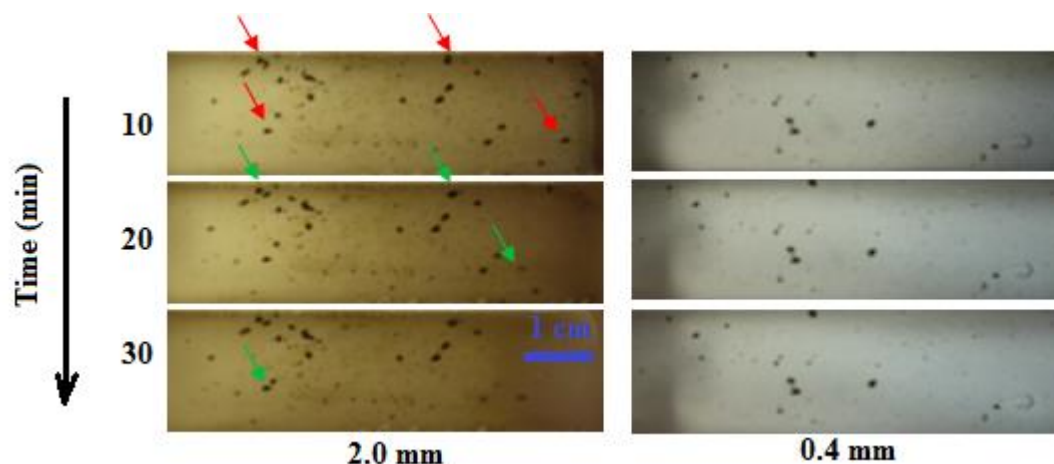


Figure 3.8. Motion of suspended particles (shown in black) inside the reaction chamber of height 2 mm (left) and 0.4 mm (right), demonstrating the presence of convection. The red and green arrows mark the initial and the final positions of the particles respectively (from top to bottom).

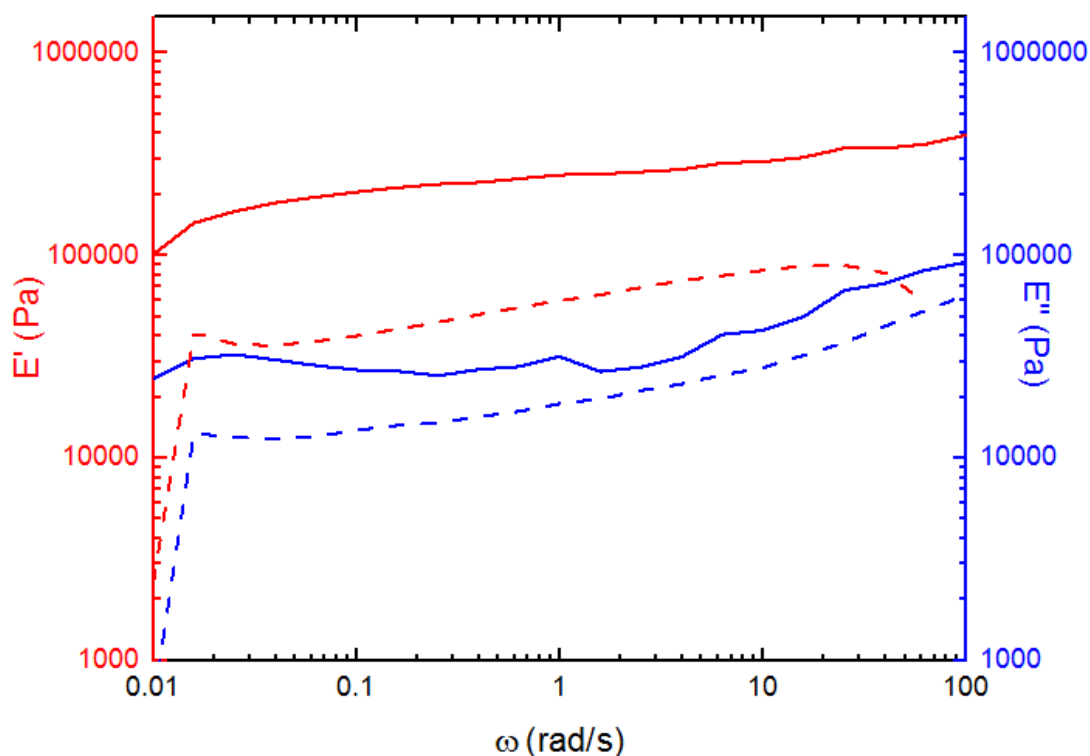


Figure 3.9. Storage (E') and loss (E'') moduli as a function of angular frequency, measured at constant strain of 0.01, for 0.4 mm thick polyacrylamide film in air (solid) and soaked in DMSO (dashed).

Having established that the gelation occurs during synthesis, the next step is to validate the hypothesis that gel formation is one of the key factors leading to low PDI values. Confined frontal polymerization experiments, as described in Chapter 2, are performed with varying acrylamide to DMSO ratios in reaction chambers of height 0.4 and 2 mm. Samples of the polymer produced are analyzed with GPC-SEC and PDI values were calculated from their MW distributions. It is observed that in presence of excess solvent, the PDI values are relatively high irrespective of the reactor height (*cf.* **Figure 3.10**), which indicates that termination is not suppressed significantly in presence of excess solvent. At relatively higher degree of dilution ($\sim < 0.2$ g/ml of acrylamide), the front did not propagate. The system cannot gel and fails to auto-accelerate because of heat dissipation. On the other hand, in presence of gelation, the

most of the exothermic heat generated goes into initiating more radicals, leading to a self-sustaining reaction front. Hence, by suitable choice of monomer/solvent systems, the gel effect can be utilized to lower chain termination rates leading to better control on polymer MW distribution.

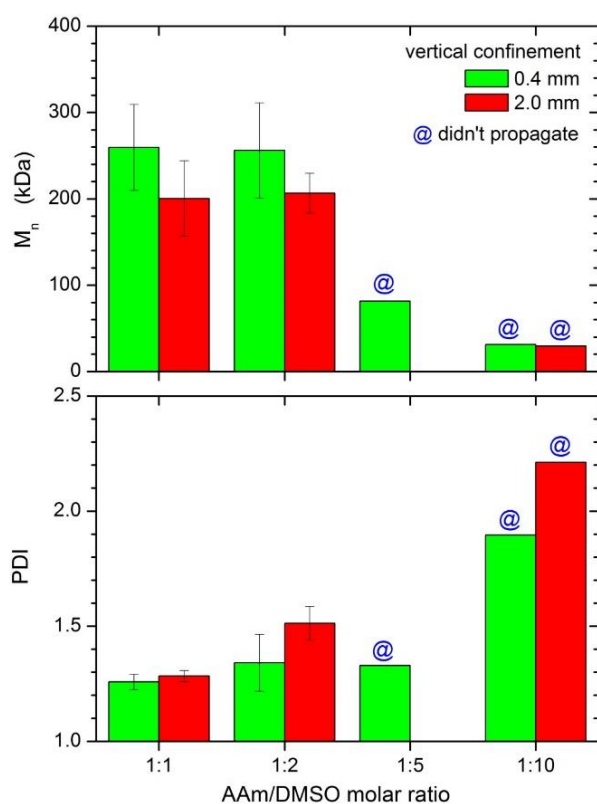


Figure 3.10. Effect of dilution on M_n and PDI for different reactor heights. For very dilute systems, the front did not propagate.

3.6 Directional heat supply

One important aspect that sets apart a frontal polymerization system from bulk polymerization is the directional nature of heat supply. To decouple the effect of directional

heat supply from gelation and vertical confinement, polymerization was carried out at the same reactor height, under two different isothermal conditions (≈ 65 and 100 °C), at same degree of dilution. These temperatures, 65° and 100 °C, correspond to those noted at the sharp back interface and the maximum value of temperature noted at any time in a frontal polymerization set-up, respectively. The polymerization products obtained under isothermal conditions were analyzed using GPC-SEC and the corresponding PDI values were calculated. It is not fair to compare the frontally grown samples for dilute systems (1:5 and 1:10, *cf.* **Figure 3.11**) with their isothermally grown counterparts. For high dilutions, the reaction front did not propagate (*cf.* **Figure 3.10**), which means that the reaction did not proceed until the same extent of conversion. However, at lower dilutions (1:1 and 1:2), the samples from confined frontal polymerization have lower PDI values than those from isothermal confined polymerization (*cf.* **Figure 3.11**) irrespective of the reactor height (0.4 and 2 mm). Further, isothermal polymerization was carried out with metal walls instead glass windows (*cf.* **Figure 3.12**). The MW and PDIs were fairly unaffected by the nature of the reactor walls (*cf.* **Figure 3.12**). Frontal mode of polymerization confines reaction to a localized zone and thereby, imparts a better temperature and diffusion control within the reactor. The lower values of PDIs for frontally-grown polymers as compared to their isothermal counterparts, corresponding to the same reactor height, further supports the hypothesis that the mode of heat supply is a key factor in achieving a better control on MW distribution.

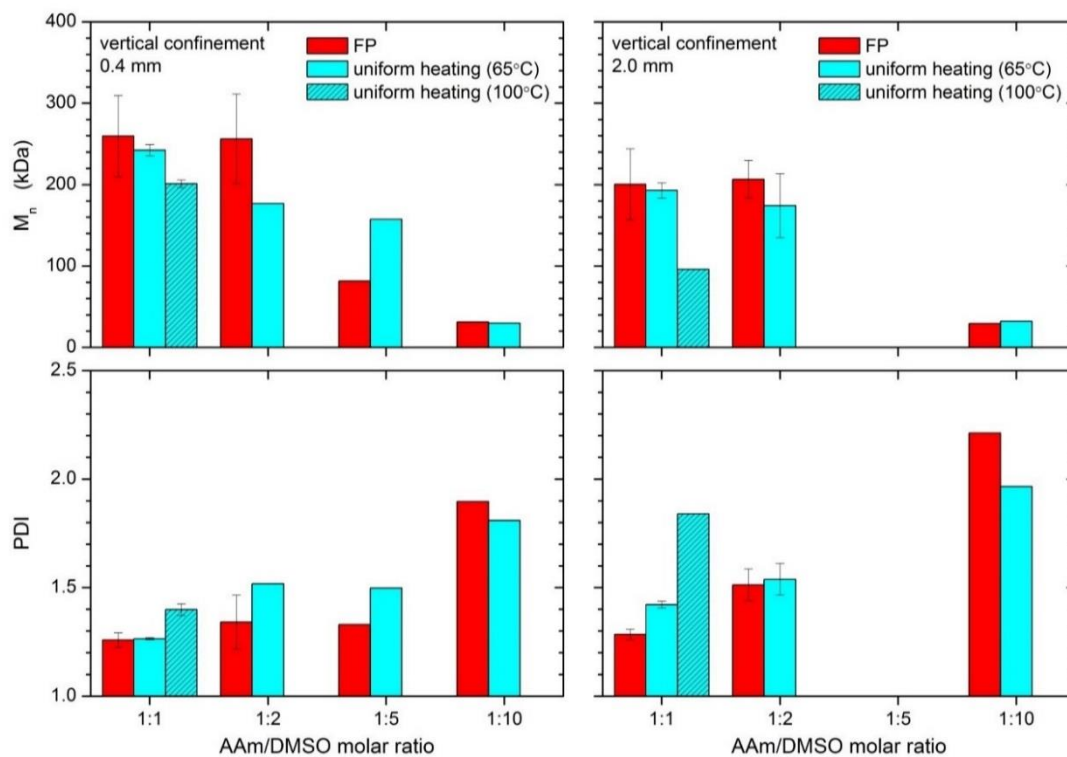


Figure 3.11. Comparison of M_n and PDI of polymers grown via frontal polymerization and uniform heating at different degrees of dilution. Note that for dilute systems (1:5 and 1:10), the front did not propagate (*cf.* **Figure 3.9**).

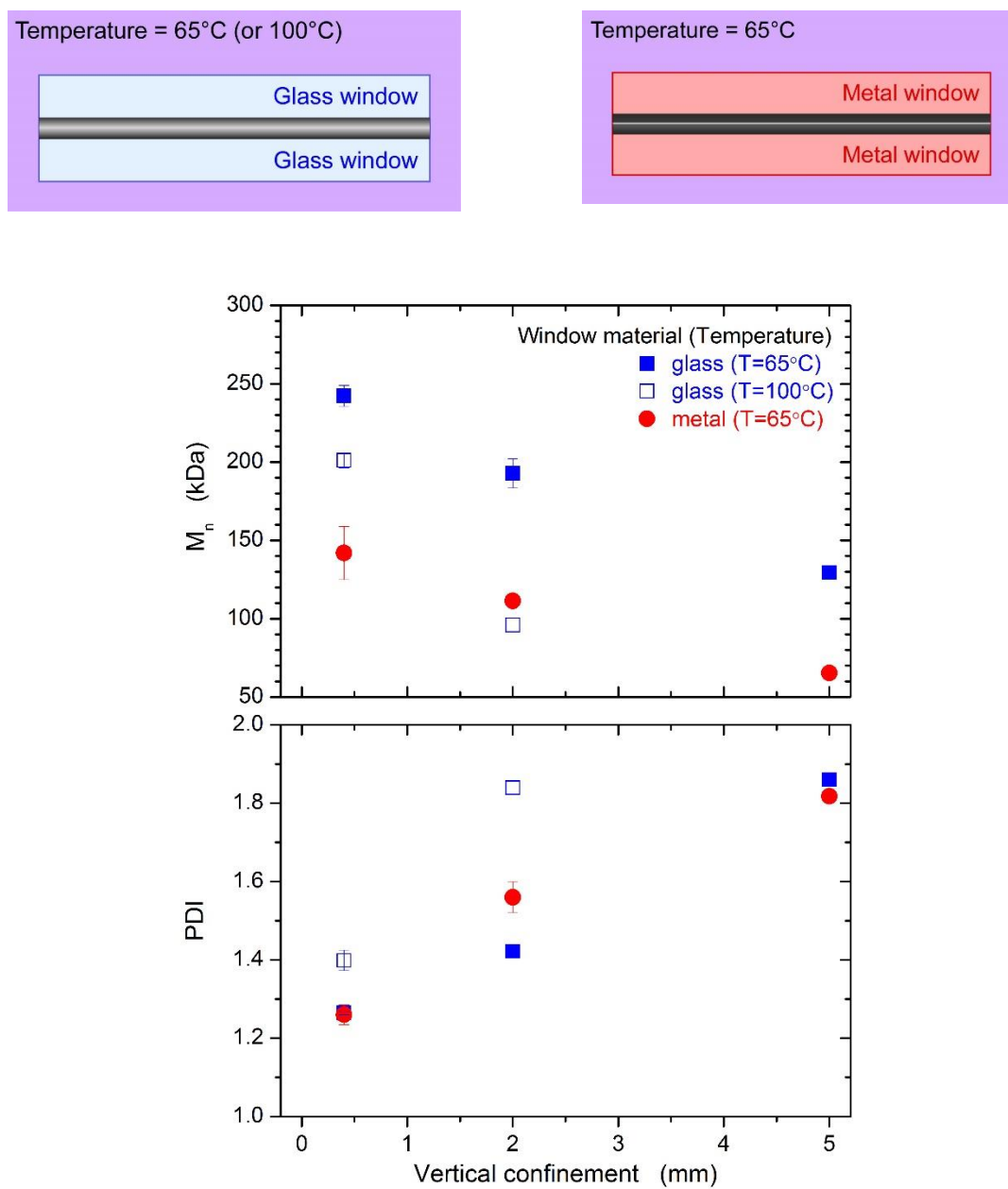


Figure 3.12. Comparison of M_n and PDI of polymers grown via uniform heating with glass and metal windows (bottom) and schematic diagram of the reactor with different windows (top).

3.7 Bimodal nature of the molecular weight distribution

The MW of a polymer sample from frontal polymerization set-up depends on the height of the reactor and its position relative to the heat source. However, the MW distribution of a given polymer sample is not unimodal. It was possible to fit two distinct Schulz-Zimm distributions to a given MW distribution. The relative contributions and parameters of individual peaks are determined by minimizing the sum of least square deviations (*cf.* **Figure 3.13**). Extensive data fitting using this approach reveals that the ratio of the M_n corresponding to the fitted peaks bear a fairly constant value of $\sim 1.5 - 2.0$, irrespective of the reactor height or the distance from heat source (*cf.* **Figure 3.14**). This is the manifestation of two different modes of polymerization occurring simultaneously. Literature on acrylamide bulk polymerization using persulfate initiators in different solvents reveals that this is indeed true. The two modes of initiation of persulfate radicals are: a) thermal decomposition and b) monomer-enhanced decomposition [25]. Depending on the mode of initiation, the exponent dependence of the rate of chain propagation on monomer concentration can vary from 1 (thermal) to 1.5 (monomer-enhanced). This implies that the relative contribution of the two polymerization modes vary with monomer concentration (or conversion). At high monomer concentration, the monomer-enhanced mode should dominate over the thermal one. To establish that the bimodal nature of the frontally grown polymer distributions arises from monomer-enhanced decomposition, differential scanning calorimetry (DSC) experiments were carried out on samples with varying ratios of monomer to initiator in DMSO. The heat flow change was measured as the sample undergoes polymerization, as exhibited by an exothermic peak in DSC heat vs. temperature curve (*cf.* **Figure 3.15**). It is to be noted that the constants obtained from DSC of such systems are not the conventional initiator decomposition constant, but the overall rate of polymerization as a function of temperature. For samples with higher monomer to initiator ratio (1500:1), the calculated rate is higher than those with lower ratio of monomer to initiator (75:1), at a given temperature. This suggests that the polymer chains resulting from monomer-enhanced initiation are on an average longer than those initiated thermally. Correlating the DSC results to the fitted MW distributions, it can be concluded that

the higher degree of polymerization peak (peak 2 – blue) corresponds to the monomer-enhanced mode and the lower peak (peak 1 – red) arises from thermally activated initiators (*cf.* **Figure 3.14**). Irrespective of the distance from heat source or the reactor height, the lower M_n fraction (peak 1) dominates. Since the frontal propagation is driven by heat, it is not surprising that the thermally initiated mode of polymerization contributing to low MW polymers is dominating. Heat transport in highly confined reactors is driven by conduction and diffusion, so the temperature decreases at larger distances from the heat source (*cf.* **Figure 3.6**). This means a smaller number of thermally initiated radicals are generated and the polymer chains can achieve greater degree of polymerization at distances away from the heat source (*cf.* **Figure 3.14**).

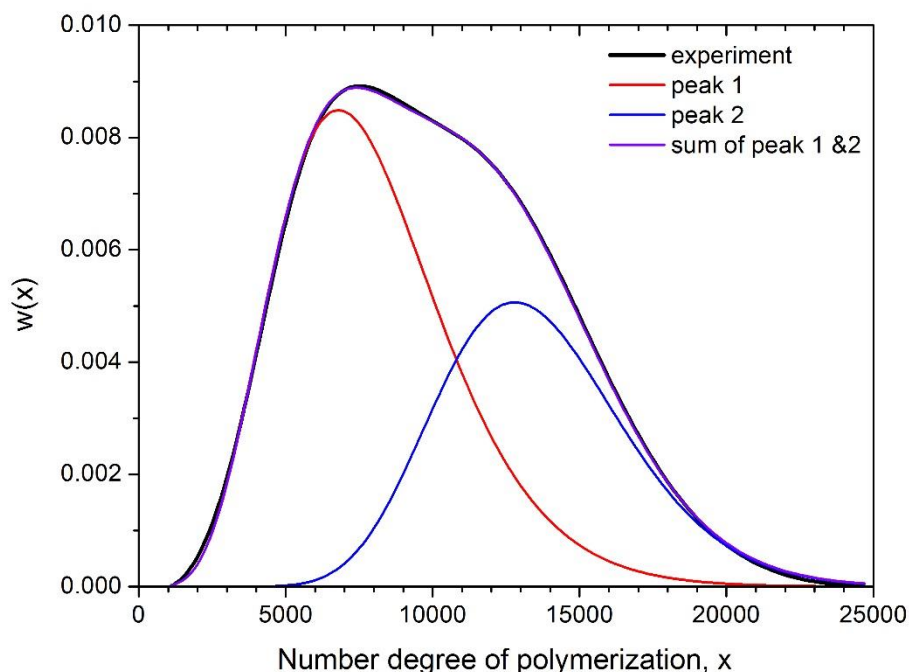


Figure 3.13. A typical example of peak resolution of degree of polymerization distribution of a polymer sample.

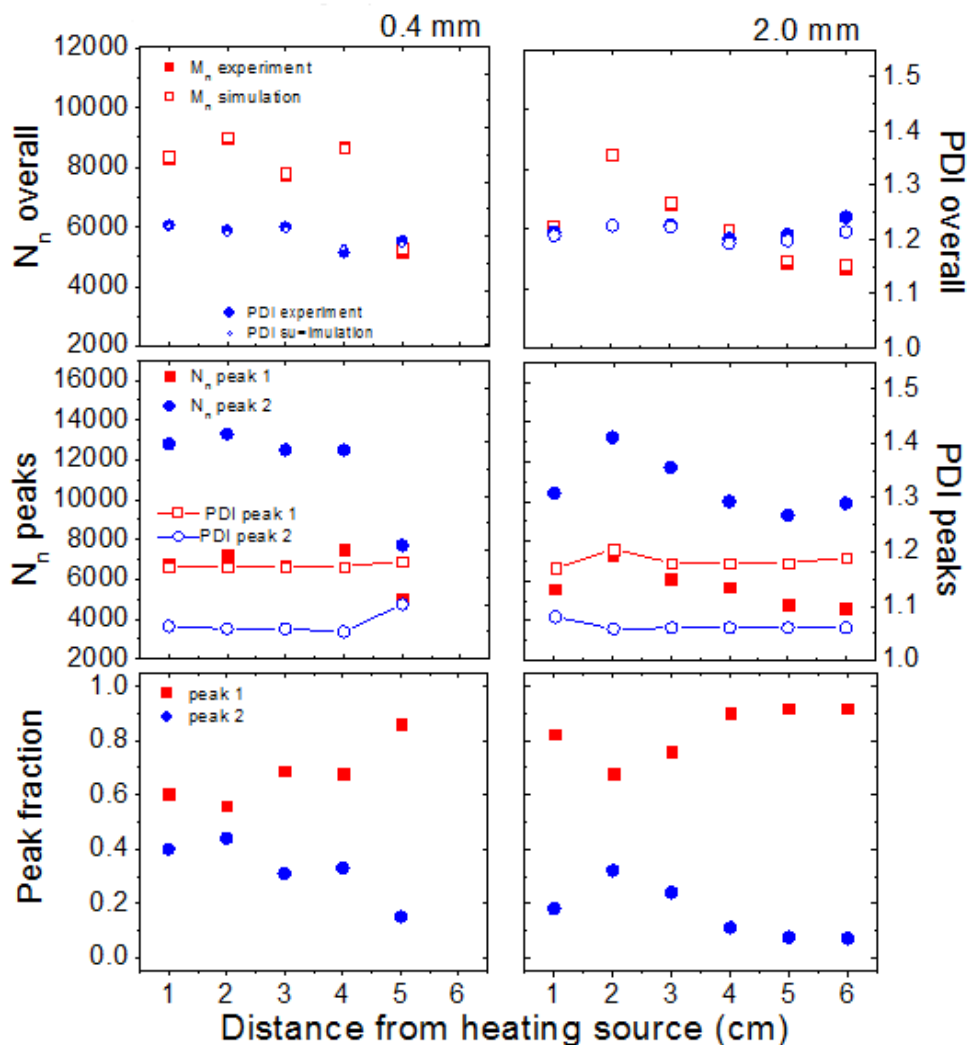


Figure 3.14. Detailed analysis of molecular weight distribution using peak fitting for polymer samples at different distances from heat source corresponding to different reactor heights (along each column). The top row compares the experimental and fitted PDI values. Peak 1 (red) and 2 (blue) correspond to the two weighted Schulz-Zimm peaks fitted to the bimodal distribution. The middle row shows the PDIs and number average degree of polymerization (analogous to M_n) for the fitted peaks. The bottom row shows the weights of the two peaks used to fit the experimental data.

It is to be noted that the PDI corresponding to each fitted peak is quite low as in the overall MW distribution. This proves that the PDIs lower than the theoretical limit of 1.5 are not the outcome of an erroneous statistical calculation. The narrow polydispersity range of each polymer population can be attributed to a combination of favorable factors: vertical confinement of the reactor, solvent-induced gelation and directional heat supply.

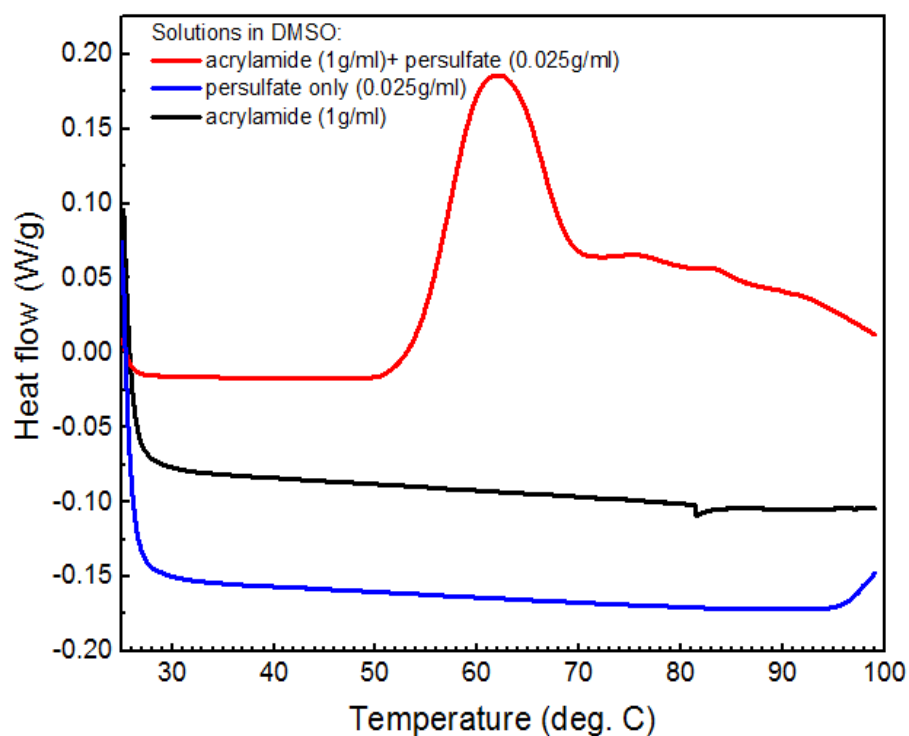


Figure 3.15. DSC curve showing exothermic peak for mixture of acrylamide and potassium persulfate in DMSO.

3.8 Discussion

The experimental observations are summarized as follows. Thermal frontal polymerization is sustained by a positive feedback of thermal energy, *i.e.*, heat supplied decomposes initiators and generates free radicals. Monomer units add to these free radicals releasing thermal energy in the chain propagation step. The local temperature rises due to the net gain in thermal energy, decomposes more initiators and thereby increases the overall rate of reaction front propagation. The vertical height of the reaction chamber was varied, keeping all the other parameters constant. In bulk or unconfined systems, convection improves thermal transport, speeds up, and deforms the front. In contrast, in highly confined systems, convection is heavily suppressed; the predominant mode of heat transfer is diffusion. The positive feedback of thermal energy drastically increases the rate of propagation reaction in bulk systems. Thus, radical generation, propagation, and chain termination take place simultaneously in bulk systems. Convection further enhances the rate of polymerization by improving thermal transport and chain mobility. The higher overall rate of polymerization in bulk systems, therefore, leads to shorter polymer chains with high PDI. In contrast, in highly confined systems the overall heat generation rates are much smaller. Thus, a smaller number of radicals are generated, resulting in a smaller number of chains with a higher MW. As the monomer conversion increases, the reaction mixture starts to gel in presence of increasing amounts of the partially soluble polymer. On the onset of gelation, polymer chain mobility is greatly reduced while monomer mobility is not much affected. As a result, the rate of chain termination decreases and monomers keep adding to growing polymer chains, further decreasing their mobility. This positive-feedback effect leads to longer MW polymers with narrow distributions even in a classical free radical polymerization. The directional mode of heat supply further localizes the reaction zone and thereby maintains a fairly constant reaction zone temperature ($\approx 65 - 70^\circ\text{C}$). These favorable environmental factors, *i.e.*, the absence of convection, gelation and localization of reaction zone, act in conjunction and lead to narrow polymer MW distributions.

In conclusion, this chapter reported on controlling polydispersity in free radical polymerization reactions by inducing gelation, tuning the degree of vertical confinement and supplying heat in a directional manner via frontal polymerization. By reducing the height of the reactor, we can suppress convective instabilities and achieve a better control on the frontal polymerization process. Under confinement, the front propagation and the overall polymerization process are slowed down, thereby producing longer and more uniform polymer chains relative to bulk polymerization under identical reaction conditions. The results also suggest that the possibility of monitoring simultaneous reactions that are otherwise impossible to decouple, using frontal polymerization set-up.

4.9 References

1. Daniel Colombani, "Chain-growth control in free radical polymerization", *Progress in Polymer Science*, 1997, **22**, 1649-1720.
2. H. Y. Zhao, Z. N. Yu, F. Begum, R. C. Hedden, S. L. Simon, "The Effect of Nanoconfinement on Methyl Methacrylate Polymerization: T-g, Molecular Weight, and Tacticity", *Polymer*, 2014, **55** (19), 4959-4965.
3. F. Begum, H. Y. Zhao, and S. L. Simon, "Modeling Methyl Methacrylate Free Radical Polymerization: Reaction in Hydrophobic Nanopores", *Polymer*, 2012, **53**(15), 3261 – 3268.
4. F. Begum, H. Y. Zhao, and S. L. Simon, "Modeling Methyl Methacrylate Free Radical Polymerization: Reaction in Hydrophilic Nanopores", *Polymer*, 2012, **53**(15), 3238 – 3244.
5. F. Begum and S. L. Simon, "Modeling Methyl Methacrylate Free Radical Polymerization in Nanoporous Confinement", *Polymer*, 2011, **52**, 1539 – 1545.
6. G. A. O'Neil & J. M. Torkelson, "Modeling Insight into the Diffusion-Limited Cause of the Gel Effect in Free Radical Polymerization", *Macromolecules*, 1999, **32**, 411.
7. G. A. O'Neil, M. B. Wisnudel & J. M. Torkelson, "An Evaluation of Free Volume Approaches to Describe the Gel Effect in Free Radical Polymerization", *Macromolecules*, 1998, **31**, 4537.

8. G. A. O'Neil, M. B. Wisnudel & J. M. Torkelson, "A Critical Experimental Examination of the Gel Effect in Free Radical Polymerization: Do Entanglements Cause Autoacceleration", *Macromolecules*, 1996, **29**, 7477.
9. M. B. Wisnudel & J. M. Torkelson, "Diffusion-Limited Photophysical Interactions as in Situ Probes of Conversion in Free Radical Polymerization: Quantitative Analysis with Predictive Free-Volume Theory", *Macromolecules*, 1994, **27**, 7217.
10. R. G. W. Norrish & R. R. Smith, "Catalyzed Polymerization of Methyl Methacrylate in Liquid Phase", *Nature*, 1942, **150**, 336.
11. J. N. Cardenas & K. F. Driscoll, "High Conversion Polymerization. I. Theory & Application to Methyl Methacrylate", *J. Polymer Sc.: Poly. Chem Ed.*, 1976, **14**, 883.
12. S. W. Benson & A. M. North, "The Kinetics of Free Radical Polymerization under Conditions of Diffusion-controlled Termination", *JACS*, 1962, **84**(6), 935.
13. T. J. Tulig & M. Tirrell, "Toward a Molecular Theory of the Trommsdorff Effect", *Macromolecules*, 1981, **14**, 1501.
14. J.A. Pojman, "Frontal Polymerization", *Encyclopedia of Polymer Science: A comprehensive reference*, 2012, **4**, 957-979.
15. J. A Pojman, J. Willis, D. Fortenberry, V. Ilyashenko and A. Khan, "Factors Affecting Propagating Fronts of Addition Polymerization: Velocity, Front Curvature, Temperature Profile, Conversion and Molecular Weight Distribution," *J. Polym. Sci. Part A: Polym Chem*. 1995, **33**, 643-652.
16. J. A. Pojman, J. Masere, E. Petretto, M. Rustici, S. D. Huh, M. S. Kim, and V. Volpert, "The Effect of Reactor Geometry on Frontal Polymerization Spin Modes", *Chaos* 2002, **12**, 56-65.
17. M. Bazile Jr., H. A. Nichols, J. A. Pojman, and V. Volpert, "The Effect of Orientation on Thermoset Frontal Polymerization", *J. Polym. Sci. Part A: Polym Chem*. 2002, **40**, 3504-3508.
18. V. A. Volpert, V. A. Volpert and J. A. Pojman, "Effect of Thermal Expansion on Stability of Reaction Front Propagation", *Chem. Eng. Sci.* 1994, **14**, 2385-2388.
19. V. A. Volpert, V. A. Volpert, J. A. Pojman and S. E. Solovyov, "Hydrodynamic Stability of a Polymerization Front", *Eur. J. Appl. Math.* 1996, **7**, 303-320.

20. J. A. Pojman, R. Craven, A. Khan and W. West, "Convective Instabilities Induced by Traveling Fronts of Addition Polymerization", *J. Phys. Chem.*, 1992, **96**, 7466-7472.
21. B. McCaughey, J. A. Pojman, C. Simmons and V. A. Volpert, "The Effect of Convection on a Propagating Front with a Liquid Product: Comparison of Theory and Experiments," *Chaos* 1998, **8**, 520-529.
22. G. Bowden, M. Garbey, V. M. Ilyashenko, J. A. Pojman, S. Solovyov, A. Taik and V. Volpert, "The Effect of Convection on a Propagating Front with a Solid Product: Comparison of Theory and Experiments", *J. Phys. Chem. B* 1997, **101**, 678-686.
23. J. A. Pojman, V. M. Ilyashenko and A. M. Khan, "Free-Radical Frontal Polymerization: Self-Propagating Thermal Reaction Waves," *J. Chem. Soc. Faraday Trans.* 1996, **92**, 2824-2836.
24. J. A. Pojman, G. Curtis and V. M. Ilyashenko, "Frontal Polymerization in Solution," *J. Am. Chem. Soc.* 1996, **115**, 3783-3784.
25. D. Hunkeler, "Mechanism and Kinetics of the Persulfate-Initiated Polymerization of Acrylamide", *Macromolecules*, 1991, **24**, 2160-2171.

4. Computer Simulation of Template Polymerization using a Controlled Reaction Scheme[†]

[†]Based on P. Datta and J. Genzer, *Macromolecules*, 2013, **46**, 2474-2484.

4.1 Introduction

The increasingly demanding industrial applications and the emerging uses of synthetic polymers require synthesis of specialty macromolecules. Synthetic homopolymers often lack perfect molecular-level definition; *i.e.*, they possess non-uniform molecular weight distribution or distribution in tacticities. In addition, synthetic copolymers often exhibit chemical non-uniformity and randomness in the sequence of different types of units along the chains. This lack of definition arises from a number of causes, the most important ones being the statistical nature of the polymerization process and the absence of specificity in chain propagation. In many biological reactions, such as DNA replication or polypeptide synthesis, low molecular weight substrates and polymeric products are present in the reaction medium together with the macromolecular compounds, called matrices or templates, which control the synthetic process. The discovery of DNA replication, an elaborate template synthesis, has inspired the development of template polymerization [1, 2]. Polymer chemists have studied the effects of templates on various types of polymerization methods, including, chain- and step-growth during homo- or copolymerization. The most notable examples are the use of DNA-templated synthesis (DTS) and nucleic acid template synthesis to either elongate DNA and oligonucleotide strands or polymerize daughter monomers from a predefined DNA sequence [3]. While DTS is an attractive platform for the production of monodisperse polymers with well-defined chemical sequences, it has so far been limited primarily to biopolymers.

Template polymerization is a process, which utilizes specific interactions between a preformed macromolecule (*i.e.*, template) and a growing chain [1-5]. It is characterized by geometrically predetermined paths of chain propagation. Template polymerization comprises three steps: 1) template-monomer complexation to form a linear array of monomers, 2) polymerization of bound monomers, and 3) separation of the daughter macromolecule from the mother template. The monomer units can bind to the template via various physical interactions, such as, hydrogen bonding, dipole-dipole or electrostatic forces, or by chemical bonding, such as disulfide bridging. In order to study template systems, one needs to compare the template process and products of the reaction with conventional bulk polymerization

carried out under identical conditions, typically replacing the template by a low molecular non-polymerizable entity. The effects of the template on the polymerization process and the product are usually called “template effect” or “chain effect” [1]. The template effects can be classified as [1, 2, 4-6]: 1) the kinetic effect (*i.e.*, increased the reaction rate, change in kinetic equation), 2) the molecular effect (*i.e.*, influence on the molecular weight and molecular weight distribution; ideally, the degree of polymerization of the daughter polymer is the same as the degree of polymerization of the template used, so-called replication), 3) the effect on tacticity (*i.e.*, the daughter polymer can have a structure complementary to the structure of the template used), and 4) the effect on the sequence distribution of units (in case of template copolymerization). In this work, we explore the effect of templation on the average molecular weight, composition and sequence distribution of the daughter polymers.

Advances in template polymerization can lead to better control of polymer properties. A few examples of influencing polymer properties, namely tacticity and chain organization, through templation have been reported in literature [7-9]. Other potential applications include synthesis of ladder-like polymers, or surface-based template polymerizations for the production of intertwined structures, free-standing two-dimensional polymers and molecular sensors [9-12]. In order to potentially harness Nature’s templation strategies to produce polymers with controlled lengths, tacticities, and sequences, we need to understand the factors that can affect template polymerization of simpler moieties. Experimental studies are often tedious and expensive because of the difficulties in separating the daughter polymer from the template. To this end, the vast parameter space can be explored easily and effectively with computer simulations.

In this work, we employ a Monte Carlo simulation scheme based on the bond fluctuation model [15] to simulate template polymerization via controlled polymerization scheme, involving copolymerization of free monomers (A) and monomers bound to a template (B) that consists of linear/ring-like substrates with equidistant sites occupied by bound monomers (B). In experiments, such a system can be setup by adsorbing monomer to liquid/solid, liquid/liquid, or air/liquid interface via physical or chemical interactions [13] and

then inducing polymerization by exposing the substrates to monomer/initiator solution. The main purpose of this work is to setup a framework for gaining an understanding of the structure of products of template polymerization under different conditions. Gaining detailed insight into the structure of the polymers grown via template polymerization will help us understand how the properties of the daughter polymers depend on the densities of free monomers, bound monomers and initiators, spacing of the bound monomers on the template, the template characteristics and the extent of monomer adsorption on the template. We vary systematically the number of free monomers, the number of initiators, the number monomers bound to the template, spacing between adjacent monomer units bound to the template, template characteristics (shape, orientation) and degree of flexibility. Upon testing the different parameters, we seek to identify the most favorable conditions for growth of template-bound polymers. Such information will ultimately assist in designing experimental conditions, leading to “optimal” and well-controlled template polymerization.

Different applications might require that polymers be prepared on a substrate comprising various geometries and dimensionalities, such as nanowires, Si/Au surfaces, a polymer with a stiff backbone, zeolites. Depending on the geometry and the dimensionality, the growing chains experience a diverse degree of confinement. For planar substrates (Si/Au wafers) [13] or nano-porous substrates [14] (zeolites), the added dimensionality can impose stronger spatial restrictions on the growing polymer chains as compared to rod-like substrates (nanowires, polymer backbones). In this paper, we deal specifically with 1-D substrates surfaces because this is perhaps the simplest geometry to model and understand as it imposes the least restriction on the polymer chains. We plan to extend the study to other geometries (planar substrates/nanoporous substrates) and that would be quite straightforward, given our present setup.

For this work, we assume that the substrates are fixed in space with a monomer layer bound to it. In experiments, this corresponds to the case when Au-thiol chemisorption or silane chemistry is utilized to create a relatively stable self-assembled monolayer. The density of the bound monomers on the substrate is a key parameter in template polymerization. Depending

on value of the grafting density, templation might be favored (due to proximity of monomer units) or hindered due to steric effects. Our work provides the framework for finding an optimum grafting density corresponding to substrates of dimensionalities. Substrate shape can potentially impose confinement effects on the growing polymer chains. We explore the two extreme cases of curvature- rod-like substrates and ring-like substrates. Experimentally, it is difficult to investigate the effect of shape of 1-D substrates on templation products. With the present set-up, extension to flat, concave or convex 2-D substrates is straightforward.

4.2 Simulation Model

We use a Monte Carlo (MC) simulation scheme to model the “living”/controlled radical polymerization (CRP) based on the bond fluctuation model (BFM) in the NVT ensemble [15]. The substrates, monomers, and polymers reside on a three-dimensional cubic lattice. All possible permutations and sign inversions of the following vector families represent the allowed set of moves: $P(2,0,0) \cup P(2,1,0) \cup P(2,1,1) \cup P(2,2,1) \cup P(3,0,0) \cup P(3,1,0)$. This prevents any bond from crossing and polymers from overlapping. In this implementation, each bead on the lattice represents an effective monomer unit. The simulation results reported here have been carried out on a cubic lattice $50 \times 50 \times 50$, with periodic boundary conditions applied in all directions. Because each monomer corresponds to 8 sites effectively, the full lattice occupancy is achieved at 15,625 sites. The computer simulations follow the general scheme of individual steps reported in an earlier work by one of the authors [16]. The values of the parameters intrinsic to the MC simulation scheme are held constant during all the runs, namely reaction probabilities for initiators and living radicals are both 1 and the probability of reaction vs. motion is 0.01. A low value of the reaction probability assures controlled polymer growth. For details of the model and the choice of parameters see Ref. 16 and 17.

In our computer simulations, the B monomers are bound to either rod-like or ring-like substrates, whose position is fixed in space (*cf.* **Figure 4.1**). The rod-like substrates are four in number and are positioned symmetrically in the cubic lattice, with either 7 or 16 bound B monomers grafted on each of the substrates. Thus, the total number of bound monomers ($[B]$)

is either 28 or 64. The grafting density of the bound monomers on the substrates (σ_B) is, defined as the ratio of the number of bound monomers that are present on a substrate relative to the maximum number of monomers that can be accommodated on that substrate. For ring-like substrates, we have 24 or 48 B bound monomers equally distributed between two rings placed symmetrically in the cubic lattice (*cf.* **Figure 4.1**). The bound monomers can be oriented in four different ways relative to the ring-like substrate: in-plane, 30° incline, 60° incline or normal (*vide infra*). **Figure 4.1** shows only the in-plane orientation of bound monomers on a ring. We refer back to the different orientations briefly in a later section (*cf.* **Figure 4.9**). The B bound monomers are attached to the substrates by either rigid or flexible bonds. For most of the simulations, we keep the B monomers bound rigidly in space. We later introduce flexibility in the bound monomers such that the bond between the substrate and the bound monomer can stretch and rotate in accordance with the BFM formalism. In addition to the bound B monomers, there are free A monomers present in bulk. Although both A and B are identical, *i.e.*, there is no interaction potential acting between A and B, we use this nomenclature to distinguish between the polymers formed of free monomeric units only and those formed of both bound and free monomeric units. In addition, there are free initiators present in bulk. The numbers of A monomers and initiators are denoted as [A] and [I], respectively. Two different types of polymers can form during the simulation: homopolymers comprising only A units (*i.e.*, A homopolymers) and copolymers containing both A and B units (*i.e.*, A-B copolymers). **Figure 4.1** shows schematically that the “degree of randomness” in the A-B copolymer depends on the spatial distribution of the B units on the template. To this end, B units spaced closely on the template form random-blocky copolymers (*i.e.*, having longer consecutive sequences of B) while sparsely distributed B monomers result in “truly random” copolymers (*i.e.*, having discretely and randomly spaced B units).

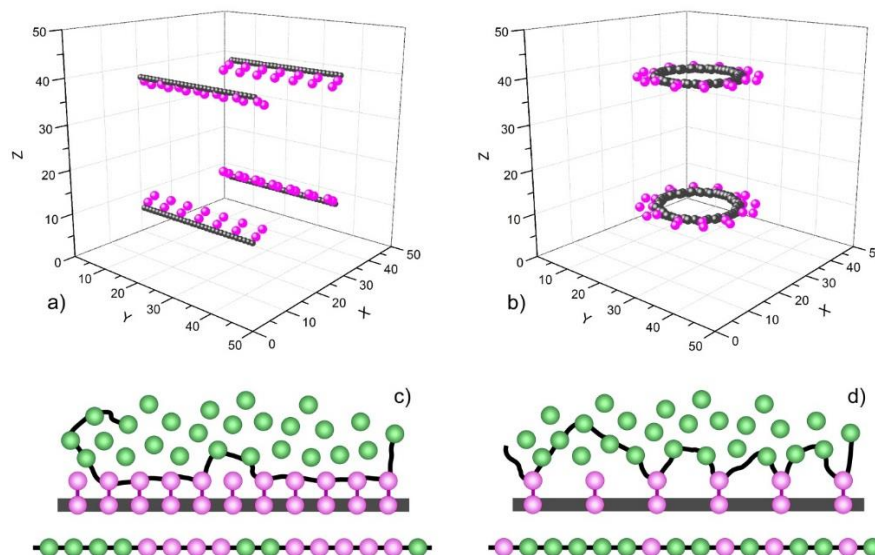


Figure 4.1. a) Rod-like substrates (black) with grafted bound monomers (magenta), (b) Ring-like substrates (black) with grafted monomers (magenta), (c) copolymers formed by combination of free monomers (green) and bound monomers (magenta) – high grafting density of monomers, (d) copolymers with bound “unimers” – low grafting density of monomers on substrate.

Our system is “truly living”, *i.e.*, the chains do not undergo termination or chain transfer [17]. The implicit solvent model (no explicit solvent molecules are included in the simulations) is presumed to be valid for modeling the growth of “living” chains under good solvent conditions [17]. The initiator molecules and free monomers are initially distributed homogeneously throughout the lattice. In our simulations, the initial number of free monomers ($[A]$) is set to be either 3125 or 6250, which corresponds to the lattice occupancy of 20% or 40%, respectively. The initial number of initiators ($[I]$) is chosen to be either 12 or 125, giving rise to a maximum number of polymers equal to 12 or 125, respectively, that can exist for a given simulation. After placing the monomers and initiators on the lattice, we perform an initial equilibration run for 10^9 Monte Carlo steps (MCS) per bead to obtain a randomly distributed configuration. We use the equilibrated configuration as the input for the MC simulation. The reactive MC algorithm commences after a secondary short equilibration run

($\approx 10^5$) and runs for a predetermined number of MCS, typically 10^9 , in order to achieve the same conversion. On an average it takes around 6 hours for each set of MC runs.

Chain statistics (*i.e.*, molecular weight, polydispersity index) and the coordinates of the monomers of each polymer and all monomers are stored periodically after several thousand MCS. In order to obtain good statistics, we perform 50 MC simulations runs for every set of input parameters. In order to understand the effect of different parameters (*i.e.*, $[B]$, σ_B , $[A]$, $[I]$, substrate shape, bound monomer orientation and flexibility), we monitor the number distribution of bound B monomers and the sequence length distribution in the A-B copolymers, normalized by the number of copolymers formed. While the number distribution gives us a quantitative estimate of the incorporation of bound B monomers in A-B copolymers, the sequence length distribution offers a qualitative insight into the co-monomer distribution in the A-B copolymers. In addition, we also report the number of A-B copolymers and the mole fraction of bound B monomers present in the A-B copolymers.

4.3 Results and Discussion

To facilitate the discussion, we set $[B] = 28$, and $\sigma_B = 0.42$. We will explore the effect of these two parameters later in the paper. In **Figure 4.2**, we plot the normalized number distribution of bound monomers $[B]$ in the A-B copolymers (upper row) and the corresponding distribution of the sequence lengths, normalized by number of copolymers (lower row) for two concentrations of free monomers ($[A]$) equal to 3125 (red squares) and 6250 (blue circles) and two free initiator concentrations ($[I]$) equal to 12 (left column) and 125 (right column). The data in **Figure 4.2** reveal that the probability of incorporating the B monomers into the A-B copolymer is not affected by the number of free A monomers. Altering the concentration of free initiators does have an effect on the likelihood of finding the B monomers inside the A-B copolymer. A more than ten-fold increase in $[I]$ (from 12 to 125) reduces the maximum number of B monomers per copolymer from ≈ 8 to ≈ 4 while concurrently increasing the occurrence of A-B copolymers that have only a single B bound monomer. Due to an increased

[I] more polymer chains are generated in the system, which reduces the number of B bound monomers available per growing chain. Thus, by increasing [I], it is more likely to form more A-B copolymers but less likely for a growing A-B chain to incorporate many bound B monomers. We will refer back to the effect of the number of initiators on the polymerization process later in this section.

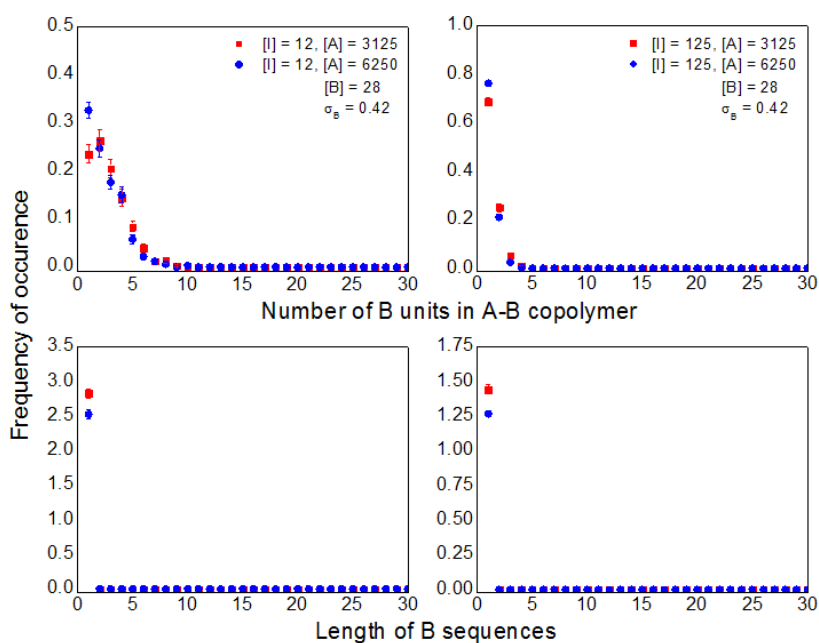


Figure 4.2. Comparison of the number and sequence length distributions of B bound monomers in A-B copolymers for different number of initiators ($[I] = 12$ and 125) and free monomers ($[A] = 3125$ and 6250) for rod-like substrates.

We now set $[I] = 12$ and $[B] = 28$ and increase σ_B from 0.42 to 1.0 . The normalized number distributions of bound B monomers per A-B copolymer chain for the different values of σ_B are plotted in **Figure 4.3**. The maximum number of B monomers per copolymer increases with increasing σ_B irrespective of the number of free monomers ($[A]$). This effect

becomes most prominent at the highest grafting ($\sigma_B = 1$); the maximum number of B per copolymer increases from ≈ 7 (for $\sigma_B < 1$) to ≈ 13 (for $\sigma_B = 1$). Note that for $\sigma_B = 1$ there is a distinct peak corresponding to 7 bound B monomers per A-B copolymer indicating that all of the 7 bound B monomers in each substrate (recall that given $[B] = 28$ and 4 identical substrates bearing the bound B monomers, there are 7 monomers per substrate) can be potentially incorporated in a single chain at the highest grafting density. This implies that we can grow polymer chains that mimic perfectly the template when the B monomeric units are spaced as close as possible along the template. We attribute this behavior to the “proximity effect”; *i.e.*, once a growing chain adds a bound monomer unit, it is more likely to add a neighboring bound B monomer than a random free A monomer. Overall, varying the concentration of free A monomers does not have an effect of the system behavior. This is due to the large excess of A monomers present in the system. In the following discussion, we thus set $[A] = 3125$ for most of the simulations.

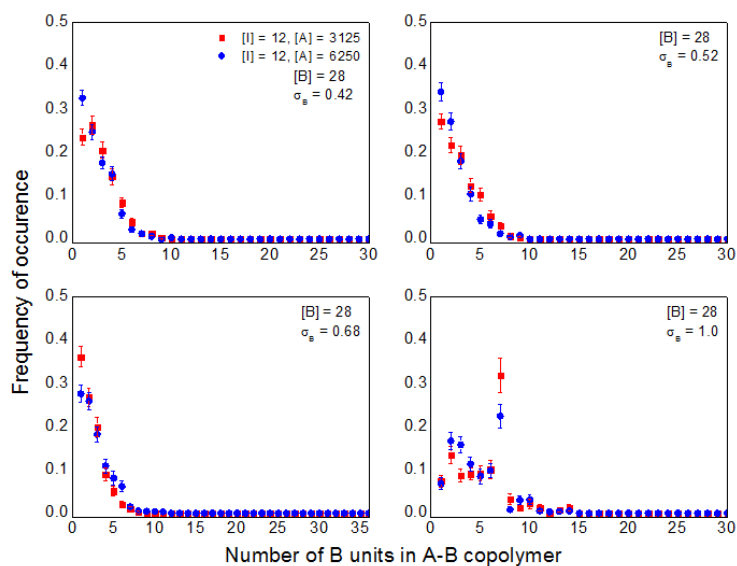


Figure 4.3. Comparison of the number distribution of B in A-B copolymers, averaged over 10 simulation runs, for different grafting densities on rod-like substrates (σ_B).

Our computer simulations indicate that for $\sigma_B < 1$ the B monomers are incorporated into the A-B copolymers as unimers; *i.e.*, there are not dimers, trimers, tetramers, *etc.* constituting consequent runs of B units within the A-B chains. Only for $\sigma_B = 1$ we detect the presence of B-mers longer than unimers. This suggests that longer sequences of consecutive B runs can be realized when the B monomers are spaced on the substrate as closely as possible. This finding also reveals that varying the absolute value of [B], while keeping $\sigma_B = 1$ should alter the population density of the various “mers”. In **Figure 4.4**, we compare the number and sequence length distributions of systems having different number of bound monomers ([B] = 28 and 64) at $\sigma_B = 1$. The sequence length distribution of B for [I] = 12 and [B] = 28 (left column, red squares) shows a distinct peak value corresponding to sequence length of 7, which corroborates the “proximity effect” (*vide supra*). Increasing [I] ten-fold results in decreasing the average number of B units per A-B chain ten times, thus attenuating this “proximity effect”; we note that the distinct peak corresponding to sequence length of 7 found at [I] = 12 is greatly diminished while the overall distribution peaks at a sequence length of 2. The trends observed for [I] = 12, are replicated when [I] = 64 (corresponding to 16 B monomers bounds on each substrate). For instance, the data in **Figure 4.4** (right column) exhibit a distinct peak at sequence length of 16. The data also reveal that in the presence of a large number of bound B monomers the A-B copolymers are more likely to incorporate a greater number of B (>13) and possess longer sequences of B (>7). This behavior holds true regardless of the number of initiators present in the system. However, the frequencies of occurrence corresponding to number of B and sequence length equal to 16 (in case of [B] = 64; *i.e.*, 16 B monomers per substrate) are much lower than the frequencies corresponding to 7 (in case of [B] = 28; *i.e.*, 7 B monomers per substrate). This implies that for a greater number of bound B monomers on each substrate, it is less likely to incorporate all the B monomers in a single chain. Thus, the template length poses a practical limitation on the replication process leading to complementary polymer chains. **Figure 4.5** shows a typical snapshot from one of the simulation runs, depicting the distribution of B monomers in A-B copolymers for [I] = 125, [B] = 64, and [A] = 6250. Each B monomer and A-B copolymer is assigned a serial number

(shown along x and y-axes of **Figure 4.5**, respectively). Monomers 1-16, 17-32, 33-48 and 49-64 are attached to substrates 1, 2, 3 and 4 respectively; the red lines demarcate the position of the substrates on **Figure 4.5**. We count the number of blocks of B in each copolymer, the corresponding block length (number of B in a block) and the serial number of each B monomer unit in a block and plot this information in **Figure 4.5** for a visual representation. For example, consider polymer 1 in **Figure 4.5**; it has two B blocks of lengths 1 and 2 shown in black and yellow respectively. **Figure 4.5** also reveals that both these blocks (monomer numbers 49, 50-51) are located on the 4th substrate.

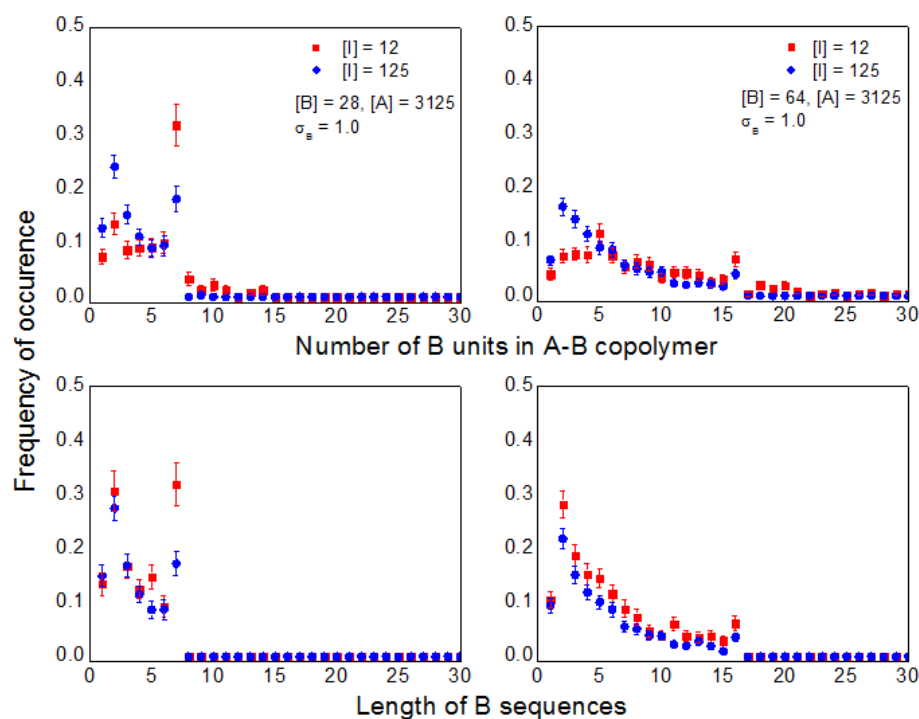


Figure 4.4. Effect of the number of initiators ($[I]$) and the number of bound B monomers ($[B]$) on the number distribution and sequence length distribution of B in copolymers A-B.

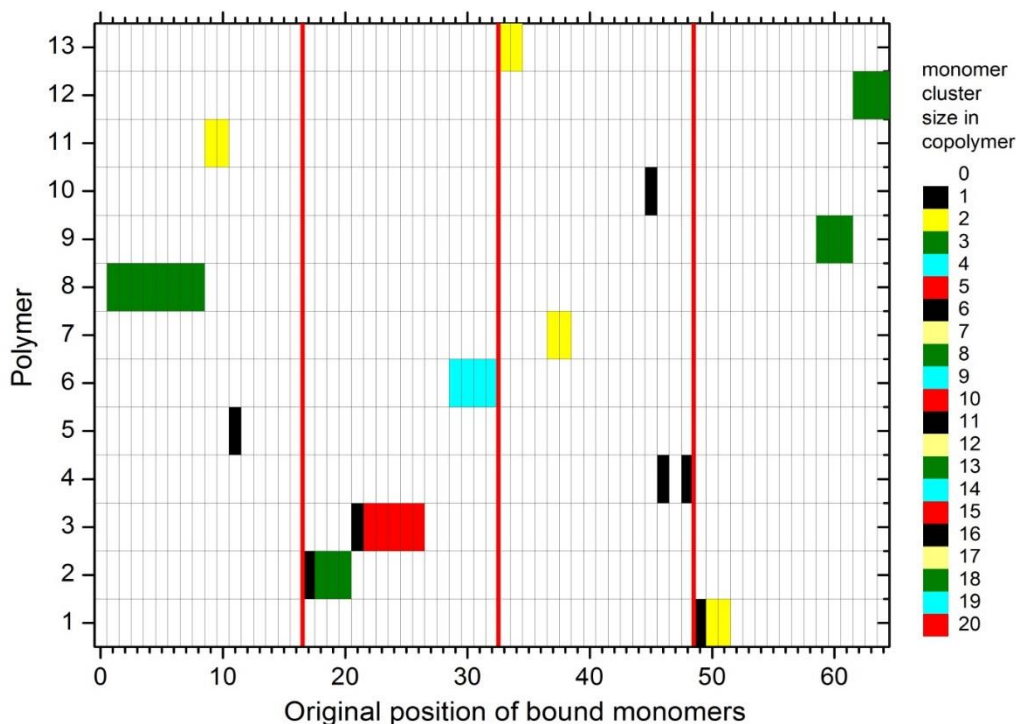


Figure 4.5. Distributions of “mers” in A-B copolymers for $[I] = 125$, $[B] = 64$, $[A] = 6250$ and $\sigma = 1$. Unimers to octamers are observed to be formed under these conditions (the red lines demarcate the different substrates).

In the results discussed thus far, we kept the position as well as the orientation of the B monomers constant. To make the system more realistic, one has to consider that the orientation of the B monomers on the substrate may change with time (while their position is fixed). This would correspond to situations, in which the B monomers are attached to the substrate via flexible linkers that allows the B units to alter their spatial orientation with time. Hence, next we explore the effect of flexibility of bound B monomers on their number distribution and sequence length distribution in the A-B copolymers. **Figure 4.6** shows a comparison of the fixed (red squares) and flexible (blue circles) bound monomer cases for two systems ($[B] = 28$ or 64) at the maximum grafting density ($\sigma_B = 1$). The flexibility of B monomers dilutes the

“proximity effect”; the average spacing between adjacent bound and flexible monomers does not remain constant through the run time, effectively reducing the overall grafting density. This is evident from the disappearance of peaks (red squares) corresponding to 7 (for $[B] = 28$) or 16 ($[B] = 64$) in the number distributions of B and the occurrence of discrete B units in sequence length distributions. Therefore, in systems featuring flexible bound B monomers one cannot polymerize all B monomers present on the substrate. Thus, the B monomers bound rigidly to the substrate (*i.e.*, no conformational flexibility) are more favorable towards templation at high grafting densities.

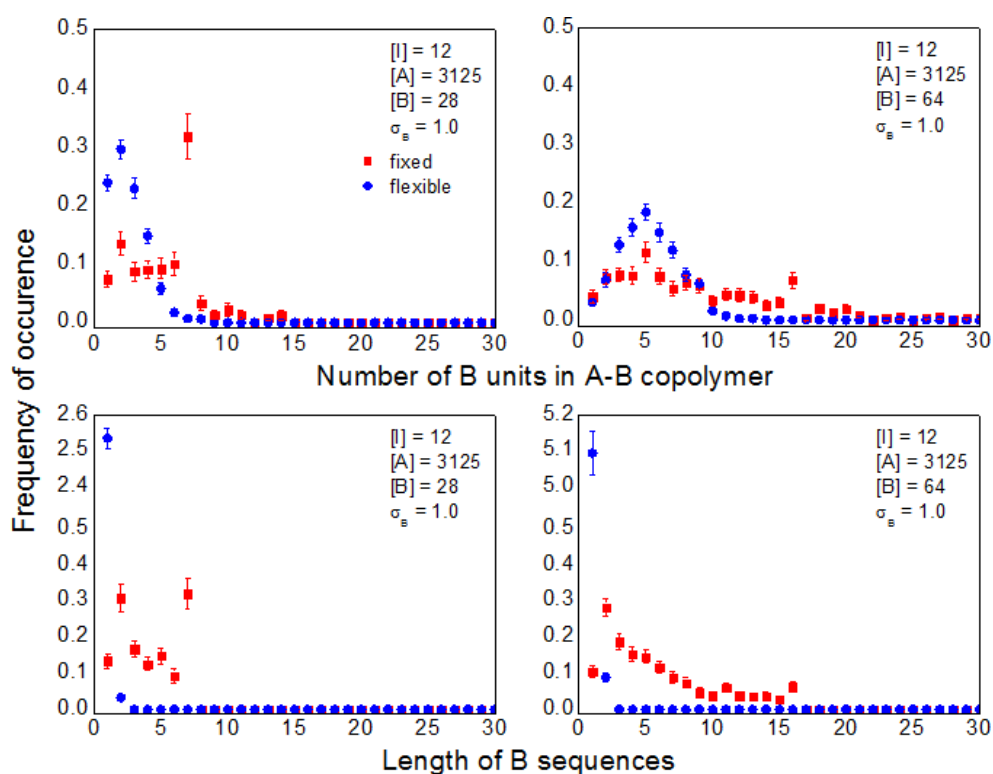


Figure 4.6. Effect of flexibility of the bound B monomers on the number distribution and sequence length distribution of B in A-B copolymers, for $[I] = 12$ and 125.

Figure 4.7 shows a comparison of the number of A homopolymers and A-B copolymers as well as the composition of A-B copolymers formed with two different numbers of initiators, *i.e.*, $[I] = 12$ (close symbols) and 125 (open symbols), at different σ_B for fixed (left column) and flexible (right column) bound B monomers. The red and blue symbols represent the data pertaining to A-B copolymers and A homopolymers, respectively. The number of A-B copolymers produced in the system is governed by the number of initiators and the number of bound B monomers. The data in **Figure 4.7** reveal that when the bound B monomers are present in excess of the initiators (*i.e.*, $[B] = 28$ and $[I] = 12$), the number of A-B copolymers formed is limited by the number of the initiators. In contrast, when the initiators are in excess ($[I] = 125$), the number of A-B copolymers formed is limited by the number of bound monomers ($[B] = 28$). This holds true at all grafting densities regardless of the flexibility of the B bound monomers. The fraction of B units in the A-B copolymers is slightly less in case of 125 initiators as compared to 12 initiators. Here, the greater the number of initiators results in more copolymers formed (*vide supra*); thus, the composition of the copolymers is limited by the number of bound B monomers present in the system. This argument is corroborated by a similar trend in the case of fixed bound B monomers. In addition, we observe that the mole fraction of fixed B in the A-B copolymers exhibits a minimum value at $\sigma_B = 0.68$ independent of $[I]$. Since the corresponding number of A-B copolymers does not show a maximum at $\sigma_B = 0.68$, we attribute the lower mole fraction of B to a lower overall number of B in the copolymers. High grafting densities can lead to steric hindrance of the growing chains, thereby attenuating the “proximity effect” that favors addition of bound B monomers. Since the steric effects increase with increasing σ_B the “proximity effect” predominates. The mole fraction data in **Figure 4.7** for systems with fixed B monomers (right column) validate our hypothesis; the fraction of B in the A-B copolymers decreases with varying σ_B until $\sigma_B = 0.68$, and peaks at $\sigma_B = 1$. For flexible B bound monomers, both the number of polymers and the composition do not change significantly with increasing σ_B , most likely due to dilution of the “proximity effect” mentioned earlier.

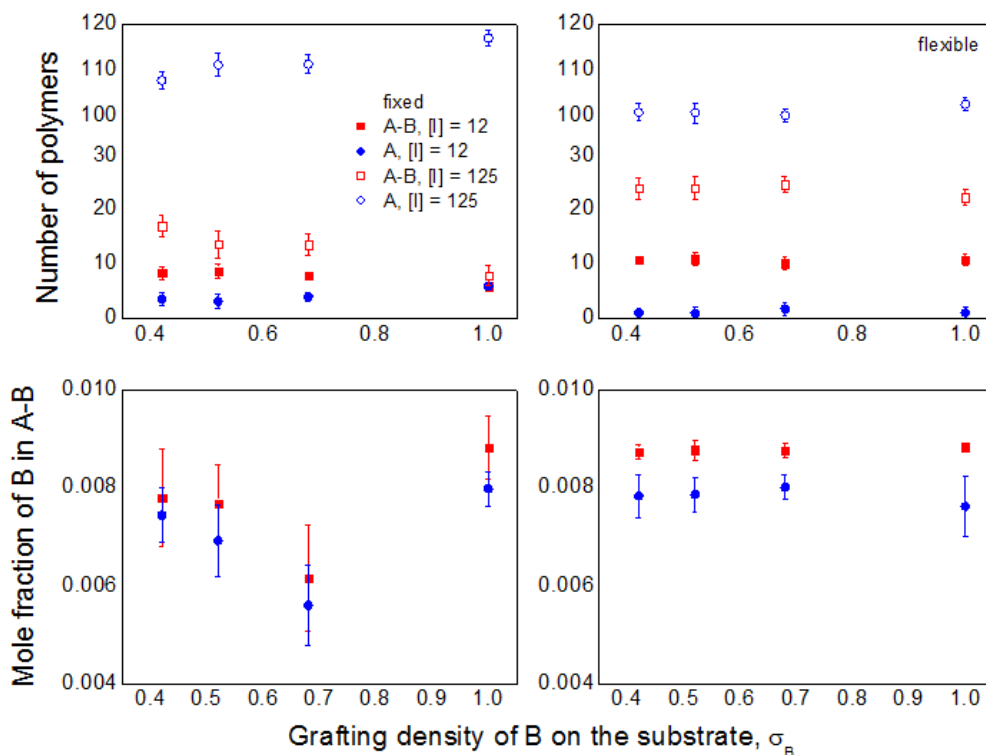


Figure 4.7. The average number of A polymers and A-B copolymers as well as the average A-B composition as a function of the grafting density of the B monomers (σ_B) in fixed (left column) and flexible (right column) conformations.

In all simulation runs that have been discussed so far, we monitored the incorporation of bound B monomers (on rod-like substrates) into growing copolymer chains over time (not shown). We observed that regardless of its location on the rod-like substrate, each bound monomer on an average was equally likely to get incorporated in a copolymer chain and there is no preferred order of chain-growth along the template (*i.e.* there were no end-effects of the linear substrates). Intuitively, this is expected because the template is one-dimensional, which means that the B monomers located far away from the ends of the templates are as accessible to growing chains as the ones located at the two ends. Thus far, we have investigated cases, in which the B monomers were placed on 4 rigid rods placed uniformly in the lattice. In order to

explore whether the geometry of the substrate plays a role in incorporating the bound B monomers into the A-B copolymers, we probe the effect of substrate shape and spatial orientation of the B bound monomers on the number distribution and the sequence length distribution of B in A-B copolymers. **Figure 4.8** shows a comparison of rod and ring substrates with the same molecular parameters (*i.e.*, $[I] = 12$, $[A] = 3125$ and $\sigma_B = 0.425 \pm 0.005$; top row). The number distributions show the same general trend for rod- and ring-shaped substrates, independent of chain flexibility. One striking observation is that both the systems (*i.e.*, rod and ring) show the same maximum number of B units per A-B copolymer. However, the maximum number of B units per copolymer is reduced when σ_B is decreased from 0.43 to 0.24. Similar to the rod-like substrates, the number distribution of B is affected by variations in σ_B ; at higher values of σ_B it is more likely to incorporate more bound B monomers in an A-B single chain. The data in **Figure 4.8** also reveal that greater number of bound B monomers (*i.e.*, $[B] = 48$) leads to an overall increase in incorporation of bound monomers per A-B copolymer and an increase in the maximum number of B per A-B copolymer. Thus, the substrate shape does not appear to affect the template polymerization process.

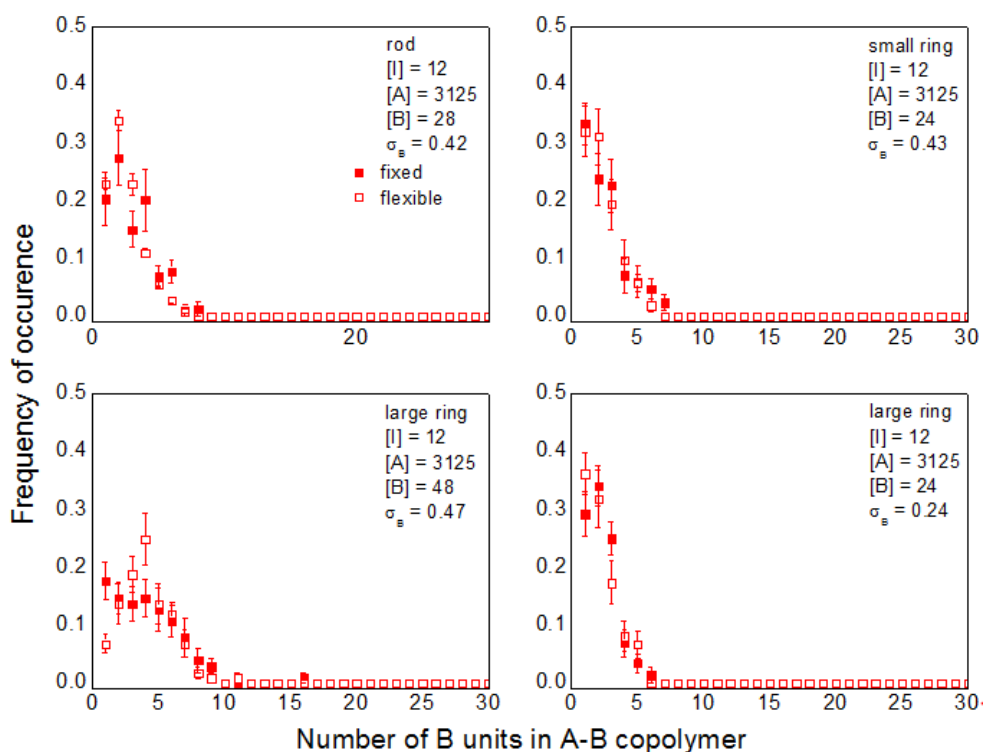


Figure 4.8. Comparison of the number distribution of B monomers in A-B copolymers for rod and ring-like substrates.

We have shown that the spatial orientation of the B monomers bound on the substrate affects the properties of the resultant A-B copolymers. In order to gain more insight into the effect of the spatial orientation of the B monomers relative to the orientation of the substrate, we placed the B monomers in various (fixed) positions along the ring-like substrate. **Figure 4.9** shows the number distribution of B per A-B copolymer for four different spatial orientations of a bound monomer relative to the ring-like substrate (depicted pictorially by the cartoons on the right in **Figure 4.9**). The maximum number of bound B monomers that can be incorporated in a single A-B chain is dictated by the orientation of a bound B monomer relative to the ring-like substrate. Each orientation is marked by a characteristic peak in the number

distribution of bound B monomers in the A-B copolymer. This peak shifts to the right as the orientation of the B monomers changes from in-plane to normal to the substrate. In ring-like substrates, the different spatial orientation of bound monomers effectively changes the spacing between adjacent bound monomers; the normal orientation is the most densely packed while the in-plane one is the least packed. All parameters being the same, the difference in effective bound monomer spacing is most likely the reason behind the shift in the peaks in the number of B monomers in the A-B copolymer. For flexible B bound monomers, a similar trend is observed (not shown). The data also reveal that the maximum number of bound monomers incorporated per A-B copolymer increases slightly as the number of bound monomers is doubled. This is similar to the trend observed in case of rod-like substrates.

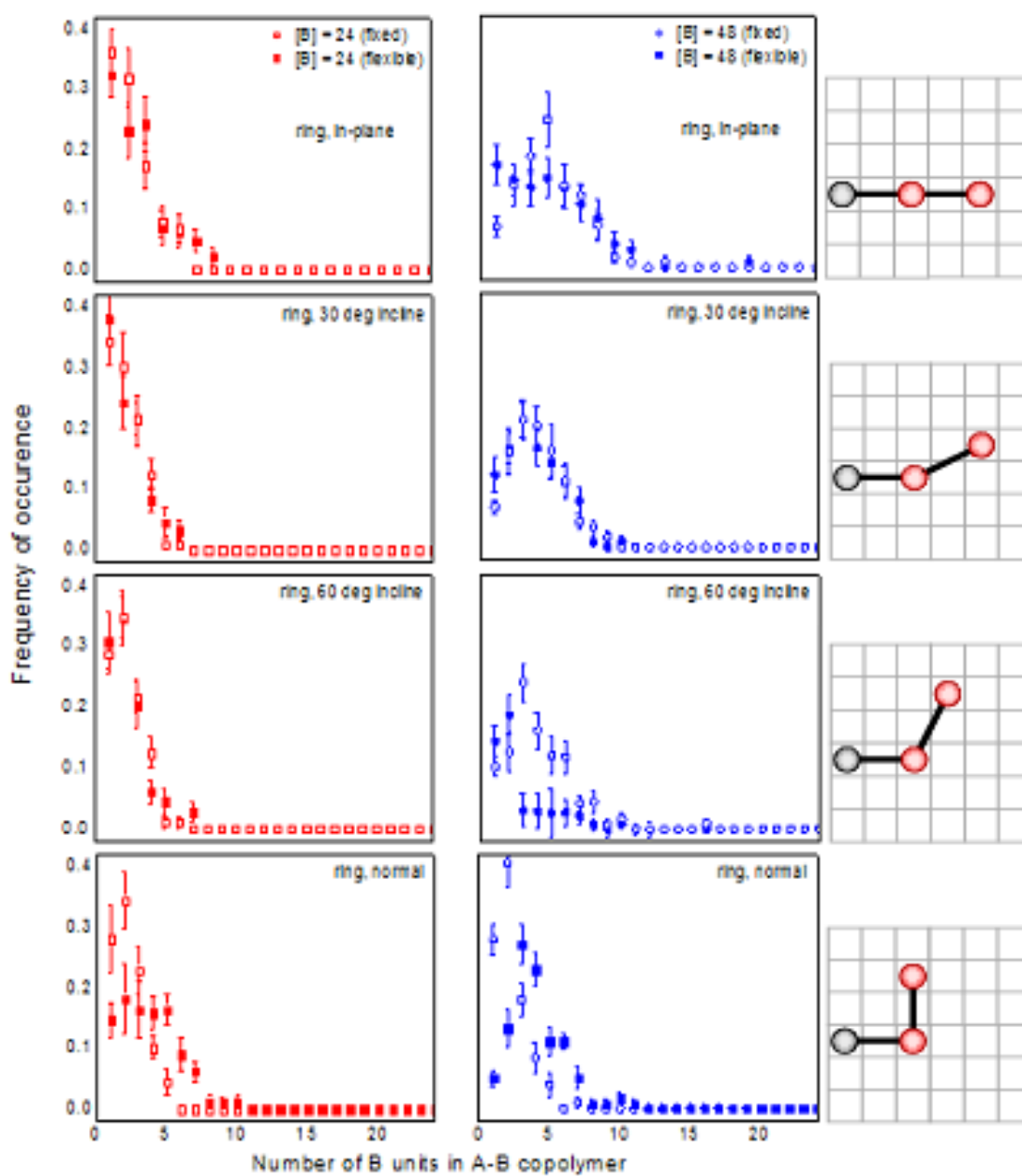


Figure 4.9. Effect of the orientation of the bound B monomer on their number distribution in A-B copolymers, for $[I] = 12$, $[A] = 3125$ and $\sigma_B = 0.47$ (blue), 0.43 (red).

4.4 Conclusions

We used Monte Carlo simulations to investigate the effect of various factors, *i.e.*, the grafting density (σ_B) and number of B bound monomers ($[B]$), the number of initiators ($[I]$), the number of free A monomers ($[A]$), and the flexibility of the bound monomers, on template polymerization involving rigid rod-like and ring-like substrates. The computer simulations ensured “true living” conditions by neglecting any chain termination or chain transfer. We noted that $[A]$ has no significant influence on the template polymerization process as long as free A monomers are in excess; we thus chose to keep the number of free monomers constant ($[A] = 3125$) for most of the simulations present in this work. We observed that increasing σ_B increases the possibility of the bound B monomers to get incorporated into the growing A-B chains. At the maximum possible grafting density ($\sigma_B = 1.0$), the maximum number of B monomers gets incorporated into a single polymer chain. In addition, the maximum sequence length of “polymerized” bound B monomers increases with increasing the number of B monomers present on a single substrate; this effect is more significant when the bound B monomers lack any flexibility. At low σ_B , it is unlikely to form sequences of B longer than unimers. This behavior has been attributed to the “proximity effect” of the bound B monomers that favors the sequential polymerization of the bound monomers into a single growing chain. We also observed that increasing the number of initiators by ten-fold (12 to 125) leads to shorter sequence lengths of bound monomers and lowers the number of bound monomers present per polymer chain. Our computer simulations show that long sequences of B bound monomers are formed mostly when the bound B monomers are immobilized in space. We attribute this behavior to the dilution of the “proximity effect” in case of flexible bound B monomers as the average spacing between the adjacent B bound monomers does not remain constant throughout the simulation run. The number of A-B copolymers produced in the system is governed by $[I]$ and $[B]$ in the system. We showed that when the initiators are in excess (*i.e.*, $[I] = 125$), the number of A-B copolymers formed is limited by the number of bound monomers (*i.e.*, $[B] = 28$). Additionally, the chemical composition of the A-B copolymers is not significantly affected by increasing $[I]$. We also investigated the effect of

substrate shape and orientation on template polymerization processes. All parameters remaining the same, the distribution of number of the bound B monomers incorporated per growing chain shows the same trend, irrespective of the shape of the substrate (rod or ring) and the flexibility of the bound monomers, therefore there are no end effects associated with the rod-substrate. We also show that the maximum number of bound B monomers that can be incorporated in a single A-B chain is dictated by the spatial orientation of a bound monomer relative to the ring-like substrate. Each orientation is marked by a characteristic peak in the number distribution of bound B monomers. This peak shifts as the orientation of the B monomers changes from in-plane to normal to the substrate. We attribute this behavior to the change in the effective spacing between adjacent bound B monomers occurring due to different spatial orientations of the B monomers. The maximum number of bound B monomers incorporated per A-B copolymer increases slightly as $[B]$ is doubled. This is similar to the trend observed in case of rod-like substrates.

In real experiments, the rod-like substrates can be realized in the form of functionalized nano-wires or macro-molecules having monomeric units attached to a rigid backbone. Our simulations do not account for any flexibility or mobility of the substrates. It would be interesting to investigate whether substrate mobility promotes template polymerization. In the present work, we assumed that the bound and free monomers have identical reactivities. It would also be useful to carry out computer simulations to explore the effect of different reactivity ratios on the incorporation of bound monomers into growing polymer chains.

4.5 Acknowledgements

We thank the National Science Foundation for supporting this work through the grants No. CBET-0853667 and DMR-1121107.

APPENDIX

4.6 Appendix

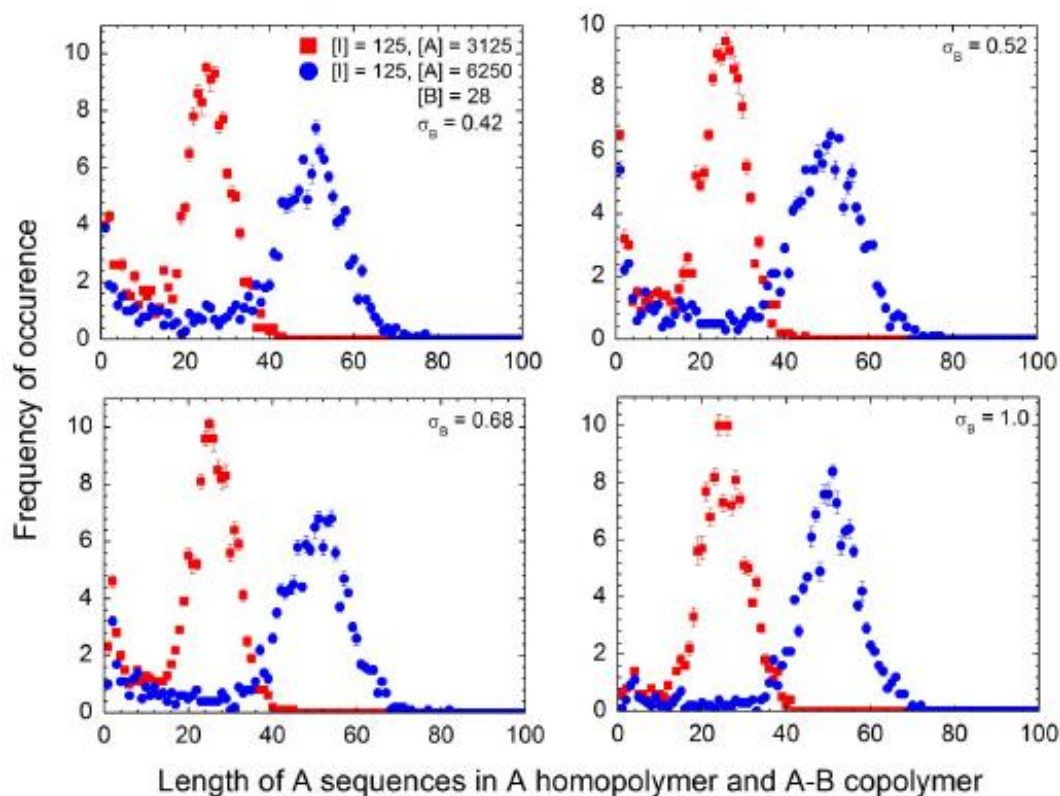


Figure A4.1. Comparison of sequence length distribution of A monomers in polymer chains at different grafting densities of bound monomers B for two different initial numbers of free A monomers in solution.

The sequence distribution of A monomers in the homopolymer chains possesses a Gaussian distribution with the mean equal to the average molecular weight of the homopolymers at all grafting densities. In contrast, the sequence distribution of A monomers in A-B copolymers shows a dependence on grafting density of the substrate-bound B monomers. In order to establish that grafting density of bound B monomers is the predominant factor affecting the sequence distribution of A and B in the A-B copolymer chains, in **Figure**

A4.1 we plot the sequence length distributions of A monomers (not normalized) at different grafting densities for two different values of initial number of free monomers, $[A] = 3125$ (red) and 6250 (blue). We observe a bimodal distribution of the sequence lengths of A monomers arising from contributions from both copolymer and homopolymer chains at low grafting densities ($\sigma_B < 1$). The maximum at low sequence length corresponds to A-B copolymers while the Gaussian-like peak corresponds to A homopolymers. The A-B copolymer maximum is unaffected by the initial number of free monomers ($[A]$), as expected. In contrast, the A homopolymer peak is Gaussian and it shifts to twice its value (i.e., from 25 to 50) when $[A]$ is increased from 3125 to 6250. The likelihood of occurrence of short sequences of A is the same irrespective of the number of free A monomers. This corroborates our conclusion that grafting density of the bound B monomers is the most important factor in determining the sequence length distribution of both A and B units in the A-B copolymer chains.

4.7 References

1. S. Polowinski, "Template Polymerization", *ChemTec Publishing*, 1997.
2. G. Challa and Y.Y. Tan, "Template Polymerization", *Pure & Applied. Chem.*, 1981, **53**, 647-651.
3. D. M. Rosenbaum and D. R. Liu, "Efficient and Sequence-Specific DNA-Templated Polymerization of Peptide Nucleic Acid Aldehydes", *J. Am. Chem. Soc.*, 2003, **125** (46), 13924-13925.
4. J. Gons, E. J. Vorenkamp, G. Challa, "Radical polymerization of methyl methacrylate in the presence of stereoregular poly(methyl methacrylate). V. Kinetics of initial template polymerization", *Journal of Polymer Science: Polymer Chemistry*, 1975, 13 (7), 1699-1709.
5. J. Smid, Y.Y. Tan, G. Challa, "Effects of poly(2-vinylpyridine) as a template on the radical polymerization of methacrylic acid—I. Influence of atactic poly(2-vinylpyridine) concentration", *European Polymer Journal*, 1983, 19 (10-11), 853-858.

6. I. Rainaldi, C. Cristallini, G. Ciardelli, P. Giusti, "Kinetics and reaction mechanism of template polymerization investigated by conductimetric measurements. Part 3. Radical polymerization of acrylic acid in the presence of poly(*N*-vinylpyrrolidone)", *Polymer International*, 2000, 49 (1), 63–73.
7. K. J. Shea and D. Y. Sasaki, "On the control of microenvironment shape of functionalized network polymers prepared by template polymerization", *J. Am. Chem. Soc.*, 1989, **111** (9), 3442-3444.
8. T. Serizawa, K. Hamada & M. Akashi, "Polymerization within a molecular-scale stereoregular template", *Nature*, 2004, **429**, 52-55.
9. K. Hamada, T. Serizawa, and M. Akashi, "Template Polymerization Using Artificial Double Strands", *Macromolecules*, 2005, **38** (16), 6759-6761.
10. V. S. Trubetskoy, V. G. Budker, L. J. Hanson, P. M. Slattum, J. A. Wolff and J. E. Hagstrom, "Self-assembly of DNA-polymer complexes using template polymerization", *Nucleic Acids Research*, 1998, **26** (18), 4178-4185.
11. J. Matsui , T. Kato , T. Takeuchi , M. Suzuki , K. Yokoyama , E. Tamiya , I. Karube, "Molecular recognition in continuous polymer rods prepared by a molecular imprinting technique", *Analytical Chemistry*, 1993, **65** (17), 2223–2224.
12. W. Wang, S. Gao, and B. Wang, "Building Fluorescent Sensors by Template Polymerization: The Preparation of a Fluorescent Sensor for d-Fructose", *Organic Letters*, 1999, **1** (8), 1209-1212.
13. J. F. Ford , T. J. Vickers , C. K. Mann , and J. B. Schlenoff, "Polymerization of a Styrene-bound Monolayer", *Langmuir*, 1996, **12** (8), 1944-1946.
14. T. Bein and P. Enzel, "Encapsulation of Polypyrrole Chains in Zeolite Channels", *Angewandte Chemie*, 1989, **28** (12), 1692-1694.

15. I. Carmesin and K. Kremer, "The bond fluctuation method: a new effective algorithm for the dynamics of polymers in all spatial dimensions", *Macromolecules*, 1988, **21** (9), 2819–2823.
16. J. Genzer, "In silico polymerization: Computer simulation of controlled radical polymerization in bulk and on flat surfaces", *Macromolecules*, 2006, **39**, 7157-7169.
17. S. Turgman-Cohen and J. Genzer, "Computer Simulation of Controlled Radical Polymerization: Effect of Chain Confinement Due to Initiator Grafting Density and Solvent Quality in "Grafting From" Method", *Macromolecules*, 2010, **43** (22), 9567-9577.

5. “Grafting Through” Polymerization involving surface-bound monomers

In the past two decades, modification of surface properties using grafted polymer assemblies has shown immense potential in a plethora of applications such as protein separation, protective and conductive coatings, vapor sensing and improvement of adhesion between different materials. While physical deposition of polymeric materials is simple, the strength of the coating relies on, typically, weak interactions between the surface and the coating material. Chemical attachment of polymers to material surfaces, frequently called chemical grafting reactions, play an important role in the modification of solid surfaces. This is due to the fact that in the course of the surface modification process covalent chemical bonds between surface and coating are established, which are in many cases stable even under quite adverse conditions. The grafting routes are often broadly classified into “grafting to” and “grafting from” reactions.

“Grafting from” route requires a surface-grafted initiator and its biggest challenge is the need to synthesize the initiator and subsequent surface-initiated polymerization, such as atom transfer radical polymerization (ATRP), which requires advanced organic chemistry techniques. In contrast, the “grafting to” approach involves anchoring prefabricated polymers with functional groups to corresponding functional groups on the substrate. Such a methodology relies on polymer diffusion, and due to stereochemical hindrance, density of grafting is not very high. An alternative approach to create assemblies of polymers tethered to surfaces is to anchor a monomer to a substrate and use a bulk polymerization reaction to chemically link the growing polymer chains to the surface-bound monomers via a so-called “grafting-through” approach. This method has the advantage of being directly applicable to existing bulk polymerization processes (*i.e.*, free radical or controlled radical polymerization). The thickness of a surface-grafted polymer layer obtained via this approach is controllable by adjusting the density of the surface-bound monomers and the conditions of the polymerization reaction in bulk, and results in uniform films on substrates with areas of several cm². These films can either completely or partially cover the bound monomer layer, presenting a way to tune interfacial properties [1-19].

Chapter 4 in this Ph.D. Thesis dealt specifically with 1-D substrates, which is perhaps the simplest geometry to model and understand as it imposes the least restriction on the polymer chains. In this chapter, the study has been extended to planar two-dimensional (2D) substrates. As seen in the previous chapter, bound monomers can be incorporated in a growing polymer chain, thereby “grafting” the polymer to the substrate/template through one or more sites. This work illustrates the effect of dimensionality of substrates on “grafting through” polymerization and combines computer simulations and surface-sensitive analytical techniques to comprehend the phenomenon.

For this work, we assume that the substrates are fixed in space with a monomer layer bound to it. In experiments, silane chemistry is utilized to create a relatively stable self-assembled monolayer of bound monomers on the substrate [18, 19]. The density of the bound monomers on the substrate is a key parameter in “grafting through” polymerization. Depending on the monomer packing density, “grafting through” might be favored (due to proximity of monomer units) or hindered due to steric effects. Our work furthers the present understanding of in-plane polymerization and the role of bound monomer packing density in the “grafting through” process.

5.1 Computer Simulation

5.1.1 Set-up and Method

The Monte Carlo (MC) simulation scheme, as described in Chapter 4 of this Ph.D. Thesis, was used to model the “living”/controlled radical polymerization in case of a 2D substrate. The substrates, monomers, and polymers reside on a 3D cubic lattice, with the substrate forming the base of the simulation box. The B monomers are covalently bound to the planar substrate, hence their positions are held fixed throughout the simulation. The simulation results reported here have been carried out on a cubic lattice of volume fixed at 125,000 lattice cells, varying the dimensions of the simulation box so that the overall lattice occupancy is constant (at ~15,625 beads) for different packing densities of B. The packing density of the bound monomers was varied by adjusting the area of the X-Y base plane (*cf.*

Figure 5.1). Periodic boundary conditions were applied in only in orthogonal directions along the plane of the substrate. As described in Chapter 4, the values of the parameters intrinsic to the MC simulation scheme are held constant at the same values during all the runs.

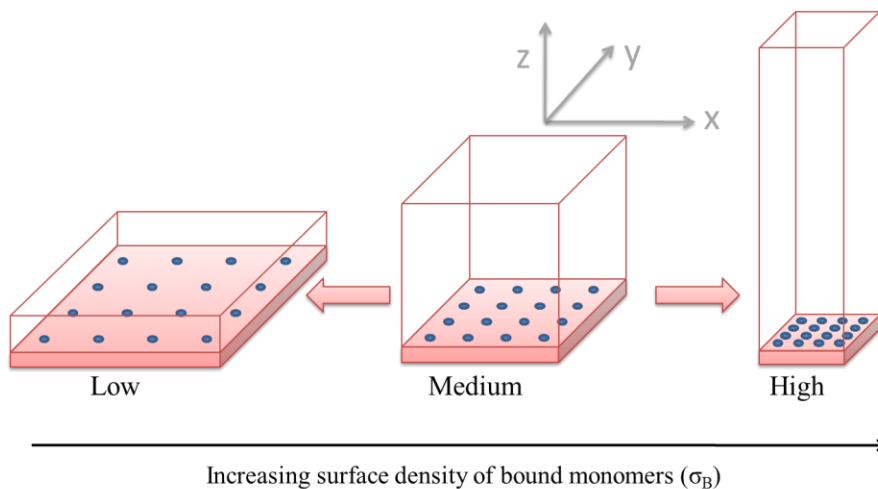


Figure 5.1. The cubic lattice for simulation – the dimensions of the box are changed to vary the bound B monomer packing density (σ_B), keeping the volume constant. The blue motifs denote the monomers bound to the substrate.

In addition to the bound B monomers, there are free A monomers present in bulk. Although both A and B are identical, *i.e.*, there is no interaction potential acting between A and B, such nomenclature is used in this Thesis to distinguish between the polymers formed of free monomeric units only and those formed of both bound and free monomeric units. In addition, there are free initiators present in bulk. The numbers of A monomers and initiators are denoted as [A] and [I], respectively. Two different types of polymers can form during the simulation: homopolymers comprising only A units (*i.e.*, A homopolymers) and copolymers containing both A and B units (*i.e.*, A-B copolymers).

Our system is “truly living”, *i.e.*, the chains do not undergo termination or chain transfer [17]. The implicit solvent model (no explicit solvent molecules are included in the simulations) is presumed to be valid for modeling the growth of “living” chains under good solvent conditions [17]. The initiator molecules and free monomers are initially distributed homogeneously throughout the lattice. In our simulations, the initial number of free monomers ($[A]$) is set to be 3125, which corresponds to the lattice occupancy of 20%. The initial number of initiators ($[I]$) is chosen to be 100, giving rise to a maximum number of polymers equal to 100, that can exist for a given simulation. After placing the monomers and initiators on the lattice, we perform an initial equilibration run for 10^9 Monte Carlo steps (MCS) per bead to obtain a randomly distributed configuration. We use the equilibrated configuration as the input for the MC simulation. The reactive MC algorithm commences after a secondary short equilibration run ($\approx 10^5$) and runs for a predetermined number of MCS, typically 10^9 , in order to achieve the same conversion.

Chain statistics (*i.e.*, molecular weight, polydispersity index) and the coordinates of the monomers of each polymer and all monomers are stored periodically after several thousand MCS. In order to obtain good statistics, we perform 50 MC simulation runs for every set of input parameters. In order to understand the effect of different parameters (*i.e.*, $[B]$, σ_B , $[A]$, $[I]$, substrate shape, bound monomer orientation and flexibility), we monitor the number distribution of bound B monomers and the sequence length distribution in the A-B copolymers, normalized by the number of copolymers formed. While the number distribution gives us a quantitative estimate of the incorporation of bound B monomers in A-B copolymers, the sequence length distribution offers a qualitative insight into the co-monomer distribution in the A-B copolymers. In addition, we also report the number of A-B copolymers and the mole fraction of bound B monomers present in the A-B copolymers.

5.1.2 Results and Discussion

To facilitate the discussion, we set $[B] = 100$ and increase packing density of B on the substrate (σ_B) from 0.18 to 1.0. Note that these numbers for packing density are calculated relative to the maximum occupancy of bound monomers on a square lattice. As in case of one-dimensional substrates, varying the concentration of free A monomers does not have an effect of the system behavior except for increasing the MW of the polymers. This is due to the large excess of A monomers present in the system. In the following discussion, we thus set $[A] = 3125$ for all of the simulations.

The normalized number distributions of bound B monomers per A-B copolymer chain for the different values of σ_B are plotted in **Figure 5.2**. Altering the concentration of free initiators does have an effect on the likelihood of finding the B monomers inside the A-B copolymer. A more than ten-fold increase in $[I]$ (from 12 to 125) reduces the maximum number of B monomers per copolymer from ≈ 40 to ≈ 8 ($\sigma_B < 1$) while concurrently increasing the occurrence of A-B copolymers that have only a single B bound monomer. Due to an increased $[I]$ more polymer chains are generated in the system, which reduces the number of B bound monomers available per growing chain. Thus, by increasing $[I]$ it is more likely to form more A-B copolymers but less likely for a growing A-B chain to incorporate many bound B monomers. We will refer back to the effect of the number of initiators on the polymerization process later in this section. The maximum number of B monomers per copolymer is fairly independent of σ_B irrespective of the number of initiators ($[I]$), at low values of σ_B . However, at the highest grafting ($\sigma_B = 1$), the maximum number of B per copolymer increases from ≈ 8 to 80 (for $[I] = 125$) and ≈ 40 to 100 (for $[I] = 12$) to 80. Note that for $\sigma_B = 1$, a non-zero value of frequency of occurrence for 100 B monomers per A-B copolymer indicates that all of the 100 bound B monomers on the substrate can be potentially incorporated in a single chain at the highest grafting density. This implies that we can bind together all the monomer units on the substrate when the B monomeric units are spaced as close as possible along the substrate template. We attribute this behavior to the ‘‘proximity effect’’; *i.e.*, once a growing chain adds

a bound monomer unit, it is more likely to add a neighboring bound B monomer than a random free A monomer. In addition to the “proximity effect” favoring addition of B monomers to a growing chain, the close packing environment prevents more growing chains to approach the substrate, thereby facilitating the already-grafted chain to add on more bound B monomers.

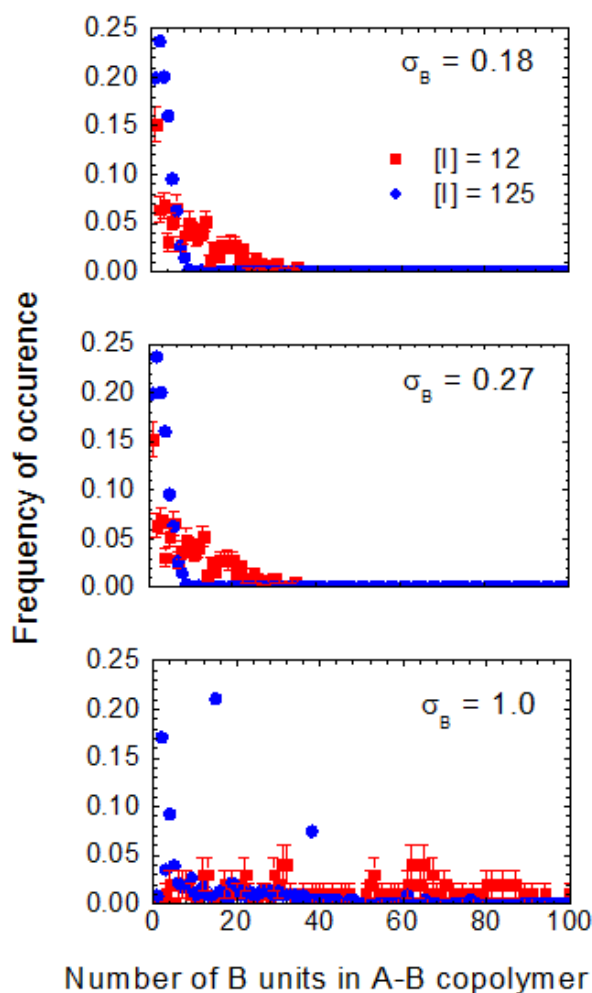


Figure 5.2. Comparison of the number distribution of B in A-B copolymers, averaged over 50 simulation runs, for different grafting densities on planar substrates (σ_B) at two different initiator concentrations ($[I] = 12, 125$).

Our computer simulations indicate that for $\sigma_B < 1$ the B monomers are incorporated into the A-B copolymers as unimers; *i.e.*, there are not dimers, trimers, tetramers, *etc.* constituting consequent runs of B units within the A-B chains. This behavior holds true regardless of the number of initiators present in the system. Only for $\sigma_B = 1$ we detect the presence of B-mers longer than unimers. In fact, we find sequences of B as long as 80 monomers in a single polymer chain. This suggests that longer sequences of consecutive B runs can be realized only when the B monomers are spaced on the substrate as closely as possible. Certain sequence lengths (18 and 40) occur more frequently than others (*cf.* **Figure 5.3**), as observed for $[I] = 125$. In-plane growth of a grafted polymer chain is self-limiting due to steric effects, which is most likely the reason behind the bias towards specific sequence lengths. In **Figure 5.3**, we compare the sequence length distributions of systems having different packing densities of bound B monomers for different number of initiators. Increasing $[I]$ ten-fold results in decreasing the average number of B units available per A-B chain ten times, thus attenuating the overall frequency of occurrence values. This implies that for a greater number of free initiators, it is less likely to incorporate all the B monomers in a single chain.

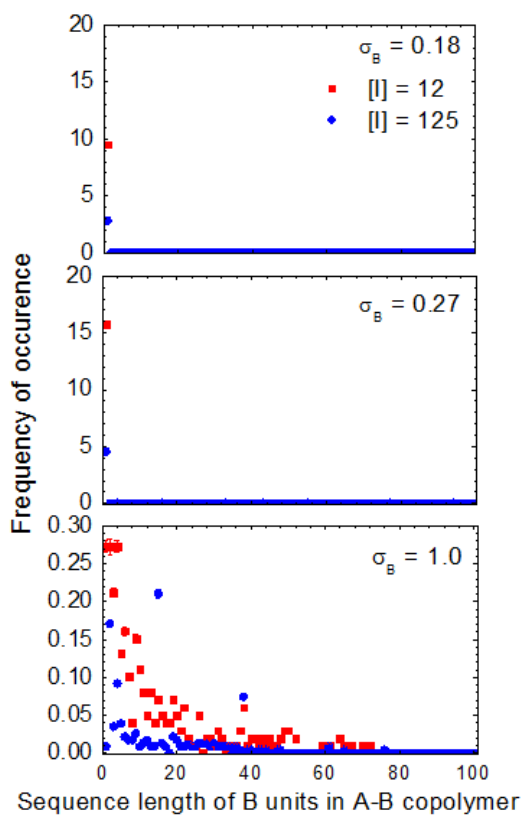


Figure 5.3. Effect of the monomer packing density (σ_B) on the sequence length distribution of B in copolymers A-B.

Figure 5.4 shows a typical snapshot from one of the simulation runs, depicting the grafted A-B copolymers for $[I] = 12$, $[B] = 100$, and $[A] = 3125$, at different values of total monomer conversion for two extremes of B monomer packing densities that are explored in this work. With increasing monomer conversion, the surface-grafted polymer chains (A-B type) grow in length often forming loops as they add on more bound B monomers. Free growing polymer chains (homopolymers) can still get grafted onto the substrate by adding on a surface-bound B monomer. However, the copolymer chains (A-B) already grafted to the substrate sterically hinders the approach of new chains and effectively shields the unreacted bound B monomers. Thus, the grafting of new polymer chains is a self-limiting process. At

the highest packing density of bound monomers, the self-limiting nature of grafting process favors the already-grafted chains to add on more B monomers that are in the proximity, and leads to long sequences or “trains” of B along the plane of the substrate. The interplay of proximity effect and steric effect dictates the addition of new B monomers into a growing chain. At low monomer packing densities, the steric effects come into play at higher monomer conversions when the grafted chains are long enough to form multiple loops. A polymer chain once grafted to the substrate, can only add another B monomer if it “loops” over the substrate to reach a neighboring B (*cf.* **Figure 5.4**). **Figure 5.5** illustrates the occurrence of the “trains” and “loops” as seen in a top-down view of the substrate, from two simulation runs, each at two extreme of monomer packing density. Each color represents a grafted polymer (A-B) chain and the numbers denote the position of the bound B monomer (shown as a solid circle) in that particular chain. Solid connecting lines between two circles, *i.e.*, two bound monomers, represent a “train”. The “loops” are not very obvious from these plots; they occur between two marked positions that are not connected by a line. **Figure 5.5** further demonstrates how a single chain can incorporate most bound monomers at the highest monomer packing density forming “trains” and preventing other chains from reaching the underlying bound monomers.

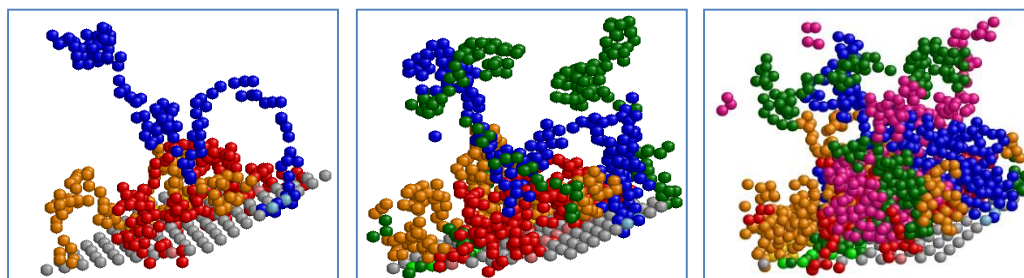


Figure 5.4. Snapshots from a typical simulation run showing the self-limiting nature of the grafting of polymer chains to the substrate. Monomer packing density is 0.18 and overall conversion is 46%, 66% and 88% respectively, from left to right. Each A-B copolymer is shown in a different color and the unreacted bound B monomers are shown in gray.

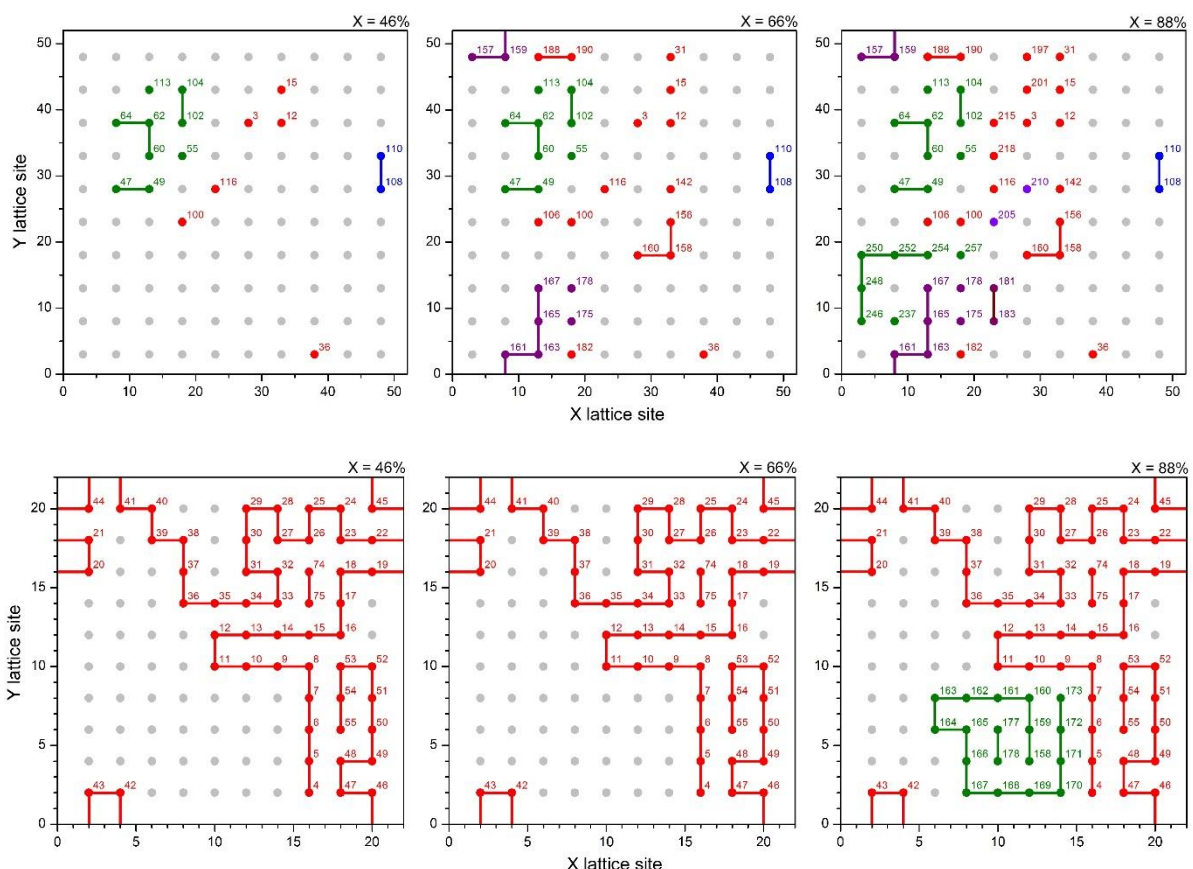


Figure 5.5. Distributions of “loops” and “trains” in A-B copolymers for $\sigma = 0.18$ and 1 (top and bottom respectively) at different monomer conversions (X). Each A-B copolymer is shown in a different color. The numbers correspond each “polymerized” bound monomer is its rank in its respective copolymer sequence. “Trains” are denoted by solid lines. “Loops” occur between successive bound monomers occurring in the same chain, but not consecutive in ranking.

The length of the “loops” formed by a surface-grafted copolymer is affected by the monomer packing density as well as the number of initiators present in the system (*cf.* **Figure 5.6**). For $\sigma_B < 1$, the distribution of loop lengths is relatively well-defined and shows a finite maximum value of loop length that varies with $[I]$. In presence of excess free A monomers ($[I] = 12$), the grafted A-B copolymers can add on more A monomers and form relatively longer

loops. We refer back to the loop lengths later in this section to understand how long loops might favor “grafting through” polymerization of bound B monomers. At the highest monomer packing density, *i.e.*, $\sigma_B = 1$, the loop length distribution covers a wider range of values and displays high scatter.

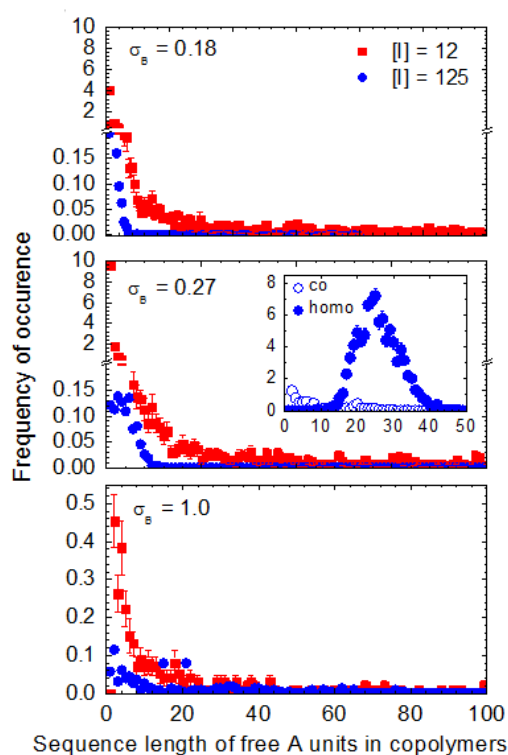


Figure 5.6. Effect of the monomer packing density (σ_B) and number of initiators ($[I]$) on the sequence length distribution of A in copolymers A-B.

Figure 5.7 shows a comparison of the number of A homopolymers and A-B copolymers as well as the composition of A-B copolymers formed with two different numbers of initiators, *i.e.*, $[I] = 12$ (red squares) and 125 (blue circles), at different monomer packing densities. The closed and open symbols represent the data pertaining to A-B copolymers and

A homopolymers, respectively. The number of A-B copolymers produced in the system is governed by the number of initiators and the packing density of bound B monomers. Overall, higher packing density of bound monomers results in fewer A-B copolymers irrespective of number of initiators. We attribute this behavior to the self-limiting nature of polymer grafting onto the surface. The data in **Figure 5.7** reveal that when the bound B monomers are present in excess of the initiators (*i.e.*, $[I] = 12$), the number of A-B copolymers formed is limited by the number of the initiators and is fairly close to the number of free homopolymers formed. The polymer chains being fewer in number can access more of the free space, grow longer loops of free A monomers, and easily reach to the substrate to incorporate bound monomers. In contrast, when the initiators are in excess ($[I] = 125$), the number of A-B copolymers formed (< 30) is significantly lower than the number of homopolymers (> 100) and is strongly affected by the bound monomer packing density. A ten-fold increase in the overall number of polymers (from $[I] = 12$ to 125), does not translate into a proportionate increase in the number of A-B copolymers. Excess number of growing chains leads to a higher probability of forming A-B copolymers; however, steric interactions between growing chains that have already grafted onto the substrate, prevent new chains from approaching the substrate. The fraction of B units in the A-B copolymers is less in case of 12 initiators as compared to 125 initiators. Here, the greater the number of initiators results in more copolymers formed with lower molecular weights (*vide supra*); thus, the composition of the copolymers is limited by the initiators present in the system. As noted earlier, the effects of bound monomer packing density is predominant in presence of excess initiators ($[I] = 125$). Increasing bound monomer packing density can lead to steric hindrance of the growing chains, thereby attenuating the “proximity effect” that favors addition of bound B monomers. The mole fraction data in **Figure 5.7** validate our hypothesis. The fraction of B in the A-B copolymers decreases with varying σ_B (for $\sigma_B < 1$) in presence of excess initiators. However, when free A monomers are in excess, these effects are smeared out and the overall copolymer composition is unaffected by σ_B (for $\sigma_B < 1$). We observe that the mole fraction of fixed B in the A-B copolymers exhibits a maximum value at $\sigma_B = 1$ independent of $[I]$. It is because in-plane growth of a grafted polymer

is extremely favored at the highest monomer packing density and leads to one or two A-B copolymers only. In addition, **Figure 5.7** shows that the molecular weights of the homopolymers and A-B copolymers are fairly similar for $\sigma_B < 1$, consistent with the experimental findings by Henze et al. [18] and Bialke et al. [19] for “grafting through” polymerization using immobilized methacrylates. Thus, by tuning the bulk parameters only, it is possible to control the properties of the surface-grafted polymers.

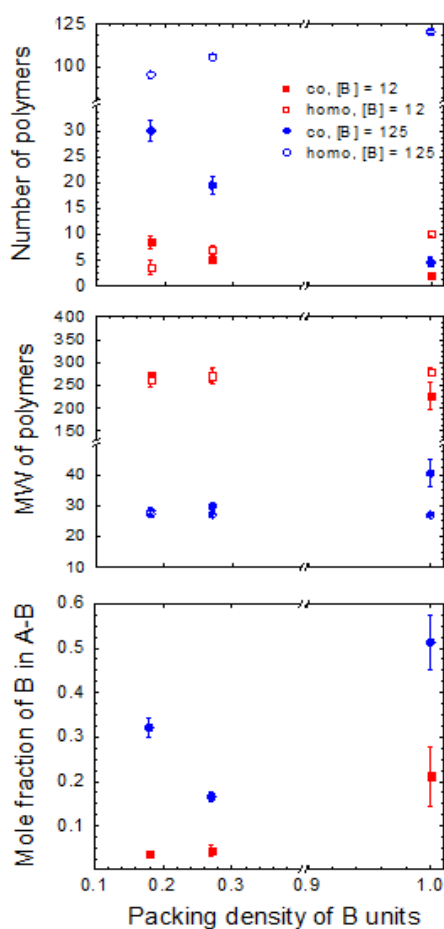


Figure 5.7. The average number of A polymers and A-B copolymers as well as the average A-B composition as a function of the grafting density of the B monomers (σ_B) for $[I] = 12$ and $[I] = 125$.

We also modeled gradient substrates, *i.e.*, substrates with varying monomer packing density along their lengths. Note that the areas corresponding to a specific grafting density are not uniform along the gradient in a simulation box. The end with highest monomer packing density ($\sigma_B = 1$) is much more likely to undergo in-plane polymerization than the remaining area ($\sigma_B < 1$) on the gradient. We attempted to quantify the dry thickness of the grafted polymer layer, by collapsing the chains onto the substrate and calculating the average height of the collapsed layer. A fairly uniform (~ 12 units in thickness) and conformal layer is formed on the planar substrate, irrespective of the gradient in bound monomer packing density. It is not surprising that the dry thickness is invariant, since the average molecular weight of A-B copolymers is fairly constant irrespective of σ_B (as evident in **Figure 5.7**).

5.2 Experimental Set-up

5.2.1. General Methods and Materials

4-Bromostyrene, azobisisobutyronitrile (AIBN), trimethylamine (TEA) and toluene were purchased from Sigma-Aldrich. Methacryolypropyl trimethoxy silane (MPS) and *n*-octyltrichlorosilane (OTS) were purchased from Gelest. Silicon wafers (111) of thickness 0.4 mm were procured from Silicon Valley Microelectronics. Prior to polymerization, styrene and bromo-styrene were passed through a column of inhibitor remover and AIBN was recrystallized from ethanol. Anhydrous toluene was used for all purposes. All other materials were used as received.

5.2.2 Sample Preparation

5.2.2.1 Methacrylate Silane deposition and modification

Silicon wafers were cut into 1 cm x 5 cm pieces, rinsed and sonicated for 20 minutes in methanol, then cleaned in a UV-Ozone chamber for 20 minutes. A gradient of OTS was created via vapor deposition following a protocol published previously [20]. We used a 1:5 mixture of OTS and mineral oil by volume and exposed the silicon wafer to OTS vapors in a

closed chamber for 5mins only. The wafers were then immediately immersed in a 0.1 vol % solution of MPS in anhydrous toluene and TEA (10:1 ratio by volume) and incubated at room temperature overnight, to backfill the OTS gradient with MPS. The samples were then removed, rinsed with toluene followed by methanol, water and methanol and subsequently dried with a stream of nitrogen gas.

5.2.2.2 Polymerization of surface-bound monomers

Inhibitor removed bromostyrene, AIBN (1:260 molar ratio as in the simulation set-up) and excess toluene and were charged to crimp-top sealable vials with rubber septa caps, and the AIBN was dissolved at room temperature. The MPS/OTS gradient wafers were then placed in these vials, which were sealed and degassed by bubbling with nitrogen for one hour. The vials were then placed in a thermocouple controlled oil bath heated to 70°C for 24 hours under gentle stirring. The polymerization solution was kept below the level of the heating oil during the entire polymerization to help maintain a uniform temperature. After 24 hrs, the vials were opened and the samples removed and sonicated in toluene for 20 mins to remove any physisorbed polymer. The samples were dried with a stream of nitrogen gas before further characterization.

5.2.3 Results and Discussion

We used OTS/MPS gradient samples as controls. The gradient controls were characterized using water contact angle goniometry and ellipsometry to measure wettability and thickness as a function of distance along the gradient. Using Cassie-Baxter equation for two-component surfaces, we converted the measured water contact angle data into fractional coverage of MPS along the gradient (calculations shown in Appendix). Henceforth, all experimental data are expressed as a function of fractional surface coverage of MPS rather than distance along the MPS/OTS gradient (*cf.* **Figure 5.9**). At one end of the gradient, the surface primarily contains inert OTS units while at the other end, the surface is rich in MPS (> 90%). It is likely that the MPS units are not homogeneously dispersed at the extremely OTS-

rich end. All measurements were carried out at 1 cm intervals along the gradients, starting from 0.5 cm away from one of the edges of the silicon wafer. Dry thickness, measured by ellipsometry, shows a slight increase in thickness with MPS fractional coverage until 0.75 coverage value. At very high MPS fraction (~ 0.90), the thickness increase is relatively smaller.

We further characterized the gradient samples with X-ray Photoelectron Spectroscopy (XPS). XPS data can provide information about the elemental composition as well as the types of chemical bonds in given sample. The reason behind the choice of 4-bromostyrene as the free monomer is that C and Br have distinct peaks in XPS. High resolution peaks of C and Br (*cf.* **Figure A5.2**) were resolved into multiple Gaussian components using a Simplex algorithm. The carbonyl component appears from MPS while Br 3d peak is exclusively from 4-bromostyrene. Since we do not have standards for calibration, we can draw qualitative inferences are based on ratios rather than absolute values. We compare the ratios of the areas under Br peak and carbonyl peak at each location on the gradient substrate (*cf.* **Figure 5.9**). It is to be noted that the penetration depth of XPS is ~ 10 nm, well beyond the thickness of the polymer layer ($\sim 2.5 - 3$ nm).

In addition, we calculated the elemental composition from XPS survey data at each location. Both sets of data show that the amount of Br (and therefore, bromostyrene) is higher at lower fractional coverage by MPS. Qualitatively, these results corroborate our simulations that show the occurrence of longer loops of free A monomer (bromostyrene in experiments) at lower values of bound B monomer packing density.

In addition to ellipsometry and XPS measurements, the samples were characterized by Time of Flight-Secondary Ion Mass Spectrometry (TOF-SIMS). TOF-SIMS is an extremely sensitive surface analysis technique with a typical analysis depth of less than 2 nm and is therefore better suited for the compositional analysis of ultra-thin layers and nanoscale sample features. In addition, TOF-SIMS can be used to characterize molecular information from organic materials. We performed TOF-SIMS measurements prior to any other experimental characterization to avoid contamination. We identified unique signature fragments for MPS, bromostyrene and OTS from an understanding of the molecular structure of each chemical

species. OTS can produce short saturated alkyl fragments only while bromostyrene can produce only aromatic fragments or long-chained unsaturated alkyl fragments [21]. Since we do not have standards for calibration, we report the fractional contribution of each species fragment to the total TOF-SIMS signal (*cf.* **Figure 5.10**). All aromatic fragments ($C_6H_5^+$, $C_{10}H_9^+$ and $C_8H_9^+$) and $C_{13}H_{11}Br^+$ increase with decreasing surface coverage by MPS. At low surface coverage (MPS fraction < 0.7), the contribution of aromatic and bromostyrene fragments do not change significantly with surface coverage. These results demonstrate the same qualitative trends as our findings from computer simulation (*cf.* **Figure 5.6**). In order to “graft through” the bound B monomer units (MPS) at low packing density (or fractional coverage by MPS < 0.7), more of free A monomers (bromostyrene) are needed to form loops that facilitate “grafting to” unreacted B monomers. At very high surface coverage (MPS fraction ~ 0.9) by MPS, in-plane “grafting through” is favored and do not require much of bromostyrene, as noted in case of $\sigma_B=1$ in simulations.

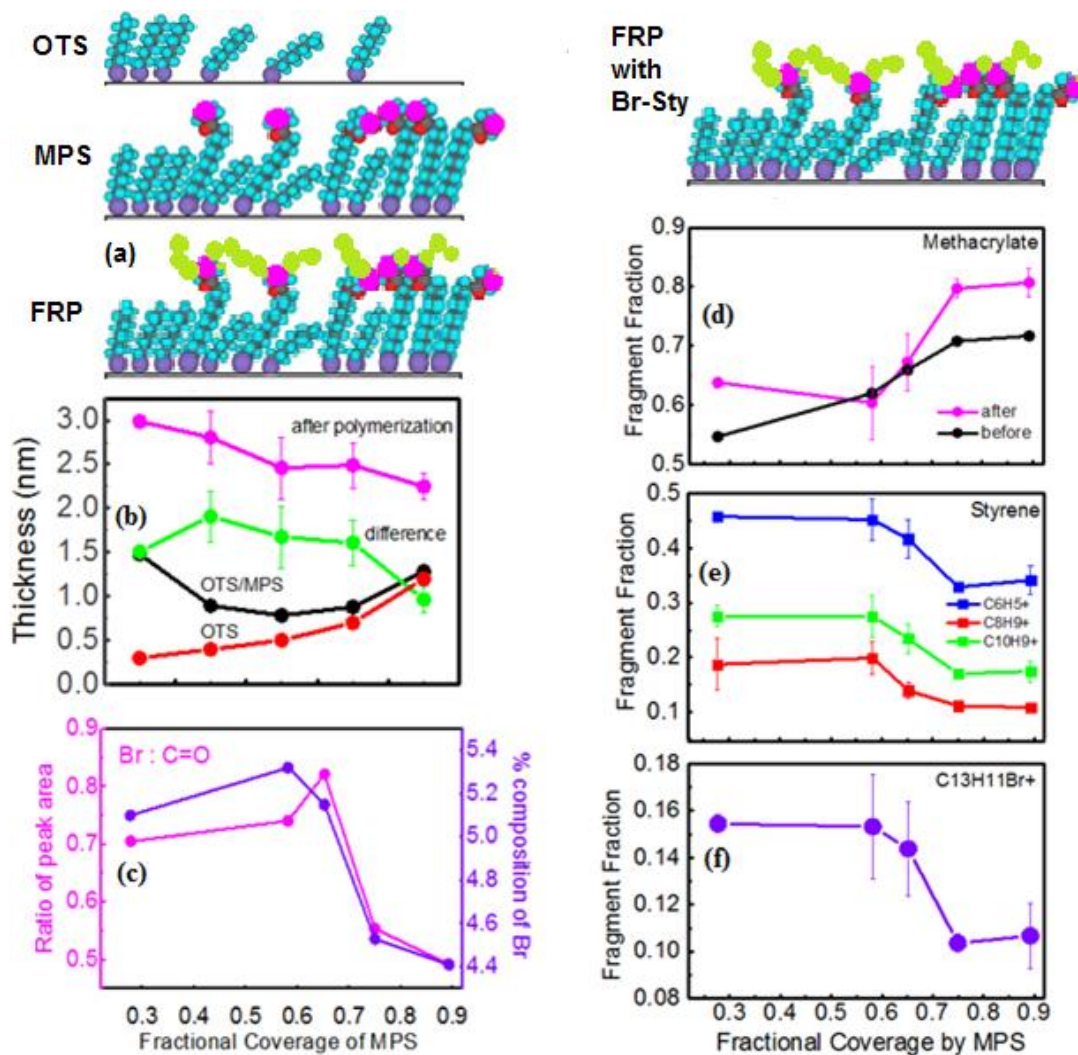


Figure 5.8. Top, left (a) Cartoon depicting the experimental procedure, (b) ellipsometry dry thickness measurements, (c) Br content estimated from XPS measurements, (d)-(f): TOF-SIMS fragments as a function of fractional coverage by MPS.

5.3. Conclusions

We used a combination of computer simulation and experiments to comprehend “grafting through” polymerization on flat 2D substrate. To our knowledge, this is the first

study that probes into this kind of systems using molecular modeling and validates the results using highly surface-sensitive analytical tools. It is to be noted that our simulation model is highly coarse-grained and lattice-based, so a direct quantitative match with fractional MPS coverage is not possible.

Our results demonstrate the effect of packing density of the surface-bound monomers on the formation and composition of the surface-bound polymers. Grafting of polymer chains to the substrate via polymerization is a self-limiting process. The proximity of the surface-bound polymerizable units promotes the “grafting through” process but prevents more free growing chains to “graft to” the polymerizable units. Our studies indicate that these two counter-active effects balance each other and do not significantly affect the overall density of the surface-bound polymer layer, except at the highest packing density of surface-bound monomers. The amount of initiator can affect “grafting through” polymerization. These results indicate that the dimensionality of the substrate/template plays a key role in “grafting through” polymerization. As reported in Chapter 4 of this Ph.D. Thesis, at the maximum possible monomer packing density ($\sigma_B = 1.0$), it is possible to incorporate all of B monomers bound to a rod-like substrate into a single polymer chain, *i.e.*, perfect templation is possible. In the present case of planar substrates, such a phenomenon is extremely unlikely since the grafting of new polymer chains is a self-limiting process.

Our experimental results show the same qualitative trends as the simulations. At the highest MPS coverage (> 0.75), the characteristics of the grafted polymer layer is distinctly different from that at lower values. The presence of higher fractions of bromostyrene fragments in the polymer at lower MPS coverage, confirms that grafting takes place by incorporating bromostyrene units, as observed in the simulations for low σ_B . The same trend is observed with XPS, which corroborates the TOF-SIMS results. The thickness of the grafted polymer layer increases slightly with increasing MPS fraction, for MPS coverage < 0.75 . On the other hand, at high MPS fraction coverage (>0.75), the change in thickness after polymerization is relatively low. This further highlights the self-limiting nature of the “grafting” process.

APPENDIX

5.4 Appendix

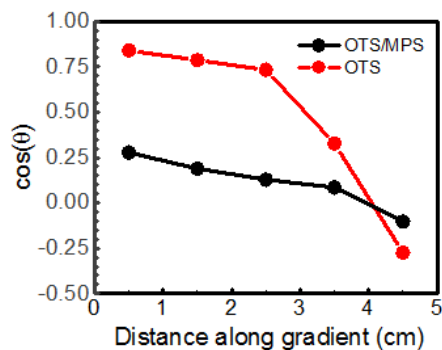


Figure A5.1. Cosine of the water contact angles measured along the length of the gradient of OTS and OTS/MPS.

The fractional surface coverage by MPS is estimated from the values of contact angle measured along the OTS/MPS gradient (*cf.* **Figure A3.1**). The MPS fraction at a given location on the gradient can be determined from water contact angle data using the Cassie-Baxter equation.

$$\cos(\theta) = f_{MPS}\cos(\theta_{MPS}) + (1 - f_{MPS})\cos(\theta_{OTS}) \quad (\text{A3.1})$$

where θ is the measured contact angle, θ_{MPS} is the water contact angle for MPS monolayer, θ_{OTS} is the water contact angle for OTS monolayer and f_{MPS} is the areal fraction of MPS. The contact angles for OTS (θ_{OTS}) and MPS (θ_{MPS}) monolayers are 110° and 70° respectively. Thus, all the contact angle data was converted to fraction of MPS as a function of distance along the gradient.

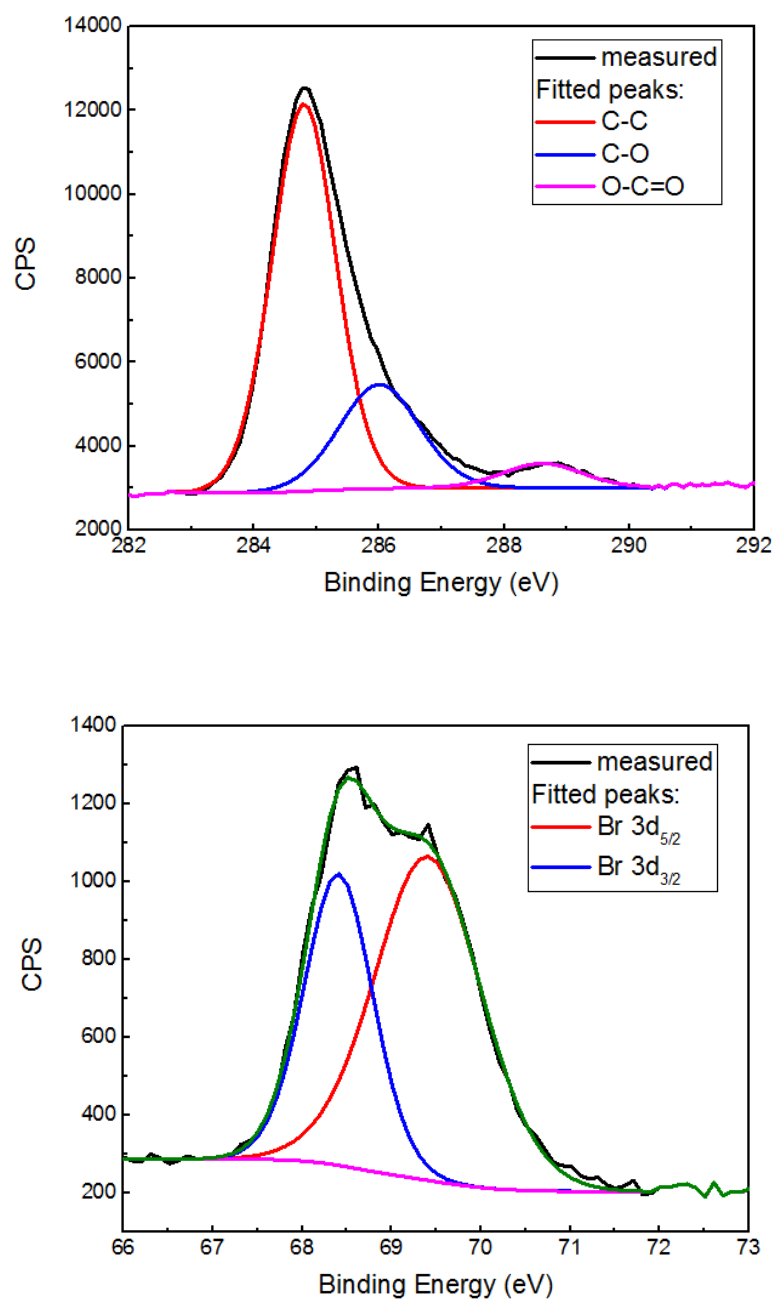


Figure A5.2. A typical high resolution XPS data showing C (top) and Br (bottom) peaks.

5.4 References

1. S. Polowinski, "Template Polymerization", *ChemTec Publishing*, 1997.
2. G. Challa and Y.Y. Tan, "Template Polymerization", *Pure & Applied. Chem.*, 1981, **53**, 647-651.
3. D. M. Rosenbaum and D. R. Liu, "Efficient and Sequence-Specific DNA-Templated Polymerization of Peptide Nucleic Acid Aldehydes", *J. Am. Chem. Soc.*, 2003, **125** (46), 13924–13925.
4. J. Gons, E. J. Vorenkamp, G. Challa, "Radical polymerization of methyl methacrylate in the presence of stereoregular poly(methyl methacrylate). V. Kinetics of initial template polymerization", *Journal of Polymer Science: Polymer Chemistry*, 1975, 13 (7), 1699–1709.
5. J. Smid, Y.Y. Tan, G. Challa, "Effects of poly(2-vinylpyridine) as a template on the radical polymerization of methacrylic acid—I. Influence of atactic poly(2-vinylpyridine) concentration", *European Polymer Journal*, 1983, 19 (10–11), 853–858.
6. I. Rainaldi, C. Cristallini, G. Ciardelli, P. Giusti, "Kinetics and reaction mechanism of template polymerization investigated by conductimetric measurements. Part 3. Radical polymerization of acrylic acid in the presence of poly(*N*-vinylpyrrolidone)", *Polymer International*, 2000, 49 (1), 63–73.
7. K. J. Shea and D. Y. Sasaki, "On the control of microenvironment shape of functionalized network polymers prepared by template polymerization", *J. Am. Chem. Soc.*, 1989, **111** (9), 3442-3444.
8. T. Serizawa, K. Hamada & M. Akashi, "Polymerization within a molecular-scale stereoregular template", *Nature*, 2004, **429**, 52-55.
9. K. Hamada, T. Serizawa, and M. Akashi, "Template Polymerization Using Artificial Double Strands", *Macromolecules*, 2005, **38** (16), 6759-6761.

10. V. S. Trubetskoy, V. G. Budker, L. J. Hanson, P. M. Slattum, J. A. Wolff and J. E. Hagstrom, "Self-assembly of DNA-polymer complexes using template polymerization", *Nucleic Acids Research*, 1998, **26** (18), 4178-4185.
11. J. Matsui , T. Kato , T. Takeuchi , M. Suzuki , K. Yokoyama , E. Tamiya , I. Karube, "Molecular recognition in continuous polymer rods prepared by a molecular imprinting technique", *Analytical Chemistry*, 1993, **65** (17), 2223–2224.
12. W. Wang, S. Gao, and B. Wang, "Building Fluorescent Sensors by Template Polymerization: The Preparation of a Fluorescent Sensor for d-Fructose", *Organic Letters*, 1999, **1** (8), 1209-1212.
13. J. F. Ford , T. J. Vickers , C. K. Mann , and J. B. Schlenoff, "Polymerization of a Styrene-bound Monolayer", *Langmuir*, 1996, **12** (8), 1944-1946.
14. T. Bein and P. Enzel, "Encapsulation of Polypyrrole Chains in Zeolite Channels", *Angewandte Chemie*, 1989, **28** (12), 1692-1694.
15. I. Carmesin and K. Kremer, "The bond fluctuation method: a new effective algorithm for the dynamics of polymers in all spatial dimensions", *Macromolecules*, 1988, **21** (9), 2819–2823.
16. J. Genzer, "In silico polymerization: Computer simulation of controlled radical polymerization in bulk and on flat surfaces", *Macromolecules*, 2006, **39**, 7157-7169.
17. S. Turgman-Cohen and J. Genzer, "Computer Simulation of Controlled Radical Polymerization: Effect of Chain Confinement Due to Initiator Grafting Density and Solvent Quality in "Grafting From" Method", *Macromolecules*, 2010, **43** (22), 9567-9577.
18. M. Henze, D. Madge, O. Prucker and J. R uhe, ""Grafting Through": Mechanistic Aspects of Radical Polymerization Reactions with Surface-Attached Monomers", *Macromolecules*, 2014, **47** (22), 2929-2937.

19. M. Bialk, O. Prucker and J. Ruhe, "Grafting of polymers to solid surfaces by using immobilized methacrylates", *Colloids and Surfaces A, Physicochemical and Engineering Aspects*, 2002, **198–200**, 543–549.
20. T. Wu, K. Efimenko and J. Genzer, "Multivariant investigation of the mushroom-to-brush transition in surface-anchored poly(acrylamide)", *J. Am. Chem. Soc.*, 2002, **124**, 9394–9395.
21. X. V. Eynde and P. Bertrande, "Quantification of polystyrene blend surfaces based on end group ToF-SIMS analysis", *Applied Surface Science*, 1999, **140**, 1-20.

6. Outlook

This Ph.D. Thesis explored two different approaches to polymerization under confinement. Chapter 2 documented the effect of vertical confinement on thermal frontal polymerization with respect to the front propagation and molecular weight of the polyacrylamide. Chapter 3 considered how molecular weight distribution of the polyacrylamide can be controlled using a combination of gelation, vertical confinement and directional heat supply. Chapters 4 and 5 reported on the importance of surface-bound monomer packing density and substrate dimensionality on template polymerization based on a “grafting through” approach. These results have opened up potential directions for research with respect to polymerization under confinement. This chapter lists the suggestions for future work that may be of interest to other polymer researchers, in particular, future Genzer group members.

6.1. Confined Frontal Polymerization as a means to synthesize low PDI polymers

Confined frontal polymerization can lead to polyacrylamide of significantly low polydispersity, in spite of the simple free-radical chemistry. It has been demonstrated that the degree of dilution, absence of convection and localization of the reaction front are the key factors that control polymer molecular weight distribution. The findings of this work suggest that it is possible to extend this synthetic technique to other monomer/solvent/initiator systems (such as acrylates) that can fulfil certain criteria, such as those outlined in Chapter 1.1. In principle, such confined reactors can be set up in parallel to get a significant amount of polymer. Compared to other controlled/“living” polymerization methods, radical-based polymerization reactions have several advantages, especially in terms of compatibility with both aqueous and organic media as well as a high tolerance toward a wide range of functional groups. The biggest strength of confined frontal polymerization lies in its potential to be extended similar monomer/solvent systems. The present work indicates that the degree of dilution governs the occurrence of gelation in the reaction mixture, which is system-specific. In order to successfully generate low PDI samples of other polymers, the reaction conditions need to be optimized accordingly.

6.2 Confined Frontal Polymerization as a separation method to study reaction kinetics

The molecular weight distribution of a polymer is the record of its polymerization kinetics. Polymer samples from different locations along the direction of front propagation in a confined frontal polymerization reactor at a certain time, correspond to different stages of monomer conversion. In principle, a confined frontal polymerization reactor can be thought of a series of plug-flow reactors with negligible mixing. Thus, a single such experiment can yield multiple samples for kinetic study without the need of collecting aliquots as in conventional kinetic-monitoring experiments. As demonstrated in this Ph.D. Thesis, the molecular weight distribution of such polymer samples can shed light on polymerization reaction kinetics. Occurrence of a multimodal molecular weight distribution implies that multiple modes of chain initiation/propagation are present. In such cases, rigorous peak fitting to the molecular weight distribution data can yield new insights into the reaction kinetics. Overall, confined frontal polymerization holds promise as an unconventional separation method for polymers of different molecular weight, which can save time, energy and resources.

6.3. “Grafting through” polymerization for molecular imprinting, replica and patterning

“Grafting through” polymerization is a relatively new and fairly unexplored means of growing substrate-grafted polymer assemblies. It has been shown that there are two counterbalancing effects coming into play- the proximity of polymerizable units favoring polymerization and the crowding of grafted polymer chains on the substrate preventing further polymerization. This work can be extended to study the feasibility of copolymer systems with different reactivity ratios of the bound and the free monomers. Furthermore, the “grafting through” approach shows promise as an emerging technique for molecular imprinting (such as DNA replication). It can be potentially used for patterning purposes on nano-scale. One prospective application of “grafting through” polymerization is stabilizing self-assembled monolayers- effectively “locking” the monolayer (of polymerizable entities) in a particular molecular orientation. In conjunction with self-assembly, it can help create the new future for nano-electronics and semiconductor applications.